

Unraveling the *in vivo* Effect of the AMD-risk Associated CFH H402 Variant

by

Michael Landowski

University Program in Genetics and Genomics  
Duke University

Date: \_\_\_\_\_

Approved:

\_\_\_\_\_  
Catherine Bowes Rickman, Supervisor

\_\_\_\_\_  
Scott Cousins

\_\_\_\_\_  
Michael Hauser, Chair

\_\_\_\_\_  
Daniel Saban

\_\_\_\_\_  
Yuan Zhuang

Dissertation submitted in partial fulfillment of  
the requirements for the degree of Doctor of Philosophy  
from the University Program in Genetics and Genomics  
in the Graduate School of Duke University

2018

ABSTRACT

Unraveling the *in vivo* Effect of the AMD-risk Associated CFH H402 Variant

by

Michael Landowski

University Program in Genetics and Genomics  
Duke University

Date: \_\_\_\_\_

Approved:

\_\_\_\_\_  
Catherine Bowes Rickman, Supervisor

\_\_\_\_\_  
Scott Cousins

\_\_\_\_\_  
Michael Hauser, Chair

\_\_\_\_\_  
Daniel Saban

\_\_\_\_\_  
Yuan Zhuang

An abstract of a dissertation submitted in partial fulfillment of  
the requirements for the degree of Doctor of Philosophy  
from the University Program in Genetics and Genomics  
in the Graduate School of Duke University

2018

Copyright by  
Michael Landowski  
2018

## Abstract

Age-related macular degeneration (AMD) is a complex retinal degeneration present in elderly populations of first world countries with limited available therapeutic interventions. Risk for AMD is strongly conferred by advanced aging but is also modulated by genetic variants and environmental stresses. One of the most replicated genetic variants associated with AMD is the *Complement Factor H (CFH) Y402H* polymorphism. CFH is a critical regulator of the complement cascade but how the H402 variant impairs its function and contributes to AMD development is unclear. Herein, the role of the H402 variant in the development of AMD-like pathologies was interrogated using two different mouse models based on advanced aging, CFH perturbation and environmental stress.

First, aged *CFH hemizygous knockout (Cfh+/-)* mice were fed a high fat, cholesterol-enriched (HFC) diet for eight weeks to induce AMD-like pathologies such as vision loss, increased retinal pigmented epithelium (RPE) damage, increased sub-RPE deposit formation and immune cell recruitment to the RPE/choroid interface. To determine if the recruitment of immune cells drives the formation of the AMD-like pathologies in aged *Cfh+/-*~HFC mice, aged *Cfh+/-* mice were concurrently treated with a systemic anti-C5a therapy during the eight week HFC diet treatment to block the complement-mediated recruitment of immune cells to the eye. However, the ocular phenotype was unchanged

in aged *Cfh+/-~HFC* mice treated with the anti-C5a therapy despite the decrease of recruited immune cells to the posterior eye. This data suggests the risk associated with the H402 CFH variant is not solely attributable to complement-mediated immune cell recruitment to the posterior eye.

Second, aged transgenic mice expressing equal concentrations of the normal human CFH Y402 (*CFH-Y:Cfh-/-*) or risk-associated CFH H402 (*CFH-HH:Cfh-/-*) protein were fed an eight week HFC diet. Remarkably, vision loss, increased RPE damage and increased sub-RPE deposit formation was only observed in aged *CFH-HH:Cfh-/-* mice following diet treatment. Biochemical analysis of aged *CFH:Cfh-/-* mice revealed differences in plasma and ocular lipoproteins, but not complement, between aged *CFH-Y:Cfh-/-~HFC* and *CFH-HH:Cfh-/-~HFC* mice. Thus, we targeted plasma lipoprotein levels through dietary intervention in aged *CFH-HH:Cfh-/-* mice and observed visual loss in these mice that coincided with dietary cholesterol-induced increases of plasma LDL. Based on our findings we hypothesize that the risk-associated with the H402 CFH variant and AMD is due to the interaction of CFH with lipoproteins and not its complement regulatory roles. These new insights may help explain why current therapies targeting complement inhibition for AMD have failed and, importantly, support targeting lipoprotein metabolism, as a treatment for AMD.

## **Dedication**

I would like to dedicate this dissertation to my family members, especially my brother, grandmother and grandfather, who are with me in spirit on this day.

# Table of Contents

Abstract .....	i
Dedication.....	iii
Table of Contents .....	iv
List of Tables.....	viii
List of Figures .....	ix
Acknowledgements .....	xii
1. Introduction.....	1
1.1 Overview on Retinal Anatomy and Physiology.....	1
1.2 Age-related Macular Degeneration.....	4
1.3 The Use of Mice in AMD Research.....	9
1.3.1 Mice as a Model Organism for AMD Studies.....	10
1.3.2 Advances in the Understanding of AMD-associated Pathobiological Mechanisms from Mouse Studies.....	18
1.3.2.1 Lipid Metabolism and Transport and Inflammation.....	19
1.3.2.2 Oxidative Stress and Inflammation.....	20
1.3.2.3 Oxidative Stress and Angiogenesis .....	22
1.3.3 Future of Mice in AMD Studies.....	24
1.4 Complement Dysregulation in AMD Pathobiology .....	25
1.4.1 Overview of Complement Biology.....	25
1.4.2 Alternative Complement Pathway and AMD.....	29

1.4.3	Complement Factor Y402H Polymorphism and AMD Risk .....	30
1.5	Interrogating the Role of CFH in AMD using Mice .....	31
2.	Effect of Anti-C5a Therapy in a Murine Model of Early/Intermediate Dry Age-Related Macular Degeneration .....	37
2.1	Introduction .....	37
2.2	Results.....	39
2.2.1	Anti-C5a Dosage and Efficacy in an Acute Model of Retinal Degeneration and of Neovascularization.....	39
2.2.2	Anti-C5a Treatment in Aged <i>Cfh</i> <sup>+/-</sup> ~HFC Mice.....	41
2.2.3	Anti-C5a Therapy Does Not Reduce Early/Intermediate Dry AMD-Like Features in <i>Cfh</i> <sup>+/-</sup> ~HFC Model .....	42
2.2.4	HFC Diet Increases Expression of Inflammation and ECM Genes in the Eyecups of Aged <i>Cfh</i> <sup>+/-</sup> Mice.....	45
2.2.5	Anti-C5a Therapy Does Not Ameliorate HFC-Induced Inflammatory and ECM Gene Expression in the Eyecups of Aged <i>Cfh</i> <sup>+/-</sup> Mice .....	47
2.2.6	Complement Anaphylatoxin Receptor 5 Is Predominantly Expressed in Mouse and Human Choroid but Not in Mouse and Human RPE .....	49
2.2.7	Anti-C5a Therapy Ameliorates Classical Monocytosis Seen in <i>Cfh</i> <sup>+/-</sup> ~HFC Mice.....	51
2.2.8	Anti-C5a Therapy Blocks Recruitment of Monocytes Into the Choroid....	53
2.3	Discussion .....	55
3.	Human CFH Y402H Causes an Age-related Macular Degeneration Phenotype in Mice .....	61
3.1	Introduction .....	61
3.2	Results .....	63

3.2.1	Fluid Phase Complement Proteins in Human CFH Transgenic Mice.....	63
3.2.2	Visual Function Decline Associates with Human H402 CFH with Aging and HFC diet.....	64
3.2.3	RPE Dymorphogenesis Increases in Mice Expressing Human H402 CFH with Age and HFC diet .....	68
3.2.4	HFC Diet-induced Sub-RPE Deposits Increase In Mice Expressing Human H402 CFH.....	69
3.2.5	HFC Diet-Induced Complement Activation is Independent of CFH 402 Variant Expressed .....	72
3.3	Discussion .....	75
4.	Dietary Cholesterol Causes Visual Loss in a Complement-Dysregulated AMD Mouse Model .....	78
4.1	Introduction.....	78
4.2	Results.....	80
4.2.1	HFC diet consumption causes NASH-like liver pathologies in <i>CFH:Cfh<sup>-/-</sup>~HFC</i> mice.....	80
4.2.2	Dietary cholesterol consumption causes NASH in aged <i>CFH-HH:Cfh<sup>-/-</sup></i> mice .....	81
4.2.3	Dietary cholesterol contributes to visual loss in aged <i>CFH-HH:Cfh<sup>-/-</sup></i> mice .....	83
4.2.4	Increased complement protein and activation levels in <i>CFH-HH:Cfh<sup>-/-</sup></i> mice occur in the high fat and high cholesterol diets compared to the normal diet.....	84
4.2.5	Diet modulates the levels of lipoproteins in aged <i>CFH-HH:Cfh<sup>-/-</sup></i> mice. ...	86
4.2.6	Plasma Low-Density Lipoprotein (LDL) Levels Are CFH Variant Dependent .....	89

4.2.7	Eyecup HDL-associated Apolipoprotein Levels Increase in CFH H402 Mice Fed HFC diet .....	92
4.3	Discussion .....	94
5.	Conclusions .....	97
5.1	Introduction .....	97
5.2	CFH acts a potential regulator of plasma LDL entering the posterior eye .....	97
5.3	Determining the Significance of Complement in Aged <i>CFH-HH:Cfh<sup>-/-</sup></i> -HFC mice .....	101
5.4	Targeting Dietary Cholesterol and its Effects in Aged <i>CFH-HH:Cfh<sup>-/-</sup></i> mice....	103
5.5	Validating the Role of the H402 CFH Variant on Lipoprotein Metabolism Using In Vitro and Population-based Studies.....	106
5.6	Conclusions.....	108
	Materials and Methods.....	109
	Appendix A.....	124
	Appendix B .....	130
	Appendix C.....	133
	References .....	134
	Biography .....	174

## List of Tables

Table 1: Summary of Current AMD Mouse Models .....	12
Table 2: Summary of Inflammatory Process and Autoimmunity Gene Expression Changes in RPE/Choroid Eyecup RNA Isolated from Old <i>Cfh</i> <sup>+/-</sup> Fed an HFC Diet Compared to Age-Matched <i>Cfh</i> <sup>+/-</sup> Fed a Normal Diet .....	124
Table 3: Supplemental Table 2: Summary of Extracellular Matrix and Adhesion Molecule Gene Expression Changes in RPE/Choroid Eyecup RNA Isolated from Old <i>Cfh</i> <sup>+/-</sup> Fed an HFC Diet Compared to Age-Matched <i>Cfh</i> <sup>+/-</sup> Fed a Normal Diet .....	127

## List of Figures

Figure 1: Anatomical features of the human eye.....	3
Figure 2: Genetic variants associated with AMD .....	6
Figure 3: Drusen are a hallmark of AMD pathology .....	7
Figure 4: Diagram of Complement Cascade .....	26
Figure 5: Ocular responses of aged C57, <i>Cfh</i> <sup>+/-</sup> and <i>Cfh</i> <sup>-/-</sup> mice after HFC diet consumption. ....	34
Figure 6: C5a dosage and efficacy studies using the sodium iodate (NaIO <sub>3</sub> ) model of retinal degeneration and laser-induced CNV model of wet AMD.....	40
Figure 7: Sustained high levels of circulating antibodies are achieved with weekly injections of 30 mg/kg of anti-C5a therapy.....	42
Figure 8 Anti-C5a therapy does not affect dry AMD-like features in <i>Cfh</i> <sup>+/-</sup> ~HFC mice. 44	
Figure 9: Overall trends of gene expression changes in inflammatory and ECM remodeling genes detected on pathway-focused PCR arrays of eye cups of aged <i>Cfh</i> <sup>+/-</sup> fed an HFC diet .....	46
Figure 10: HFC-induced expression of inflammatory and ECM-related genes in eyecups of aged <i>Cfh</i> <sup>+/-</sup> mice is not decreased by anti-C5a therapy.....	48
Figure 11: <i>C5ar1</i> expression in mouse retina, RPE, and choroid/sclera. RNA was isolated from mouse retinal, RPE, and choroid/scleral tissue .....	50
Figure 12: C5AR1 expression in human RPE and Choroid and immortalized human RPE .....	51
Figure 13: (A) Flow cytometry was performed on peripheral blood mononuclear phagocytes in <i>Cfh</i> <sup>+/-</sup> ~ND, <i>Cfh</i> <sup>+/-</sup> ~HFC and <i>Cfh</i> <sup>+/-</sup> ~HFC + anti-C5a therapy .....	53
Figure 14: Extravascular choroidal mononuclear phagocytes are increased in <i>Cfh</i> <sup>+/-</sup> ~HFC mice and are ameliorated by anti-C5a therapy .....	54

Figure 15: <i>CFH-Y:Cfh-/-</i> and <i>CFH-HH:Cfh-/-</i> mice have equivalent fluid phase complement protein levels .....	64
Figure 16: Decreased visual function loss occurs in only aged <i>CFH-HH:Cfh-/-</i> ~HFC mice. ....	66
Figure 17: Rod dominant ERG responses are impaired in aged <i>CFH-HH:Cfh-/-</i> mice following HFC diet .....	67
Figure 18: Increased RPE dysmorphogenesis is only in aged <i>CFH-HH:Cfh-/-</i> ~HFC mice	69
Figure 19: Aged <i>CFH-HH:Cfh-/-</i> ~HFC mice have increased sub-RPE deposits .....	71
Figure 20: HFC diet-induced complement activation is <i>CFH:Cfh-/-</i> genotype independent. ....	74
Figure 21: Aged <i>CFH:Cfh-/-</i> mice develop non-alcoholic steatohepatitis-like (NASH) liver pathologies after HFC diet consumption .....	81
Figure 22: Aged <i>CFH-HH:Cfh-/-</i> mice develop NASH liver pathologies that is dietary cholesterol consumption dependent .....	82
Figure 23: Visual function loss in aged <i>CFH-HH:Cfh-/-</i> mice consuming dietary cholesterol .....	83
Figure 24: Diet-induced complement activation is independent of visual function loss in aged <i>CFH-HH:Cfh-/-</i> mice .....	85
Figure 25: Dietary cholesterol modulates the circulating lipoprotein levels in aged <i>CFH:Cfh-/-</i> mice. ....	87
Figure 26: Plasma ApoE in <i>CFH-HH:Cfh-/-</i> is dietary cholesterol dependent. ....	88
Figure 27: Plasma lipoprotein levels are <i>CFH:Cfh-/-</i> variant dependent. ....	91
Figure 28: Posterior eyecup apolipoprotein levels are <i>CFH:Cfh-/-</i> variant dependent. ...	93
Figure 29: Schematic of CFH-mediated regulation of plasma LDL ingestion by the RPE. ....	100

Figure 30: Vision loss in response to the HFC diet in mice expressing human H402 CFH is advanced aging dependent.....	130
Figure 31: Increased RPE dysmorphogenesis in response to the HFC diet in mice expressing human H402 CFH is advanced aging dependent.....	131
Figure 32: Deposit formation in <i>CFH:Cfh<sup>-/-</sup></i> mice is dependent on advanced age.....	132
Figure 33: Apolipoprotein content of FPLC-fractionated <i>CFH-HH:Cfh<sup>-/-</sup></i> plasma after HFC diet .....	133

## Acknowledgements

I would like to acknowledge my advisor Dr. Catherine Bowes Rickman for her mentorship, training and advice throughout my graduate school years. She has guided me to successfully complete my projects and deliver presentations. Without her support, I would not have developed the skill set needed for me to be successful in my future research endeavors. Also, members of the Bowes Rickman were critical for my successes in graduate school. Notably, conversations with and training by Una Kelly has honed my critical thinking skills as well as given me a valuable of molecular biology skillset. I would also like to acknowledge my thesis committee, Dr.'s Scott Cousins, Michael Hauser, Daniel Saban and Yuan Zhuang, for their intellectual support and guidance during the development and progression of my thesis project. Lastly, I would like to thank the support and countless wine nights I have had with family, friends and colleagues during my pursuit for my degree.

# 1. Introduction

Maintaining a healthy eye is critical for our ability to perform daily activities such as reading and driving. Losses of visual function are often devastating and lead to a lesser quality of life. In this introduction I will discuss age-related macular degeneration (AMD), a blinding disease in elderly populations with very limited therapeutic options. The lack of therapies, in part, is due to a lack of animal models that faithfully recapitulate pathobiological processes contributing to AMD development and progression. As we gained a better understanding of the processes driving AMD pathobiology using human specimens and genetic association studies, new AMD mouse models have been generated and are being utilized to identify and test novel AMD therapies.

## ***1.1 Overview on Retinal Anatomy and Physiology***

The mammalian eye evolved to allow light to penetrate through the cornea and be focused by the lens onto the center of the neural retina in the back of the eye (Fig. 1A). The neural retina is a specialized layered nervous tissue containing 5 distinct classes of neurons: photoreceptors, bipolar cells, ganglion cells, horizontal cells and amacrine cells (2). These cells are organized and wired such that following light detection and the initiation of phototransduction in photoreceptors there is a graded change in membrane potential and subsequent change in the rate of neurotransmitter release onto bipolar and

ganglion cells (Fig. 1B). This signal originating from the photoreceptors travels through ganglion cells' axons in the optic nerve to reach the visual cortex in the occipital lobe of the brain for further image processing (Fig. 1A).

In humans and non-human primates, there is a specialized 5.5 mm diameter sized region in the center of the retina known as the macula (Fig. 1A). The macula contains the highest density of photoreceptors and is responsible for our sharpness of vision or visual acuity. In the center of the macula, there is anatomical distinct area known as the fovea that allows for light to readily penetrate photoreceptors (Fig. 1A). There are two types of photoreceptors in the retina, rods and cones, that contain the molecular machinery responsible for phototransduction (3). Furthermore, in humans, there are three different cone types containing different opsins allowing for the detection of different light wavelengths resulting in the brain's perception of colors (4). Phototransduction occurs when a photon of light isomerizes the vitamin A derived 11-cis-retinal attached to either rod rhodopsin or cone opsin in the photoreceptor outer segment to 11-trans-retinal (5). Activation of 11-trans-retinal leads to the activation of a G coupled signaling pathway in the photoreceptor causing hyperpolarization and blocking photoreceptor glutamate release to the bipolar cell (3).

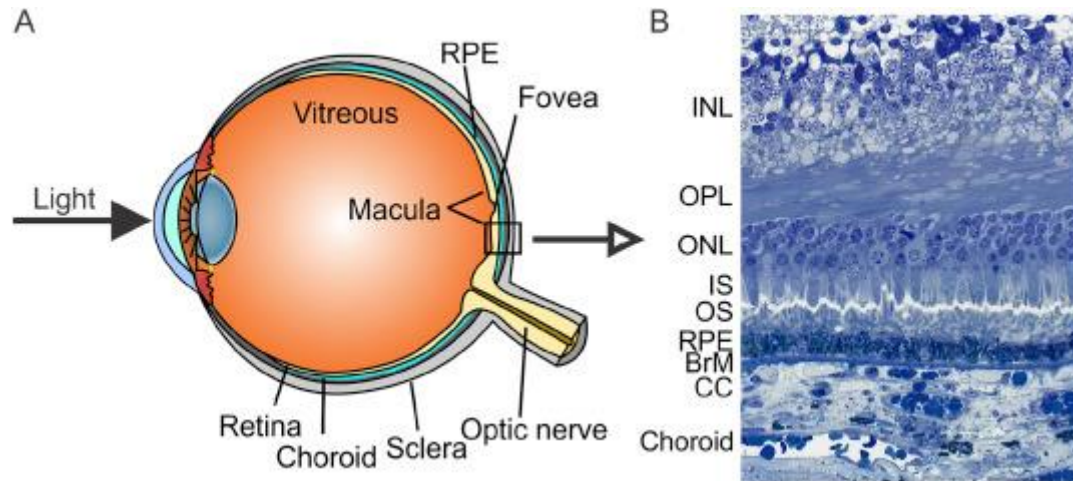


**Figure 1: Anatomical features of the human eye. A) Cartoon representation illustrating the path of light through the human eye. B) Histological cross section showing the complex layered design of the human retina. Light would enter from the top of the image passing through the ganglion cell layer and inner plexiform layers (not shown), inner nuclear layer (INL), outer plexiform layer (OPL), photoreceptor (PR) outer nuclear layer (ONL), and PR inner segments (IS) before reaching the PR outer segments where phototransduction occurs. RPE, retinal pigment epithelium; BrM, Bruch's membrane; CC, choriocapillaris. [Image adapted from (1)].**

A monolayer of cells underlying the neural retina known as the retinal pigmented epithelium (RPE) functions to preserve photoreceptor health (Fig. 1A, B). These functions include recycling of retinoids needed for phototransduction known as the visual cycle; phagocytosing photoreceptor outer segments; sustaining the blood-retina barrier via its tight junction complexes; capturing stray light with its pigment granules; coordinating cytokines; delivering nutrients and oxygen to photoreceptors; and secreting the inter-photoreceptor matrix (6). Beyond the RPE is capillary bed known as the choriocapillaris and a network of blood vessels known as the choroid that delivers

oxygen, nutrients, lipids and proteins to the RPE and photoreceptors through fenestrations located in the choriocapillaris (Fig. 1A, B). The RPE is critical for choriocapillaris health with its secretion of vascular endothelial growth factor (VEGF) (7). Loss of VEGF secretion by the RPE leads to choriocapillaris loss, choroidal thinning and photoreceptor degeneration in mice (8). In addition, the RPE blocks growth of retinal vessels into the photoreceptor layer via secretion of pigment epithelium-derived factor (PEDF) (6).

Separating the RPE and the choriocapillaris is a pentalaminar extracellular matrix (ECM) known as Bruch's membrane (BrM) (Fig. 1B). BrM serves as a basement membrane to the RPE cells as well as the choriocapillaris (9). It also acts as a critical barrier to circulating proteins reaching the RPE (10). Both the RPE and choroid deposit ECM proteins into BrM to sustain its integrity (9). With age there is an increase of lipids deposited within BrM that causes it to thicken (11). It is widely believed these age-related changes in BrM set the stage for the development of age-related macular degeneration (AMD) (11, 12).

## ***1.2 Age-related Macular Degeneration***

AMD is a leading cause of blindness in populations over the age of 55 in the United States and other countries (13-15). It is a late-onset, progressive deterioration of the macula leading to irreversible central visual loss although there are some peripheral

retinal changes (16). These characteristics separate AMD from other prominent blinding conditions such as glaucoma (peripheral visual loss), diabetic retinopathy (earlier onset) and cataracts (reversible vision loss).

The etiological risk factors for AMD include advanced aging, genetic variants and environmental stressors. Advanced aging is the strongest associated risk factor for AMD (17, 18). An individual's risk for developing AMD at age 55 is 0.7% but exponentially increases to 22.5% when they reach the age of 80 (19). Genetic variants also contribute to development of AMD and account for 28-43% of the disease risk depending on the estimated prevalence of AMD in the population (20). There are currently 34 AMD-associated loci within genes encoding proteins involved in inflammation, ECM remodeling, lipid metabolism and transport and angiogenesis (Fig. 2) (21). Environmental stressors modulate the effects of aging and genetic variants on AMD development. Exposure to cigarette smoking strongly influences the risk for AMD while diet, obesity, hypertension, sunlight exposure and alcohol consumption are mildly associated with disease risk (22-27). However, it remains unclear how advanced aging, genetic variants and environmental stressors predispose the eye to the development of AMD.

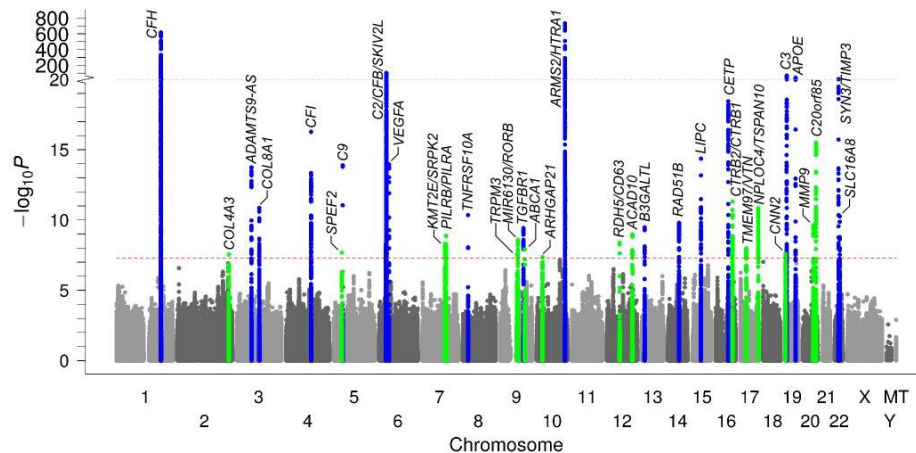


**Figure 2: Genetic variants associated with AMD.** Manhattan plot depicts dots representing single nucleotide polymorphisms (SNPs) that are associated with increased or decreased risk for AMD. Currently, there are 34 genetic loci associated with AMD. Of note, the strongest AMD-associated SNPs occur within *Complement Factor H (CFH)* on chromosome 1q32 and *Age-Related Maculopathy Susceptibility 2 (ARMS2)* and *Htra Serine Peptidase 1 (HTRA1)* on chromosome 10q26. [Adapted from (21)].

The early to intermediate stages of AMD are usually fairly benign but can progress to its vision-impairing late stages. Early pathologies consist of impaired dark adaptation reflecting rod photoreceptor dysfunction, RPE pigmentary changes and the presence of intermediate-sized (63 to 124  $\mu\text{m}$ ) focal lipid- and protein-containing deposits known as drusen (Fig. 3) (28). While the presence of a few small ‘hard’ drusen or basal laminar deposits is a normal, non-vision-impairing part of aging, the deposition of large diffuse drusen, or basal linear deposits, in the macula is vision impairing and indicative of early AMD (11). The size, type and location of drusen have been directly linked to AMD progression (29, 30). As AMD progresses to its late stages, it is known as

either exudative or nonexudative AMD. The presence of choroidal neovascularization characterizes the exudative, or 'wet,' form of late AMD where the formation of immature blood vessels from the choroid advances into the RPE and sub-retinal space causing fibrosis and scarring and irreparable vision loss (16). Non-exudative, or 'dry,' AMD is described as geographic atrophy (GA) where there is macular loss of RPE and photoreceptors (31). Most of the AMD-afflicted population has early/intermediate or late 'dry' AMD while 10% of patients present with 'wet' AMD (31). The prevalence of AMD is estimated to double by 2020 and increase the burden of AMD on our society and economy (32).

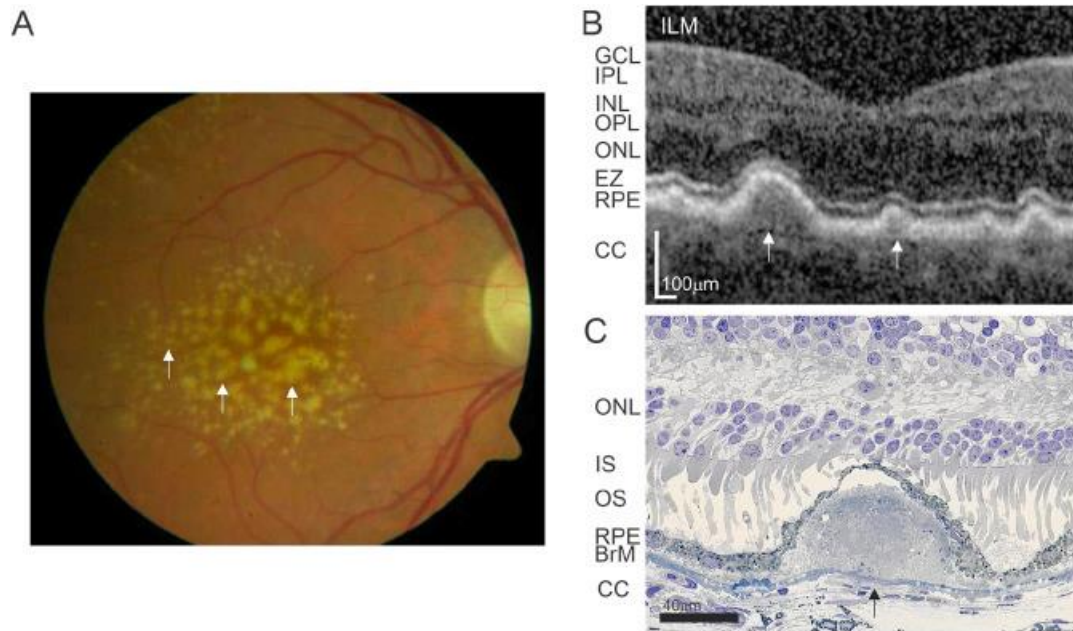


**Figure 3: Drusen are a hallmark of AMD pathology. A) Druse appears as yellowish punctate spots on fundus photographs of human eyes. B) Spectral domain optical coherence tomography (SD-OCT) imaging shows druse occurs between the retinal**

**pigmented epithelium (RPE) and choroicapillaris (CC). C) Closer histological examinations of AMD donor eyes reveals pathogenic druse develop between the RPE and elastic layer of Bruch's membrane (BrM). Arrows depict druse. GCL, ganglion cell layer; IPL, inner plexiform layer; INL, inner nuclear layer; OPL, outer plexiform layer; ONL, outer nuclear layer; EZ, ellipsoid zone. [Adapted from (1)].**

Recent advancements in intravitreal anti-vascular endothelial growth factor (VEGF) have enabled successful treatment of the 'wet' form of AMD. However, the second form of late AMD, GA, remains difficult to treat and a significant cause of vision loss. While there are several therapies used to treat wet AMD including anti-VEGF-A antibodies bevacizumab (Avastin, Genentech/Novartis) and ranibizumab (Lucentis, Genentech/Novartis) or the fusion protein receptor trap targeting VEGF-A, aflibercept (Eylea, Regeneron/Bayer) (33, 34), not all 'wet' AMD patients respond positively (35). Other therapies are available for the treatment of AMD such as Age-Related Eye Disease Supplement (AREDS), an oral supplement containing vitamin C, vitamin E, lutein/zeaxanthin and zinc that enhances protection against oxidative stresses in the eye (36). Still, AREDS will only slow the five year progression of early/intermediate AMD to late-stages of the disease by 25% (37). Given the substantial burden of disease of AMD, elucidating the risk factors and pathogenesis of the disease remains a significant research priority. We have focused on developing animal models based on multiple AMD risk factors that faithfully recapitulate aspects of AMD to gain a better

understanding of the pathobiological processes underlying its development and progression and to identify novel targets for AMD therapies for AMD.

### ***1.3 The Use of Mice in AMD Research***

Understanding the role of disease-associated mechanisms contributing to AMD development and progression will advance the treatments for AMD. Historically, much of our understanding of AMD pathobiology originates from studies on human AMD donor eyes and genetic association studies. A number of cellular and animal models have been characterized to study these disease-associated mechanisms but no model exists that faithfully recapitulates all of the aspects of the complex nature of AMD. Scientists often debate the usefulness of the cellular and animal models in AMD research but studies involving these models allow for the direct interrogation of AMD-associated pathological mechanisms in controlled environments, an attribute lacking in AMD studies involving humans. The question remains how to best leverage these models to effectively test the role of disease-associated mechanisms in AMD that will lead to the development of novel therapies. Cellular models are excellent for their ability to be directly manipulated by various treatments while animal models retain the complex anatomical architecture of the posterior eye that allows investigators to study the interactions between these tissues. Here, the advantages and disadvantages as well as the successes of using mice in AMD research will be further discussed.

### **1.3.1 Mice as a Model Organism for AMD Studies**

AMD can be modeled using a variety of organisms including zebrafish, mice, rats, and non-human primates. Of all the models, only non-human primates possess a macula, but these animals are generally prohibitively expensive to maintain and very difficult to manipulate and follow longitudinally due to their long life-span and because they outlive the duration of most grant awards (38). Non-mammalian models like zebrafish are advantageous in that they produce large quantities of offspring and allow for easy assessment of eye phenotypes due to their transparency as juveniles, but they differ from mammals in their retinal vasculature organization and develop photoreceptor degenerations beginning in the larval stage and not in the adult fish (39, 40). Mice are the most practical organisms for modeling AMD due to their short life span, genetic manipulability, relatively low maintenance cost and retinal architecture that is similar to humans. Importantly, the mouse does not possess a macula or even an area centralis like pigs or dogs, but rather a rod-rich retina that is similar to the rod-rich parafovea in humans (41). The lack of a macular region in the murine retina has called into the question the usefulness of mice in AMD research; however, studies involving AMD mouse models have greatly aided our understanding of AMD development and progression.

The most commonly used mouse models in AMD research largely fall into two groups that represent either early and intermediate dry AMD or ‘wet’ or neovascular AMD, although there are a few models that aim to model late dry AMD or geographic atrophy (Table 1). One important consideration for an AMD mouse model is the incorporation of advanced aging as aging is the strongest risk factor for human AMD. Many early and intermediate dry AMD mouse models incorporate advanced aging effectively incorporating the effect of chronic processes that drive the development of early/intermediate AMD pathology. In contrast, models of neovascular and geographic atrophy are often based on acute insults to young mice that consequently develop retinal pathology in a short time frame (*e.g.* one to two weeks) (42-44). One exception is the wet AMD model using aged HTRA1 overexpressing mice where pathologies were observed at one year of age (45-47). Therefore, these models may not faithfully reflect the complex pathological cues and/or mechanisms that cause late stages of AMD.

A subset of AMD mouse models have been developed based on mutations in genes that cause inherited macular degenerations in humans including C1QTNF5 in late-onset retinal macular degeneration (48, 49), EFEMP1 in Malattia Leventinese/Doyme’s honeycomb retinal dystrophy (50, 51), TIMP3 in Sorsby’s fundus dystrophy (52), and ABCA4 in recessive Stargardt’s disease (STGD1) or ELOVL4 in dominant Stargardt’s (STGD3) (53-56) (Table 1). Inherited retinal degenerations differ

**Table 1: Summary of Current AMD Mouse Models**

	Mouse Model	Abbreviation	Comments
<u>Mouse Models of Inherited Macular Degeneration:</u>	<i>ATP-binding cassette, sub-family A (ABC1), member 4 (Abca)</i> Knockout Mouse	<i>Abca4<sup>-/-</sup></i>	Mouse model of recessive Stargardt's disease that have been used in studies of complement activation (57), lipofuscin and novel drug development for AMD (58).
	<i>C1q and tumor necrosis factor related protein 5 (C1QTNF5)</i> Serine to Arginine at Amino Acid 163 (S163R) Knockin Mouse	<i>C1QTNF5<sup>S163R</sup></i>	Mouse model of late-onset retinal degeneration generated by a introduction of the S163R mutation into the mouse <i>C1QTNF5</i> gene (48) as well as viral delivery of human <i>C1QTNF5<sup>S163R</sup></i> to the RPE of C57BL/6J mice (49).
	<i>EGF-containing fibulin-like extracellular matrix protein 1 (Efemp1)</i> Arginine to Tryptophan at Amino Acid 345 (R345W) Knockin Mouse	<i>Efemp1<sup>R345W</sup></i>	Mouse model of Malattia Leventinese/ Doyne's Honeycomb Dystrophy revealed a vital role of complement in sub-RPE deposit formation (59) which was replicated using cell culture (60).
	<i>Elongation of very long chain fatty acids protein 4 (Elovl4)</i> Five Base Pair Deletion Knockin Mouse	<i>Elovl4<sup>mut/-</sup></i>	Mouse model of dominant Stargardt's disease characterized by defects in very long chained-polyunsaturated fatty acids in the retina (61).
	<i>Metalloproteinase inhibitor 3</i>	<i>Timp3<sup>S156C</sup></i>	A mouse model of Sorsby's dystrophy

	( <i>Timp3</i> ) Serine to Cysteine at Amino Acid 156 (S156C) Knockin Mouse		used in angiogenesis studies (62).
<u>Mouse Models of 'Wet' AMD</u>	<i>Htra1</i> overexpressing Mouse Exposed to Cigarette Smoke (CS)	<i>HTRA1</i> ~CS	12 month old HTRA1 overexpressing mice were exposed to cigarette smoke for 30 minutes per day, 5 days per week for 12 weeks and resulted in increased CNV and sub-RPE basal deposits (46).
	Laser-induced Choroidal Neovascularization (CNV)		Commonly used acute model that has been interrogated in multiple transgenic mice (i.e. <i>Cflr</i> <sup>-/-</sup> (63), <i>Ahr</i> <sup>-/-</sup> (64) and <i>Cx3cr1</i> <sup>-/-</sup> (65) and used for testing novel therapies for 'wet' AMD (44).
<u>Acute Models of AMD:</u>	Blue Light Exposure		Acute light induced insult that results in damage to the neural retina that has been used to differentiate microglia and bone marrow-derived macrophages in the retina(66).
	Intravitreal Injection of Paraquat		Acute insult that results in increased oxidative stress damage and subsequent damage to the neural retina that is used for anti-oxidant therapy studies (67).
	Oral Hydroquinone		16 month old C57Bl/6J female mice were given oral hydroquinone in their drinking water that resulted in the development of sub-RPE basal deposits

			(68).
<u>Mouse Models of Geographic Atrophy:</u>	Intravenous Injection of Sodium Iodate		Acute insult causing RPE damage resulting in RPE atrophy and death, retinal degeneration and immune cell recruitment by three days post injection (42, 43, 69).
	RPE-specific <i>Dicer</i> Knockdown Mouse	<i>Dicer</i> <sup>-/-</sup>	Acute mouse model where <i>Dicer</i> has been knocked down by Cre-LoxP recombination and results in increased <i>Alu</i> mRNA and frank RPE cell death mediated by inflammasome activation (70).
	Inducible Cre recombinase Driven by the <i>Monocarboxylate Transporter 3</i> Promoter and <i>Diphtheria Toxin A (DTA)</i> with LoxP-flanked Stop Codon Double Transgenic Mouse	RPE(CreER)/DTA	RPE(CreER)/DTA mice have 60-80% RPE cell death that results in ERG and retinal pathology and serves as a valuable model for stem cell-derived RPE transplantation studies (71).
<u>Mouse Models of 'Early' and 'Intermediate' AMD</u>	Human <i>Apolipoprotein B100 (APOB100)</i> Mouse Fed a High Fat (HF) Diet	<i>APOB100</i> ~HF	C57Bl/6J mice that contain the full length human <i>APOB</i> gene were fed a HF diet and aged to 12 months but no apparent phenotypic differences were observed between <i>APOB100</i> mice fed a normal mouse chow and HF diet (72).
	Human <i>Apolipoprotein E</i> isoform 4 ( <i>APOE4</i> ) Mouse Fed	<i>APOE4</i> ~HFC	Aged <i>APOE4</i> ~HFC develop more severe AMD-like pathology than aged <i>APOE2</i>

	a High Fat, Cholesterol-enriched (HFC) Diet		and <i>APOE3</i> mice fed a HFC diet (73).
	<i>Aryl hydrocarbon receptor (Ahr)</i> Knockout Mouse	<i>Ahr</i> <sup>-/-</sup>	Chronic mouse model based on <i>Ahr</i> activity and protein concentration decreases with age in human RPE cells (74).
	C57BL/6J Mouse Exposed to Cigarette Smoke (CS)	C57BL/6J~CS	Two month old C57BL/6J mice were exposed to cigarette smoke for five hours a day and 5 days a week for 6 months that resulted in ultrastructural changes to Bruch's membrane and RPE apoptosis (68).
	C57BL/6J Mouse Fed a High Glycemic (HG) Diet	C57BL/6J~HG	16 month old C57BL/6J mice were fed a HG diet until 23.5 months of age and developed more AMD-like pathologies that correlated with changes in the microbiome (75).
	C57BL/6J Mouse Immunized with Carboxyethylpyrrole (CEP)-adducted BSA	CEP Immunized C57BL/6J	Chronic mouse model with increased inflammasome activation (76) and increased pro-inflammatory macrophage infiltration (77).
	<i>Complement factor h (Cfh)</i> Knockout Mouse	<i>Cfh</i> <sup>-/-</sup>	Absence of CFH leads to excess complement activation resulting in no reservoir of plasma complement proteins and subtle retinal damage in aged <i>Cfh</i> <sup>-/-</sup> mice (63, 78, 79).

	Heterozygous <i>Cfh</i> Mouse Fed a HFC Diet	<i>Cfh</i> <sup>+/-</sup> ~HFC	Aged <i>Cfh</i> <sup>+/-</sup> ~HFC provides the first multifactorial AMD mouse model suited to test the role of complement components on AMD-like pathology development (80, 81).
	Human <i>Complement Factor H</i> Mouse	<i>CFH:Cfh</i> <sup>-/-</sup>	Mice containing the full-length human <i>CFH</i> gene encoding either the Tyrosine (Y) or Histidine (H) at amino acid 402 were crossed to <i>Cfh</i> <sup>-/-</sup> mice to generate mice that produce only human CFH Y402 or H402 protein, respectively, that functions with mouse complement proteins (79).
	Chimeric, transgenic <i>Cfh</i> Mouse	Chimeric <i>Cfh</i>	Mouse <i>Cfh</i> was genetically modified to include short consensus repeat domains 6 through 8 of human <i>CFH</i> and included either the Y402 or H402 amino acid but no difference in phenotype was observed between mice expressing these variants (82).
	<i>Ceruloplasmin (cp)</i> and <i>hephaestin(Heph)</i> Double Knockout Mouse	<i>Cp</i> <sup>-/-</sup> <i>Heph</i> <sup>-/-</sup>	Chronic mouse model in which pathologies result from increased oxidative stress from retinal iron overload as supported by the protection against pathologies with the iron chelator deferiprone (83).

	<i>C-X3-C motif chemokine receptor 1 (Cx3cr1)</i> Knockout Mouse	<i>Cx3cr1</i> <sup>-/-</sup>	Chronic mouse model used to interrogate the role of APOE (84) and CFH (85) in AMD.
	<i>Nuclear factor-like 2 (Nrf2)</i> Knockout Mouse	<i>Nrf2</i> <sup>-/-</sup>	Chronic mouse model that has been used in oxidative stress studies (86).
	<i>Nrf2</i> Knockout Mouse Fed a HF Diet	<i>Nrf2</i> <sup>-/-</sup> ~HF	12 month old <i>Nrf2</i> <sup>-/-</sup> mice were fed a HF diet for 16 weeks developed a more robust AMD-like phenotype that correlated with interleukin 17-producing $\gamma\Delta$ T-cells (87).
	<i>Superoxide dismutase 1 (Sod1)</i> Knockout Mouse	<i>Sod1</i> <sup>-/-</sup>	Chronic mouse model with a susceptibility to oxidative stress damage as shown by increased retinal damage after a intravitreal injection of paraquat (88).
	RPE-specific <i>Superoxide dismutase 2 (Sod2)</i> Knockdown Mouse	<i>Sod2</i> <sup>-/-</sup>	Chronic mouse model where Sod2 has been knockdown using a viral-delivered ribozyme and Cre-LoxP recombination that has been used to test the efficacy of RPE65-programmed bone marrow-derived cells <i>in vivo</i> (89).

from AMD since they are caused by a single genetic mutation and present earlier in life (90-94). Regardless of the different etiologies between these diseases, the mouse models of these macular degenerations recapitulate many of the cardinal features of their respective inherited macular degeneration and some features of AMD (48, 50-55, 95, 96). Utilizing these mouse models may yield insight into the development of AMD pathologies. In fact, studies using the *EFEMP1*<sup>PR345W</sup> knock-in mouse model of Malattia Leventinese/Doyme's honeycomb retinal dystrophy revealed a role of the complement system in the development of sub-RPE basal deposits seen in many AMD mouse models (59).

A popular strategy for generating AMD mouse models has been to subject them to acute insults aimed at reproducing AMD-relevant environmental stressors and assessing retinal damage after a few days and/or weeks. Because oxidative stress has been implicated in AMD many of these acute insults increase the oxidative stress burden in eye. These include systemic sodium iodate treatment (42, 43), intravitreal paraquat (67), oral hydroquinone (97) and blue light exposure (98-100). The most commonly used acute AMD mouse model is laser-induced choroidal neovascularization (CNV), which is meant to model wet or neovascular AMD (44). Importantly, it has been a reliable animal surrogate in the development of therapeutics to <sup>treat</sup> wet AMD including predicting the

clinical efficacy of anti-vascular endothelial growth factor (VEGF) therapy for wet AMD (101). In laser-induced CNV laser photocoagulation is used to disrupt Bruch's membrane, stimulating growth of new choroidal blood vessels toward the retina (44). The laser-induced CNV mouse model produces quick results within a few weeks, but it is a wounding model unlike neovascular AMD (102). Unlike in humans, the CNV in rodents spontaneously regresses after a few weeks to months and there is considerable variation in outcome between mouse strains, genotypes, age and their origin (103). Still, the laser-induced CNV mouse model is widely used in studies evaluating exudative AMD therapeutics.

Overall many AMD pathological hallmarks have been recapitulated in different mouse models but few models faithfully display a combination of these AMD changes. Examples of the following AMD-associated functional deficits and morphological changes that have been modeled in AMD mice include: vision loss (71, 74, 78-80, 86, 104-107); photoreceptor degeneration (45, 65, 74, 78-80, 104-106, 108-110); RPE atrophy (45, 46, 73, 74, 80, 86, 105, 106, 108, 109, 111), RPE hypopigmentation (73, 74, 86, 109), RPE hyperpigmentation (73, 74, 86) and RPE multinucleation (74, 80, 107); choriocapillaris atrophy (63, 74, 86); accumulation of lipofuscin within the RPE (74, 78, 86, 104, 105, 112); subretinal infiltration of immune cells (65, 80, 82, 86, 108, 112) and choroidal

neovascularization (CNV) (45, 46, 65, 73, 86, 106, 109, 112). Although mice do not develop drusen they do accumulate sub-RPE basal deposits resembling basal laminar deposits (45, 46, 72-74, 79, 80, 82, 86, 104, 105, 108, 110, 113) that share many of the same constituents found in drusen. These include complement components (65, 78-80, 82, 86, 87, 105, 107, 108, 112), apolipoproteins (107), amyloid beta (107), extracellular membranous debris (79, 86, 110), and long-spaced collagen (72, 74, 79, 109). However, in general most AMD mouse models recapitulate a limited number of the spectrum of pathologies associated with AMD. Mouse models of AMD that are based on multiple risk factors associated with AMD and display more complex phenotypes that resemble more aspects of AMD will be discussed in detail below.

### **1.3.2 Advances in the Understanding of AMD-associated Pathobiological Mechanisms from Mouse Studies**

The studies providing initial insights behind the pathobiological nature of AMD only establish correlations and not causations. As previously noted multiple AMD mouse models have been characterized and helped to establish a causative relationship between pathobiological mechanisms and AMD-like pathology development in rodents. These AMD mouse models established important roles of inflammation, lipid transport and metabolism, ECM remodeling, complement dysregulation, oxidative and

cellular stress, autophagy, and angiogenesis (16, 31). Here, we describe some successful studies interrogating multiple AMD-associated mechanisms through the use of mice.

### 1.3.2.1 Lipid Metabolism and Transport and Inflammation

Dysregulated lipid and cholesterol metabolism has been linked with AMD pathology by genetic studies linking variants in proteins involved in these pathways (21) and the identification of a number of lipid and cholesterol species as well as a number of apolipoproteins such as apolipoprotein E (ApoE, human protein; *APOE* human gene) in drusen (114-117). ApoE exists as three isoforms that differ at two amino acid positions: ApoE2 (Cys112, Cys158), ApoE3 (Cys112, Arg158), and ApoE4 (Arg112, Arg158) (118). Aged, transgenic *APOE* mice with targeted replacement of mouse *ApoE* with human *APOE2*, *APOE3*, or *APOE4* were fed a high fat cholesterol-enriched diet (HFC) for eight weeks and assessed for an AMD-like phenotype (73). Only aged mice that expressed human *APOE4* and fed a HFC diet (*APOE4*~HFC) developed an AMD-like ocular phenotype including decreased visual function, CNV, RPE damage and basal laminar deposit accumulation (73). Interestingly, the AMD-like phenotype in *APOE4*~HFC mice could be blocked by systemic anti-amyloid immunotherapy (119). The AMD phenotype of *APOE4*~HFC mice contrasts genetic association studies in which the *APOE4* gene decreases while the *APOE2* gene increases the risk for AMD development (120).

In a recent study of the *APOE* targeted replacement mice found that *APOE2*, not *APOE4*, accelerated accumulation of sub-retinal mononuclear phagocytes in the sub-retinal space in *APOE* mice aged to twelve months, exposed to bright light or treated with laser-induced CNV (84). However, two key pathological hallmarks of AMD, sub-RPE deposit formation and RPE atrophy, were not observed in these animals and visual function was not measured (84). A possible explanation for these differences is ApoE4 binds better to glycosaminoglycans (GAGs) than ApoE2 and ApoE3 (121). GAGs are abundantly found in Bruch's membrane (9) and may allow greater accumulation of ApoE4-containing lipoproteins. Hence, *APOE4*-HFC mice would develop a RPE-BrM interface primed for inflammation as evidenced by increased deposition of C3 fragments within the sub-RPE deposits (107). In fact, treating *APOE4*-HFC mice with an antibody targeting amyloid beta, a known activator of complement (122) prevented visual loss and RPE damage although there was no change in sub-RPE deposits (107). Results from *APOE4* mice fed an HFC diet suggest targeting proinflammatory constituents of deposits may be a viable therapy for AMD.

### **1.3.2.2 Oxidative Stress and Inflammation**

The contribution of the innate immune system to the chronic inflammation seen in AMD has been tested in AMD mouse models (123, 124). For example, a role for

inflammasome activation was tested in the RPE-specific *Dicer1* knockdown mouse model of geographic atrophy (111). DICER1 is a member of the RNase III endoribonuclease family that aids in the formation of mature microRNAs (125). *Dicer1* knockdown increases *Alu* mRNA and increased *Alu* mRNA has been documented in eyes with geographic atrophy (111). Increased *Alu* mRNA leads to RPE degeneration through the activation of the NLRP3 inflammasome *in vivo* (111). Recent work with the ceruloplasmin and hephaestin double knockout (*Cp<sup>-/-</sup>Heph<sup>-/-</sup>*) mouse model further exemplifies a pathogenic role of inflammasome activation in AMD. *Cp* and *Heph* are critical iron exporters needed to maintain iron homeostasis in the eye. 12-month-old *Cp<sup>-/-</sup>Heph<sup>-/-</sup>* mice develop retinal iron overload and a consequent AMD-like phenotype (109). Further characterization of these mice found iron overload leads to increased *B1* and *B2* mRNA, analogues of *Alu* mRNA, and activation of the NLRP3 inflammasome (126).

Similarly, inflammasome activation was identified in the eyes of the carboxyethylpyrrole (CEP)-immunized mouse model of AMD. CEP is one of the most abundant oxidatively modified species in drusen and forms from the oxidation of docosahexaenoic acid, an abundant polyunsaturated fatty acid found in the retina (117, 127). Two-month-old C57BL/6J mice were immunized with CEP-adducted mouse serum

albumin (CEP-MSA) and aged to 12-14 months (128). These mice developed sub-RPE deposits, thicker Bruch's membrane, large RPE vacuoles, increased complement activation, and subretinal F4/80+ macrophage infiltration (128). Similar to the *Dicer1* knockdown and *Cp-/-Heph-/-* mice, CEP-immunized mice had increased levels of NLRP3 inflammasome activation in their retinal macrophages (76). Interestingly, CEP immunization of *C-C chemokine receptor type 2* knockout (*Ccr2-/-*) mice, which have impaired recruitment of macrophages to the eye (129), were protected from the development of the age-dependent retinal damage seen in the CEP-immunized C57BL/6J mice (77). These lines of data suggest targeting inflammasome activation may protect against the development of early/intermediate pathologies. However, there have been conflicting studies using the laser-induced CNV mouse and non-human primate models on the therapeutic potential of targeting inflammasome activation in 'wet' AMD (76, 130-132). The laser-induced CNV model of 'wet' AMD results from an acute insult and may not reflect the chronic processes at play in the CEP-immunized, *Dicer-/-* and *Cp/Heph-/-* mouse models.

### 1.3.2.3 Oxidative Stress and Angiogenesis

In addition to genetic association of *CFH* with AMD risk (which will be discussed later), GWAS studies have strongly implicated genes located on chromosome

10q26 with AMD risk (133, 134). This chromosomal region contains three tightly linked genes: *PLEKHA1*, *ARMS2* and *HTRA1*. To date only the role of *HTRA1* in AMD has been interrogated in mice (135), likely due to the fact that there is no *ARMS2* homologue in mice, an issue that highlights a limitation of mouse usage in AMD research. *HTRA1* is a serine protease that can degrade ECM proteins (135). The *HTRA1* variant associated with AMD susceptibility is located in the promoter region and increases *HTRA1* expression (136-138). Young mice with overexpression of *HTRA1* develop polypoidal choroidal vasculopathy (PCV) (45), a manifestation that occurs in exudative AMD patients (139, 140). In another study, *HTRA1* overexpressing mice developed CNV after one year of age (46). Since exposure to cigarette smoke has been widely associated with AMD (141), 12-month-old *HTRA1* overexpressing mice were exposed to 30 minutes of cigarette smoke for 5 days a week for 8 weeks (46), but this smoke exposure did not significantly change the CNV rates in these mice (46). This may be because the smoke exposure paradigm was not severe enough; in related studies, 5 hours of cigarette smoke for 5 days a week for 6 months (113, 142) were required to induce cigarette smoking related ocular damage. Another approach combined exposure to cigarette smoke with an additional environmental stressor based on diet (97). Specifically, 16-month-old C57BL/6 female mice were fed a Purina high fat (HF) diet for 4.5 months and after a

month, subjected to 2 hours a day of smoke for 5 days a week for 3.5 months in addition to the HF diet (97). These studies exemplify the importance of standardized protocols for researchers working with AMD mouse models to follow in order to reach similar results and conclusions.

### **1.3.3 Future of Mice in AMD Studies**

Studies using mice to mimic the pathology seen in AMD have generated a multitude of models for researchers that have led to varying, incremental advances in our understanding of AMD. The models that incorporate multiple risk factors (*e.g.* advanced aging, genetic risk, and environmental stressors) have and are likely to continue to contribute to elucidating the mechanistic underpinnings of AMD development in humans. These afford us a model for understanding how these three factors interact with one another to contribute to the development of AMD. Future studies utilizing cell culture models and AMD donor eyes will unquestionably yield new insights and contribute to the evolution of current AMD mouse models. Furthermore, the development of new strategies to manipulate gene expression in the RPE such as CRISPR/Cas9 genome editing and tetracycline-inducible RPE-specific Cre will enable researchers to generate RPE-specific knockout mouse models (143). Future studies will contribute to the wealth of knowledge gained from the numerous previous

studies on AMD mouse models and to development of successful AMD therapies.

## **1.4 Complement Dysregulation in AMD Pathobiology**

Pathohistological, immunohistochemical and proteomic examinations of human donor eyes revealed colocalization of complement proteins within druse and suggests a critical role of complement in AMD pathogenesis (117, 123, 144, 145). These studies were further supported by genetic studies associating variants in proteins involved in the complement cascade with risk for AMD development and progression (146-154). The most strongly associated genetic risk factors for AMD are variants found within the *Complement Factor H (CFH)* gene that encodes CFH, the soluble regulator of complement activation. This observation lead to the hypothesis that overactivation of the complement cascade contributes to the development of AMD (155). However, to date, no clinical trial evaluating inhibitors of the complement cascade for AMD have been successful (156). Here, the functions of the complement cascade and CFH will be discussed to illustrate their possible roles in AMD pathobiology.

### **1.4.1 Overview of Complement Biology**

Complement is a cascade of more than 40 proteins found in primitive organisms such as jellyfish up to higher order mammals like humans (Fig. 4) (157). It is a component of the innate immune system that aids in the opsonization, elimination and

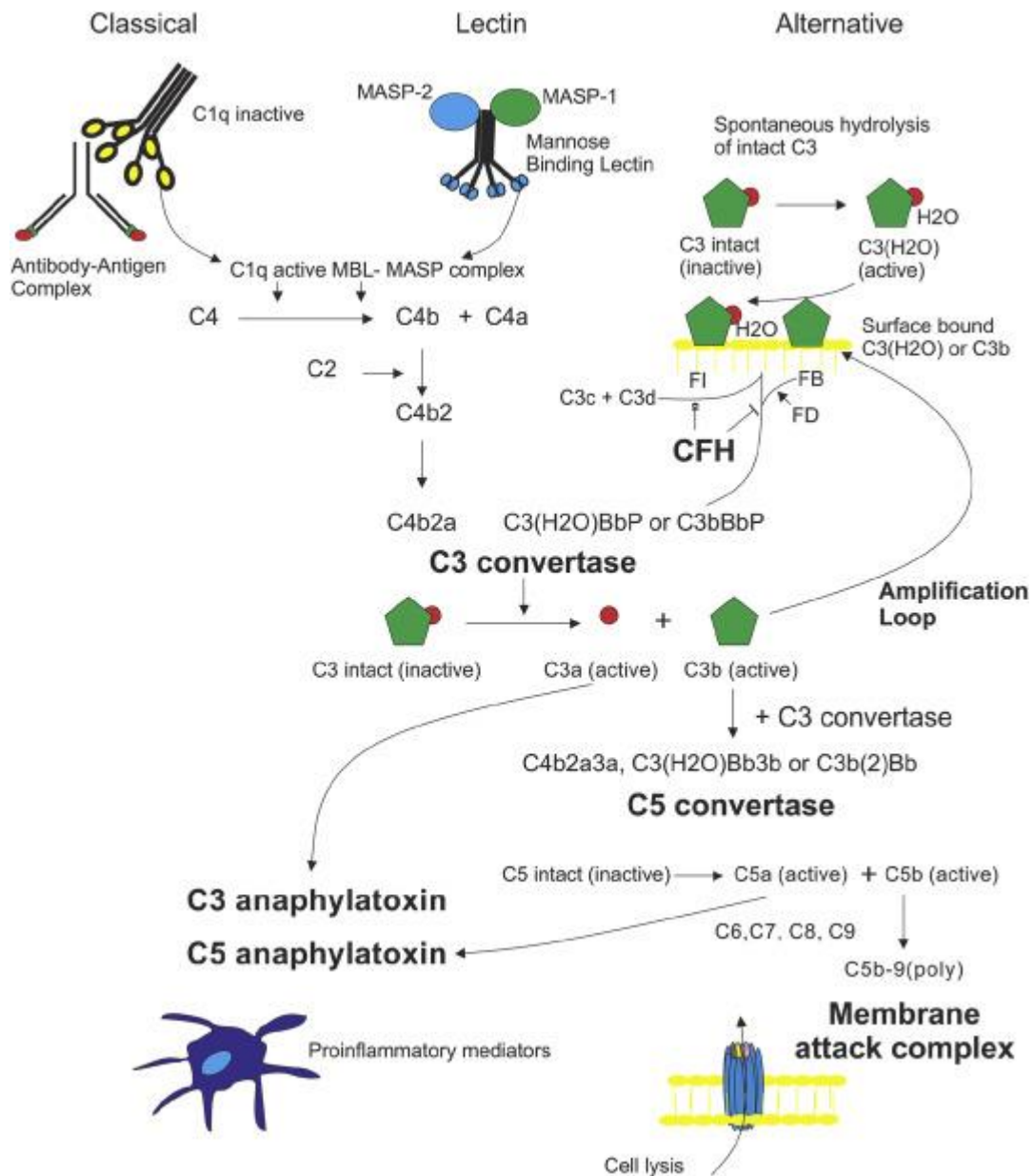


**Figure 4: Diagram of Complement Cascade.** Complement consists of three pathways enabling it to survey the bloodstream for a large repertoire of pathogens and debris. Once complement is activated, it forms the C3 convertase and subsequent C5 convertase. This leads to the cleavage of immune cell-recruiting anaphylatoxins and cell-lysing membrane attack complex. [Adapted from (1)].

lysis of microbial pathogens and apoptotic cells (158). To perform these functions, the complement cascade consists of the classical, lectin and alternative pathways differing by their activating signal. Antigen-antibody complexes and mannan-binding lectin recognition of microbial carbohydrates initiate the classical and lectin pathways, respectively (158). In contrast to the classical and lectin pathway, the self-proteolytic cleavage, or 'tick-over,' of C3 into C3a and C3b primes the alternative complement pathway (158). All three pathways converge onto the formation of a C3 convertase which amplifies complement activation (158). This leads to an abundant supply of C3b which binds to cellular membranes and forms more C3 convertases and ultimately the C5 convertase (158). The C5 convertase cleaves C5 into C5b and C5a (158). C5b binds to cellular membranes and recruit C6 through C9 to form the terminal endpoint of complement activation, the membrane attack complex (MAC) (158). MAC creates a pore in cells and causes their lysis if a sufficient amount of MAC forms on the membrane (158). Another important consequence of complement activation is the formation of the anaphylatoxins C3a and C5a. C3a and C5a direct resident and circulating immune cells to sites of tissue damage allowing for removal of danger-associated molecular antigens and secretion of proteins needed to restore tissue homeostasis (159) . To ensure protection against complement-mediated attack, there are soluble and membrane-bound

complement inhibitors (158). Together, these proteins maintain homeostasis and protect an organism from microbial invasions and apoptotic cell debris.

In addition to its roles in maintaining extracellular homeostasis, complement has noncanonical roles in adaptive immune responses and neural development. The most well-known noncanonical function of complement is amplifying the production of antibodies by B cells (160). Mice lacking the *Complement receptor 2* (*Cr2*<sup>-/-</sup>) gene that recognizes C3 fragments have impaired T cell dependent antigen-induced humoral responses (160). In fact, when antigens are coated with C3 fragments, the humoral responses to those antigens are 100 to 10,000X higher than those not coated with C3 fragments (161). Inappropriate interactions between self-antigens coated with C3 fragments and B cells are thought to lead to the development of autoimmune diseases (162). Another important function of C3 fragments *in vivo* is the labeling and pruning of synapses by microglia via the classical complement pathway (163). Mice with deficiencies in C1q, the first protein to interact with antigen-antibody complexes via the classical pathway, display epilepsy phenotypes (164). Interestingly, risk for developing schizophrenia, a psychiatric illness with synaptic dysfunction (165), is associated with copy number variations in C4, another protein in the classical pathway (166).

Emerging evidence suggests complement may play a role in regulating intracellular homeostasis. Intracellular C3a functions to sustain homeostasis as well as aid in differentiation and metabolic reprogramming between classes of T-cells (167, 168). Other tissues such as adipose tissue can be influenced by the presence of C3a. C3a can interact with the C3a receptor (C3aR) on adipocytes and lead to the activation of diacylglycerol o-acyltransferase 1 (DGAT1) (169). DGAT1 is an intracellular protein involved in triglyceride synthesis and a potential therapeutic target for the treatment of obesity (170). Although only a correlation, there is a link between complement and obesity as indicated by increased complement components in obese individuals (171). More studies are needed to elucidate the importance of the complement system in metabolic regulation.

#### **1.4.2 Alternative Complement Pathway and AMD**

Although the exact mechanisms underlying the associations between complement and AMD pathobiology are unknown, multiple lines of evidence suggest a critical role of the alternative complement pathway in AMD. First, many of the AMD-associated variants in complement protein-encoding genes are in components of the alternative complement pathway: *C3*, *Factor B (FB)*, *Factor I (FI)*, *Factor D (FD)* and *CFH* (Fig. 4) (146-154). Second, proteins involved in the alternative complement pathway, not

the classical or lectin pathway, colocalize within drusen in human donor eyes (117, 123). Third, inhibitors of the alternative pathway can attenuate laser-induced CNV lesions in mice (172-174). In fact, lampalizumab, an inhibitor of FD that is a positive regulator of the alternative pathway, showed promise on phase II clinical trials as a therapy for geographic atrophy (175). However, the 2 separate clinical trials (Chroma and Spectri, Roche) evaluating lampalizumab for the treatment of geographic atrophy failed to meet their endpoints during its phase III and raises the question on how dysregulation of the alternative complement pathway functions in AMD(176).

### **1.4.3 Complement Factor Y402H Polymorphism and AMD Risk**

In 2005 four independent studies were published on the association of increased risk for AMD development with the tyrosine (Y) to histidine (H) polymorphic substitution at amino acid 402 in CFH (146-149). Individuals heterozygous and homozygous for the H402 CFH variant are 2.5X and 6X more likely to develop AMD, respectively (146). As noted earlier, CFH is the main soluble regulator of the alternative complement pathway (177). It functions to prevent the formation of the alternative complement pathway's C3 convertase by acting as a cofactor for FI-mediated proteolytic inactivation of C3b (178) and as a decay accelerator that prevents binding of FB to C3b (Fig. 4) (179). The importance of CFH in regulating the formation of the C3 convertase is

exemplified by the absence of intact plasma C3 in *Cfh* knockout (*Cfh*<sup>-/-</sup>) mice due to uncontrolled C3 cleavage (80, 180). However, the H402 polymorphism does not impact the ability of CFH to regulate the alternative complement pathway in the fluid phase (181, 182). The Y402H polymorphism lies within the short consensus repeat (SCR) 7 of CFH. This region is critical for the binding of CFH to GAGs on cellular membranes and other biomolecules to regulate complement activation (183). The H402 polymorphism has been shown to decrease the binding of CFH to multiple biomolecules such as heparin (182, 184), M6 protein of *Streptococcus pyogenes* (184, 185), C-reactive protein (CRP) (182, 184-186), BrM (187), malondialdehyde (MDA) epitopes (188) and oxidized phospholipids (189). However, the significance of these binding differences in AMD is unclear due to the lack of an animal model to interrogate the pathogenicity due to the H402 variant.

### **1.5 Interrogating the Role of CFH in AMD using Mice**

The association of the CFH Y402H polymorphism with AMD risk motivated the pursuit to understand the role of CFH on eye health using mice. In addition to its implicated roles in AMD, CFH is critical for the prevention of membranoproliferative glomerulonephritis type II (MPGN II) or dense deposit disease (DDD) in humans (190, 191). MPGN II is a kidney disease characterized by mesangial hypercellularity, endocapillary proliferation, and capillary wall remodeling with mesangial interposition

and duplication of glomerular basement membranes (192). *Cfh*<sup>-/-</sup> mice were created to recapitulate the pathological overactivation of the complement cascade seen in human MPGN II (180). An interesting observation by Dr. Gregory Hageman linked the presence of mesangial deposits with macular drusen in the eyes of MPGN II patients and led to the study of the ocular phenotypes of aged *Cfh*<sup>-/-</sup> mice (193). The absence of CFH in two-year old *Cfh*<sup>-/-</sup> resulted in some visual loss and BrM thinning (78). In contrast, in other studies, thickening of BrM, outer nuclear layer thinning, and retinal vascular leakage was noted in similarly aged *Cfh*<sup>-/-</sup> animals (63, 194, 195). The differences in these ocular phenotypes of aged *Cfh*<sup>-/-</sup> mice may be due to the vivarium locations and consequent microbiome changes (196).

Despite the information gained from studies using *Cfh*<sup>-/-</sup> mice (63, 78, 194, 195), more robust animal models are needed to understand the significance of CFH in AMD. The significance of CFH in predisposing an aging eye to AMD development and progression can be gleaned from the study of aged *Cfh* hemizygous (*Cfh*<sup>+/-</sup>), knockout (*Cfh*<sup>-/-</sup>) mice and control age-matched wild type C57BL/6J (B6) mice exposed to an environmental stressor (80). Aged *Cfh*<sup>+/-</sup> mice fed an eight week high fat, cholesterol-enriched (HFC) diet develop AMD-like pathologies including rod-mediated visual dysfunction, increased retinal pigmented epithelium (RPE) damage and increased sub-RPE or basal

laminar deposits while, paradoxically, aged *Cfh*<sup>-/-</sup> mice only develop increased basal laminar deposits after diet treatment (Fig. 5) (80). The major difference between these mice is the absence of a circulating reservoir of complement proteins in *Cfh*<sup>-/-</sup> mice due to the lack of Cfh (80, 180). The protection against the development of an AMD-like phenotype in aged *Cfh*<sup>-/-</sup>HFC mice could be due to either a lack of a reservoir of complement components or a compensatory increase in the expression of other complement regulators due to excess complement activation in these mice (194, 197). Support for the former possibility comes from the increase of plasma C5a and consequent immune cell recruitment detected in eyes of aged *Cfh*<sup>+/-</sup>HFC mice compared to aged *Cfh*<sup>-/-</sup>HFC mice. This study demonstrated that the difference between the aged *Cfh* hemizygous and null mouse responses to the HFC diet may lie at the interplay between complement activation and consumption of a HFC diet in aged mice (80).

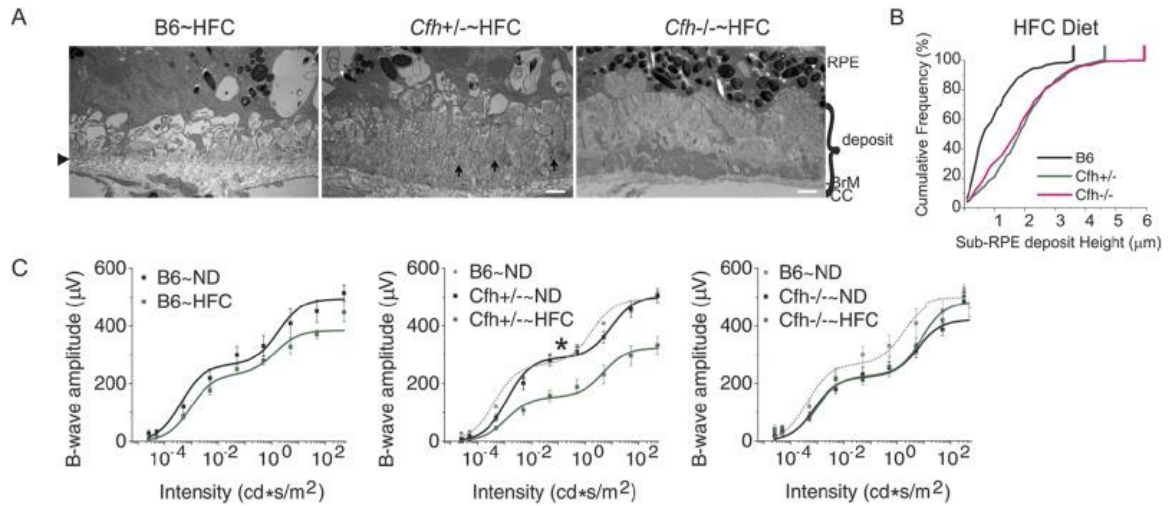


**Figure 5: Ocular responses of aged C57, *Cfh*<sup>+/-</sup> and *Cfh*<sup>-/-</sup> mice after HFC diet consumption.** Aged (>90 weeks of age) C57, *Cfh*<sup>+/-</sup> and *Cfh*<sup>-/-</sup> mice were maintained for an additional eight weeks on normal diet (ND) or switched to a HFC diet. (A-B) Only *Cfh*<sup>+/-</sup>~HFC and *Cfh*<sup>-/-</sup>~HFC diet mice develop increased sub-RPE deposits while C57~HFC mice do not. (C) In contrast, only *Cfh*<sup>+/-</sup>~HFC mice develop attenuated ERG responses while C57~HFC and *Cfh*<sup>-/-</sup>~HFC do not. This suggests deposit formation is contingent on CFH levels while visual loss is dependent on complement levels. \* represents  $P < 0.05$  by ANOVA comparing genotype versus diet. [Adapted from (1)].

Although the *Cfh*<sup>+/-</sup>~HFC mouse has increased complement activation and may model aspects of the risk associated with the H402 CFH variant, it is important to keep in mind that studies investigating plasma CFH concentrations and AMD risk have yielded mixed conclusions (198-201).

In order to mechanistically study the function of CFH H402 variant in AMD pathogenesis *in vivo*, we generated transgenic mouse lines with human *CFH* bacterial artificial chromosomes expressing the full-length human normal Y402 or risk-associated

H402 variant of the CFH protein (*CFH-Y* and *CFH-H*, respectively) (195). These mouse lines were then crossbred with *Cfh*<sup>-/-</sup> mice to remove mouse CFH (*CFH-Y:Cfh*<sup>-/-</sup> and *CFH-H:Cfh*<sup>-/-</sup>, respectively) (195). Expression of human CFH in these mice prevents the retina damage caused by the *Cfh* deletion. Additionally, human CFH protein inhibits cleavage of mouse C3 and factor B in plasma and in RPE/choroid/sclera, establishing that human CFH in these *CFH-Y:Cfh*<sup>-/-</sup> and *CFH-H:Cfh*<sup>-/-</sup> mice, regulates the activation of the mouse alternative pathway, effectively replacing mouse CFH (195). Mice that produce the risk-associated H402 variant have more visual loss and thicker sub-RPE deposits compared to mice expressing the normal Y402 variant (195). These results differ from the severe retinal phenotype observed in transgenic mice that produce a chimeric CFH consisting of mouse SCRs 1-5, human SCRs 6-8 that includes either the Y402 or H402 variant, and mouse SCRs 9-20 (82). This unexpected retinal phenotype may be because chimeric CFH protein expression in this mouse model is being driven by a human *APOE* promoter (82), leading to ectopic expression of chimeric CFH in the neural retina (116, 146, 202).

One major caveat with the *CFH-Y:Cfh*<sup>-/-</sup> and *CFH-H:Cfh*<sup>-/-</sup> murine strains is their CFH expression. *CFH-Y:Cfh*<sup>-/-</sup> mice produce twice the amount of CFH compared to *CFH-H:Cfh*<sup>-/-</sup> mice, thus any phenotypic differences between these mice may be

explained by either CFH concentration or variant or both (79). For this reason, we crossed *CFH-H:Cfh<sup>-/-</sup>* mice with each other to generate homozygous *CFH-HH:Cfh<sup>-/-</sup>* mice. These mice now express the same concentrations of CFH as the *CFH-Y:Cfh<sup>-/-</sup>* mice, exhibit equal levels of complement activity - as shown by a hemolytic assay using sheep erythrocytes - and provide similar protection against the development of MPGN II-like kidney disease compared to *CFH-Y:Cfh<sup>-/-</sup>* mice (79). The *CFH-HH:Cfh<sup>-/-</sup>* and *CFH-Y:Cfh<sup>-/-</sup>* strains allow for the direct interrogation of the H402 CFH variant in AMD pathogenesis using mice.

In the next three chapters of this dissertation, I will present experimental data derived from analyses of these complement-based multifactorial models we have developed that suggests the risk associated with the H402 variant *is not due to complement activation but rather lipoprotein metabolism*. This important observation may explain why complement inhibitors have failed for the treatment of AMD.

## 2. Effect of Anti-C5a Therapy in a Murine Model of Early/Intermediate Dry Age-Related Macular Degeneration<sup>1</sup>

### 2.1 Introduction

The H402 CFH variant is widely thought to increase complement activation in the posterior eye and lead to the development of AMD (155). One major consequence of complement activation is the generation of the anaphylatoxin C5a. C5a is a critical chemoattractant protein responsible for the recruitment, activation and maintenance of immune cells (203). Consequently, we observed an increase in extravascular recruitment of mononuclear phagocytes (MNPs) to the RPE/choroid in aged *Cfh*<sup>+/-</sup>HFC compared to *Cfh*<sup>-/-</sup>HFC mice, suggesting a potential role of C5a in the development of AMD-like pathologies seen in this dry AMD model (80). C5a is increased in the plasma of AMD patients (200, 201, 204) and is a constituent of drusen (205). C5a was shown to increase the expression of proteins in tissues implicated in AMD such as intercellular adhesion molecule-1 (ICAM1) (206), interleukin-17 (IL-17) (207), interleukin-18 (IL-18) (208), interleukin-22 (IL-22) (207), and vascular endothelial growth factor a (VEGF-A) (209). Intraocular anti-VEGF therapy injections are current standard treatments for patients

---

<sup>1</sup> This chapter is modified from my first paper that I was co-first author: Toomey CB, Landowski M, et al. (2018) Effect of Anti-C5a Therapy in a Murine Model of Early/Intermediate Dry Age-Related Macular Degeneration. Invest Ophthalmol Vis Sci 59(2):662-673..

with “wet” AMD. Similarly, antibodies and an aptamer targeting C5a have decreased the lesion size in the acute laser-induced CNV mouse model of wet AMD and show promise as a potential therapy for wet AMD (205, 210, 211).

In this study, we tested the role of C5a in the development of early/intermediate AMD-like pathologies to determine if the risk associated with the H402 variant is due to increased C5a generation and recruitment of immune cells to the posterior eye. Aged *Cfh*<sup>+/-</sup> mice fed a HFC diet were treated with weekly systemic injections of an anti-C5a antibody (4C9; Pfizer). Although anti-C5a therapy has a significant effect in an acute model of retinal degeneration and neovascularization, it did not appear to protect *Cfh*<sup>+/-</sup>~HFC mice from the development of early/intermediate dry AMD-like features, including reduced electroretinogram (ERG) responses, increased RPE damage, increased sub-RPE basal laminar deposits, and increased inflammatory and extracellular matrix (ECM) gene expression. Since C5a acts as a chemoattractant and C5a receptor 1 (*C5aR1*) expression is confined to the choroid in the eye, we quantified immune cell populations in the RPE/choroid after anti-C5a therapy and found reduced MNP recruitment in treated aged *Cfh*<sup>+/-</sup>~HFC mice. These results establish that the blockade of C5a is not sufficient to protect mice from the development of early/intermediate dry AMD-like pathologies in aged *Cfh*<sup>+/-</sup>~HFC despite blocking the recruitment of MNPs to the

RPE/choroid. This observation suggests that the risk associated with the H402 CFH variant is not due to C5a generation and immune cell recruitment to the posterior eye.

## **2.2 Results**

### **2.2.1 Anti-C5a Dosage and Efficacy in an Acute Model of Retinal Degeneration and of Neovascularization**

The dose response of our novel mouse monoclonal anti-C5a antibody, 4C9, was determined in the NaIO<sub>3</sub> model of retinal degeneration (42, 43). Administration of NaIO<sub>3</sub> results in the ablation of scotopic b-wave in C57BL/6J mice (69). ERGs were performed 3 days after mice were treated with either an intravenous injection of 3, 10, 20, 30, or 60 mg/kg anti-C5a or 60 mg/kg isotype control and were then subjected to an intravenous injection of NaIO<sub>3</sub>. We observed a statistically significant rescue in ERG responses in mice receiving the 20, 30, and 60 mg/kg doses of anti-C5a at the 0.1 ( $P < 0.05$ ) and 2.5 ( $P < 0.001$ ) cd\*s/m<sup>2</sup> flash intensity (Fig. 6A). We validated the intermediate anti-C5a dosage (30 mg/kg) in the laser-induced CNV model for wet AMD (103, 212). The antiangiogenic effects of anti-C5a therapy were measured by fluorescein angiography in the rodent CNV model by scanning laser ophthalmoscopy. Neovascular lesion size was measured following administration of either anti-C5a and/or the standard of care, anti-VEGF, in a dose–response manner. Lesion size was used to determine whether (1) the anti-C5a antibody alone reduces CNV lesion size and (2) combination therapy with anti-VEGF synergizes with complement blockade to further enhance the therapeutic effect of VEGF

inhibition. Anti-C5a therapy significantly reduced CNV lesion size in mice compared to IgG control at 30 mg/kg ( $P < 0.05$ ) (Fig. 6B). In addition, administration of 30 mg/kg anti-C5a, as a combinatorial therapy, significantly enhanced the efficacy of subtherapeutic doses of anti-VEGF at 2 and 5 mg/kg ( $P < 0.05$ ) (Fig. 6B). Thus, the anti-C5a antibody is able to reduce CNV lesion size as a monotherapy and as a combinatorial therapy with anti-VEGF as supported by others (205, 210, 211).

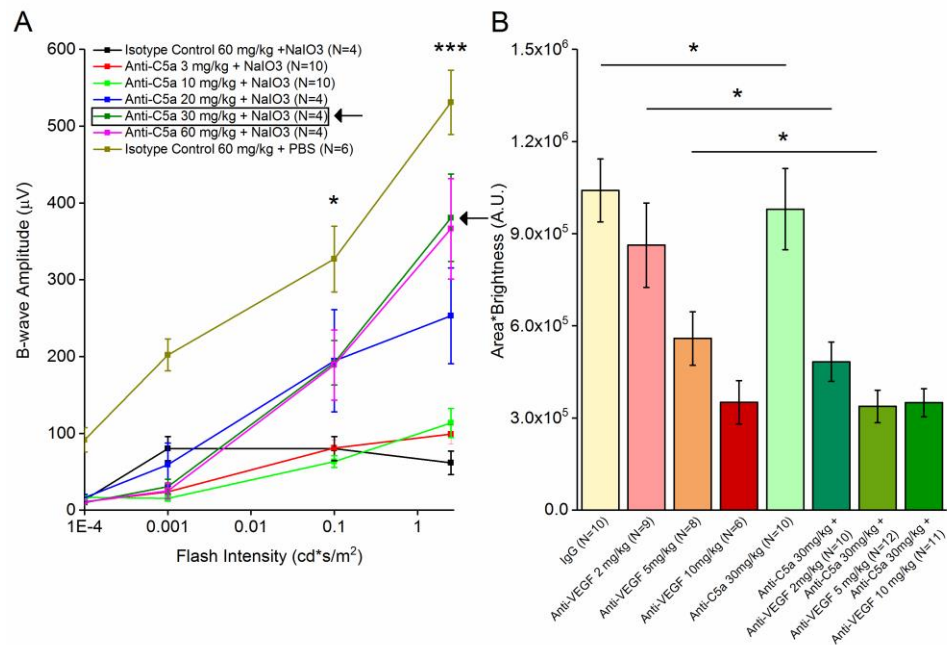


**Figure 6: C5a dosage and efficacy studies using the sodium iodate (NaIO<sub>3</sub>) model of retinal degeneration and laser-induced CNV model of wet AMD. (A) C5a dose–response therapy following NaIO<sub>3</sub>. To determine the in vivo dose response of anti-C5a (4C9) in the context of posterior eye inflammation, mice were treated with increasing concentrations of anti-C5a (3, 10, 20, 30, and 60 mg/kg) or 60 mg/kg isotype control (Iso 60 mg/kg), delivered by a single injection IP, followed by the intravenous injection of NaIO<sub>3</sub> at 25 mg/kg. Scotopic electroretinogram (ERG) B-wave amplitudes are presented at increasing flash intensities of light. Mice receiving 20, 30, and 60**

mg/kg doses of anti-C5a therapy had significantly higher ERG amplitudes than those receiving a PBS injection following NaIO<sub>3</sub> treatment. The asterisks (\* and \*\*\*) represent statistical significance by ANOVA comparing treatments with post hoc Tukey test comparing 20, 30, or 60 mg/kg anti-C5a-treated mice to PBS-treated mice after NaIO<sub>3</sub> at P < 0.05 and P < 0.001, respectively. We chose the intermediate therapeutic dose of 30 mg/kg for our studies (arrow). N , number of mice. (B) The efficacy of the 30 mg/kg dosage of anti-C5a therapy was confirmed using the laser-induced choroidal neovascularization (CNV) mouse model. CNV lesion size was assessed following administration of either IgG isotype control or anti-C5a alone or in combination with anti-VEGF. Individual lesions were quantitated via ImageJ and arbitrary units per lesion were plotted. Asterisk (\*) indicates statistical significance using the Student's t-test for P < 0.05 comparing IgG control or anti-VEGF at various doses in combination with 30 mg/kg anti-C5a therapy.

### 2.2.2 Anti-C5a Treatment in Aged *Cfh*<sup>+/-</sup>~HFC Mice

In our previous study of aged *Cfh*<sup>+/-</sup> and *Cfh*<sup>-/-</sup> mice fed a HFC diet we observed a striking correlation between complement dysregulation and RPE damage and visual function impairment (80). These findings make the *Cfh*<sup>+/-</sup>~HFC a suitable model to test the effects of C5a with an anti-C5a therapy on early/intermediate dry AMD-like features. *Cfh*<sup>+/-</sup> mice aged at least 90 weeks were switched to a HFC diet and administered weekly IP injections of 30 mg/kg anti-C5a for 8 weeks. Plasma anti-C5a antibody levels ranged from 119 to 179 µg/mL 24 hours post injection, and after 7 days, antibody levels ranged from 58 to 99 µg/mL (Fig. 7A). Following 8 weeks of weekly IP injections, anti-C5a levels ranged from 153 to 80 µg/mL (mean of 99.4 µg/mL ± 26.8) 24 hours post final injection (Fig. 7B). Thus, sufficiently high plasma levels were maintained throughout the 8 weeks of HFC diet treatment in *Cfh*<sup>+/-</sup>~HFC mice.

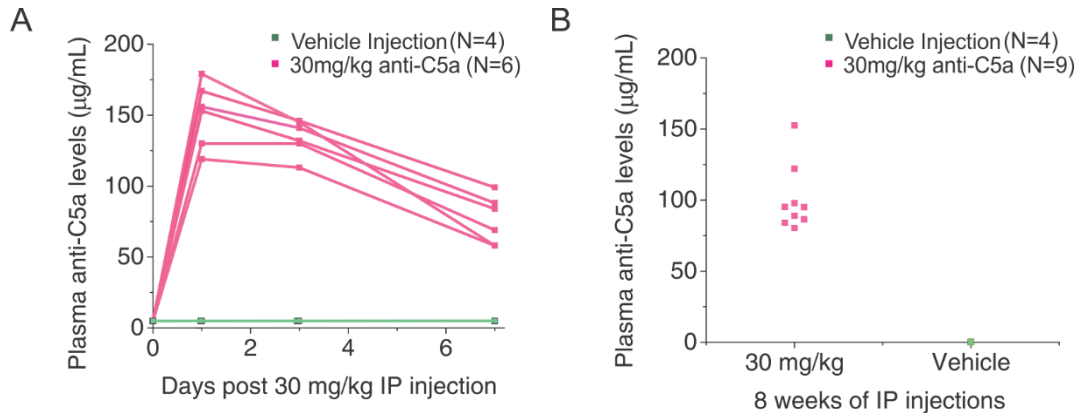


**Figure 7: Sustained high levels of circulating antibodies are achieved with weekly injections of 30 mg/kg of anti-C5a therapy. (A) Mice were injected IP with 30 mg/kg anti-C5a at day 0 and bled at days 1, 3, and 7 to establish the circulating antibody levels maintained throughout the week following weekly 30 mg/kg anti-C5a dosing. Antibody levels were determined by anti-C5a ELISA on plasma samples. (B) At the end of 8 weeks, most mice treated with 30 mg/kg anti-C5a maintained high circulating levels of anti-C5a therapy.**

### 2.2.3 Anti-C5a Therapy Does Not Reduce Early/Intermediate Dry AMD-Like Features in *Cfh*<sup>+/-</sup>~HFC Model

Extracellular lesions that form between the RPE and BrM characterize early AMD (213). The effect of anti-C5a therapy on the thickness of sub-RPE basal laminar deposits that accumulate in *Cfh*<sup>+/-</sup>~HFC mice was analyzed by quantitative electron microscopy of RPE/BrM as previously described (79). As we have previously shown, the majority of the sub-RPE deposits seen in the *Cfh*<sup>+/-</sup>~HFC model were 2- to 3-µm basal laminar deposits, and this did not change following anti-C5a therapy (Fig. 8A) (80). Quantitative analysis of sub-RPE basal laminar deposit thickness confirmed that anti-C5a therapy did not affect the amount of sub-RPE basal laminar deposits that

accumulate in *Cfh+/-*~HFC mice (Figs. 8B, 8C), suggesting that C5a blockade is not sufficient to inhibit the accumulation of sub-RPE basal laminar deposits in the *Cfh+/-*~HFC mouse model.

We measured the damage to the RPE cells in aged *Cfh+/-* mice by quantifying dysmorphic, multinucleate RPE cells on RPE flat mounts stained with Hoechst 33342 to detect the nuclei and immunostained with the tight junction-associated protein, ZO-1, to reveal the cell borders (Fig. 8D). As previously reported, exposure to a HFC diet resulted in a statistically significant increase in the number of enlarged, multinucleate RPE cells in the *Cfh+/-* mice ( $P < 0.05$ ) (Fig. 8E) (80). We found no statistical difference between *Cfh+/-*~HFC mice treated with and without anti-C5a therapy ( $P > 0.05$ ) (Fig. 8E). These data demonstrate that anti-C5a therapy does not appear to protect mice from the RPE dysmorphogenesis seen in the *Cfh+/-*~HFC mice.

As previously reported, *Cfh+/-* mice develop a statistically significant decline in scotopic visual function measured by electroretinography following 8 weeks of HFC diet compared to age-matched wild-type controls on HFC (80). Systemic anti-C5a immunotherapy did not protect the *Cfh+/-*~HFC mice from losing visual function (Fig. 8F).

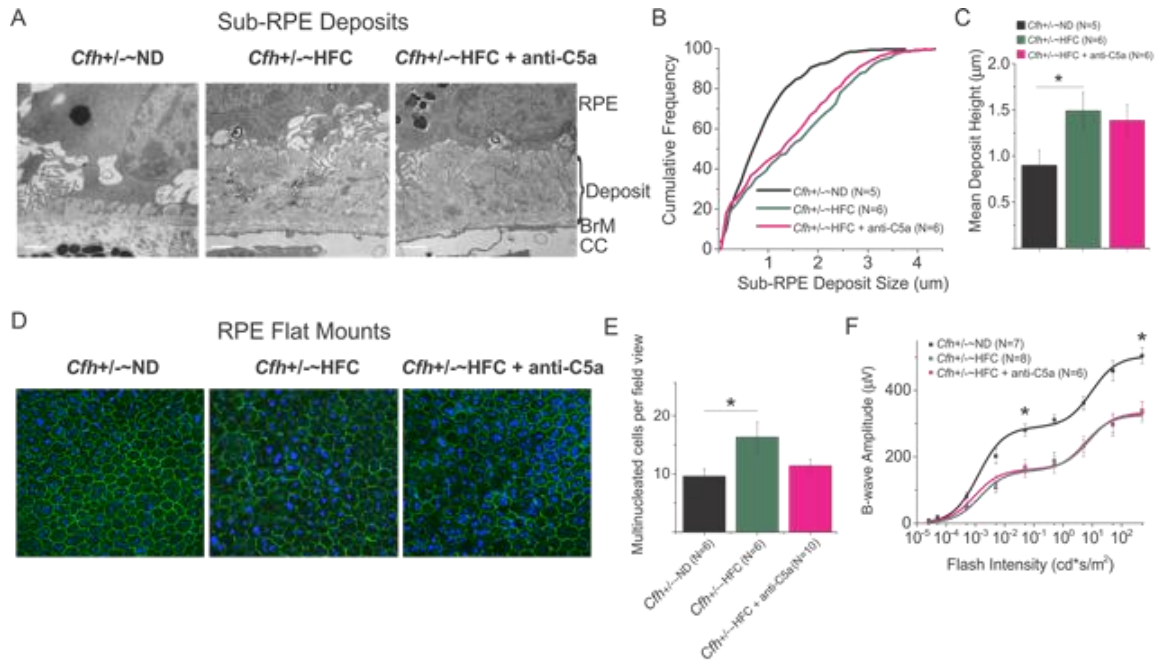


**Figure 8** Anti-C5a therapy does not affect dry AMD-like features in *Cfh+/-~HFC* mice. (A) Representative transmission electron micrograph images of basal laminar deposits along Bruch's membrane (BrM). Large (>2 μm) deposits were often seen in the *Cfh+/-~HFC* and *Cfh+/-~HFC* mice treated with 30 mg/kg anti-C5a, while only minimal sub-RPE deposit could be detected in aged-matched *Cfh+/-* fed a normal diet (*Cfh+/-~ND*). Scale bars: 1 μm. (B) Quantitative analysis of sub-RPE basal laminar deposits using cumulative frequency curves shows that no change in the size of sub-RPE basal laminar deposits was detected between *Cfh+/-~HFC* mice and *Cfh+/-~HFC* mice treated with anti-C5a therapy. (C) Quantitative analysis of mean deposit size per mouse shows no difference could be detected between *Cfh+/-~HFC* mice and *Cfh+/-~HFC* mice treated with anti-C5a therapy. Asterisk (\*) indicates statistical significance at P = 0.05 by Student's t-test analysis. (D) Confocal fluorescence images of central RPE flat mounts from >90-week-old *Cfh+/-* mice fed a ND or HFC diet treated with 0 or 30 mg/kg anti-C5a that were stained with Hoechst 33342 (blue, nuclei) and anti-ZO-1 (green) and imaged with the RPE apical side up with the neural retina removed. In *Cfh+/-~HFC* mice there are many more enlarged, multinucleate cells following HFC diet, whereas in some mice RPE cells appear to be protected from damage in *Cfh+/-~HFC* mice treated with 30 mg/kg anti-C5a. Scale bars: 20 μm. (E) Quantification of multinucleate (nuclei ≥ 3) RPE cells per field view demonstrates that some *Cfh+/-~HFC* mice treated with 30 mg/kg anti-C5a appear to be protected, but no statistically significant differences are detected. Asterisk (\*) indicates statistical

significance at  $P < 0.05$  by Student's t-test analysis. (F) Scotopic electroretinogram (ERG) flash responses in *Cfh*<sup>+/-</sup> fed a ND or HFC diet treated with 0 or 30 mg anti-C5a therapy. Stimulus-response curves of b-wave amplitudes. Data are expressed as mean  $\pm$  SE of the stimulus-response curve overlaid with  $B = (B_{max1} * I / I + I1) + (B_{max2} * I / I + I2)$  comparing ND (black), HFC (green), and HFC treated with 30 mg/kg anti-C5a (pink). *Cfh*<sup>+/-</sup>~HFC mice  $\pm$  anti-C5a treatment were significantly worse following HFC diet. Asterisk (\*) indicates statistical significance at  $P < 0.05$  by Student's t-test analysis for the indicated flash intensities comparing *Cfh*<sup>+/-</sup>~ND and *Cfh*<sup>+/-</sup>~HFC.

#### **2.2.4 HFC Diet Increases Expression of Inflammation and ECM Genes in the Eyecups of Aged *Cfh*<sup>+/-</sup> Mice**

Based on the association between AMD-like pathology in the *Cfh*<sup>+/-</sup>~HFC model with RPE/choroid inflammation and accumulation of ECM debris (80), we analyzed expression of inflammatory and ECM genes using pathway-focused PCR arrays. Transcript levels for inflammatory and ECM remodeling genes were measured using PCR arrays of inflammatory and ECM genes to characterize changes in these pathways that occur in the posterior eyecup (RPE/choroid/sclera) of *Cfh*<sup>+/-</sup>~HFC mice compared to *Cfh*<sup>+/-</sup> mice fed a normal diet (*Cfh*<sup>+/-</sup>~ND). These arrays contain 84 genes and have previously been used to interrogate the expression of inflammatory and ECM genes in the murine eye (214, 215). A complete list of inflammatory and ECM genes and their fold changes is included in Tables 2 and 3 in Appendix A, respectively. Sixty-five inflammatory genes were detected in the pooled *Cfh*<sup>+/-</sup> RPE/choroid eyecup RNA samples; of these, 35 genes were unchanged, 29 genes were upregulated, and only 1 gene (*Ccl11*) was downregulated due to the HFC diet (Table 2 and Fig. 9A). Similarly, 80

ECM genes were detected, of which 29 were unchanged, 47 were upregulated, and 4 were downregulated in response to the HFC diet (Table 3 and Fig. 9B). These results indicate that there is increased expression of inflammatory and ECM genes in the aged *Cfh*<sup>+/-</sup> due to the HFC diet.

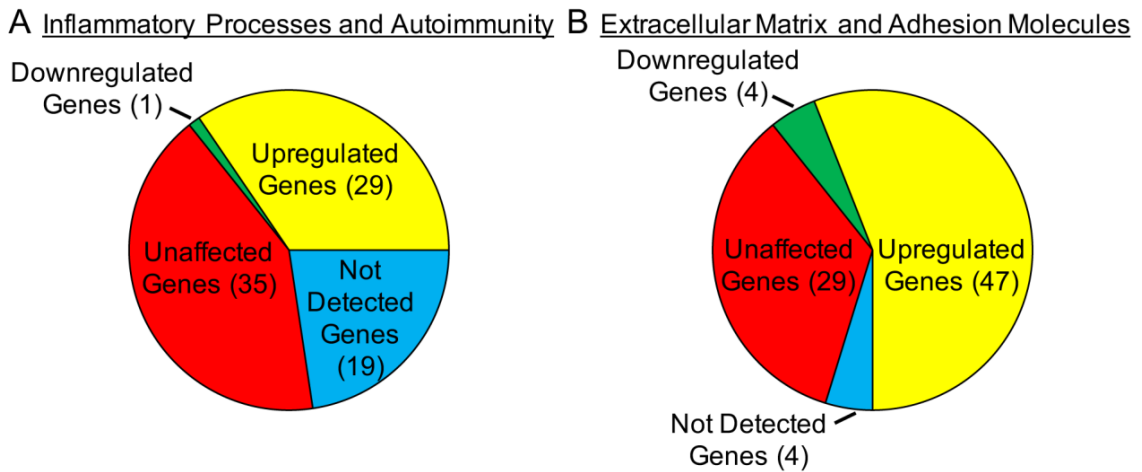


**Figure 9: Overall trends of gene expression changes in inflammatory and ECM remodeling genes detected on pathway-focused PCR arrays of eye cups of aged *Cfh*<sup>+/-</sup> fed an HFC diet. Graphic representation illustrating the change in expression of the 84 genes on the Inflammatory Processes and Autoimmunity and on the Extracellular Matrix and Adhesion Molecules pathway-focused PCR arrays (Qiagen). For these analyses, a gene was considered to be upregulated or downregulated if the fold change was greater than  $\pm 1.25$ . (A) An upregulation of 29 genes involved in inflammation was detected in the eye cups of aged *Cfh*<sup>+/-</sup> mice fed an HFC diet compared to age-matched *Cfh*<sup>+/-</sup> mice fed a normal diet. (B) 47 genes involved in extracellular matrix remodeling were upregulated in the eye cups of aged *Cfh*<sup>+/-</sup> mice fed an HFC diet. Together these gene expression changes indicate support that there is inflammation and extracellular matrix remodeling in the eyes of aged *Cfh*<sup>+/-</sup> mice fed the HFC diet. All genes and their fold changes are shown in Tables 2 and 3 in Appendix A.**

### 2.2.5 Anti-C5a Therapy Does Not Ameliorate HFC-Induced Inflammatory and ECM Gene Expression in the Eyecups of Aged *Cfh*<sup>+/-</sup> Mice

After obtaining a profile of inflammatory and ECM gene expression in the eyecups isolated from aged *Cfh*<sup>+/-</sup> mice fed the HFC diet, we validated the expression of a subset of these genes that had a fold change of 1.25 or more (Fig. 10). We also investigated the effect of blocking C5a on the expression of these same genes in *Cfh*<sup>+/-</sup>~HFC mice (Fig. 10). There was a statistically significant increase in the expression of the inflammatory genes *Ccl2*, *Ccl8*, *Ccl12*, *Cxcl1*, *Cxcl10*, *Il-1beta*, and the ECM genes *Cntn1*, *Col2a1*, *Mmp13*, *Vcan* plus *Icam1* (gene for an intracellular adhesion molecule on ECM array) in the pooled eyecups of *Cfh*<sup>+/-</sup>~HFC mice compared to *Cfh*<sup>+/-</sup>~ND mice (Fig. 10). Expression of these sampled genes was increased in eyecups of the *Cfh*<sup>+/-</sup>~HFC mice treated with anti-C5a, but no decreases were observed comparing *Cfh*<sup>+/-</sup>~HFC mice and *Cfh*<sup>+/-</sup>~HFC mice treated with anti-C5a (Fig. 10). Interestingly, of these there was only a statistically significant increase in *Ccl2* in *Cfh*<sup>+/-</sup>~HFC mice treated with anti-C5a antibody compared to *Cfh*<sup>+/-</sup>~HFC mice (Fig. 10). These findings show that C5a does not appear to contribute to the increased expression of ECM or inflammatory genes in the eyecups of *Cfh*<sup>+/-</sup>~HFC mice.

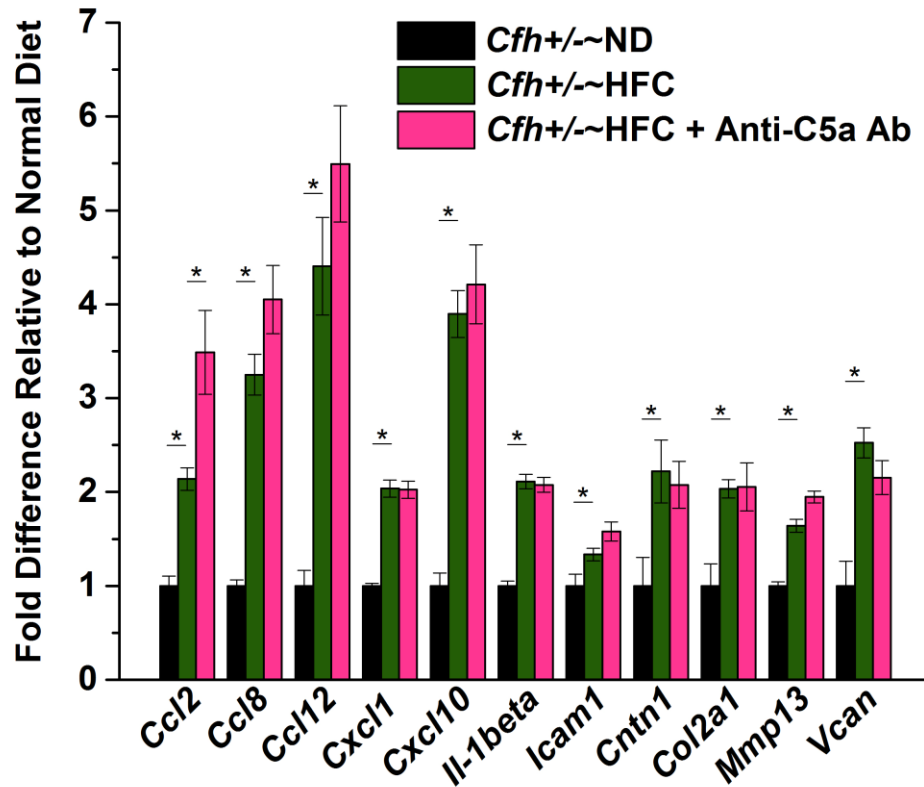
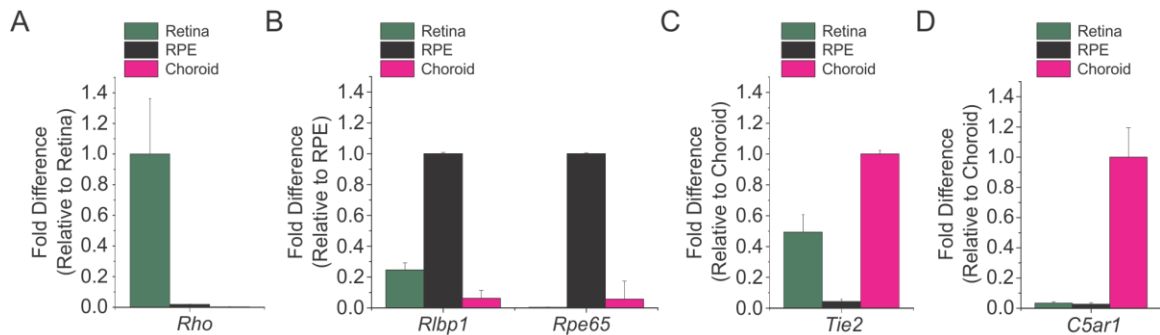


Figure 10: HFC-induced expression of inflammatory and ECM-related genes in eyecups of aged *Cfh*<sup>+/-</sup> mice is not decreased by anti-C5a therapy. Expression of inflammatory and ECM-related genes in the RPE/choroid/sclera of *Cfh*<sup>+/-</sup>~ND, *Cfh*<sup>+/-</sup>~HFC, and *Cfh*<sup>+/-</sup>~HFC + anti-C5a therapy mice. Increases in the mRNA expression of *Ccl2*, *Ccl8*, *Ccl12*, *Cxcl1*, *Cxcl10*, *Il-1beta*, *Icam1*, *Cntn1*, *Col2a1*, *Mmp13*, and *Vcan* were detected in both *Cfh*<sup>+/-</sup>~HFC and *Cfh*<sup>+/-</sup>~HFC mice treated with anti-C5a antibody and suggest that the HFC-associated increases of these genes is C5a independent. Interestingly, statistically significant increases in *Ccl2* were observed in *Cfh*<sup>+/-</sup>~HFC mice treated with anti-C5a antibody compared to *Cfh*<sup>+/-</sup>~HFC mice. Data are presented as normalized averages of triplicate RT-PCR reactions relative to four pooled eyecups from normal diet age-matched *Cfh*<sup>+/-</sup> mice. Error bars represent standard deviations. Asterisk (\*) represents statistical significance at P < 0.05 using ANOVA statistical analysis with post hoc Tukey test comparing gene expression between four pooled eyecups of normal and HFC diet-fed mice or mice fed a HFC diet and those fed a HFC diet and treated with anti-C5a.

### **2.2.6 Complement Anaphylatoxin Receptor 5 Is Predominantly Expressed in Mouse and Human Choroid but Not in Mouse and Human RPE**

C5a has been shown to increase the expression of inflammatory and ECM remodeling genes such as *Ccl2* and *Icam1* in the murine posterior eye (129, 206) but the anti-C5a therapy did not change the expression of these genes in the eyecups of *Cfh+/-*~HFC mice. To localize the effect of the anti-C5a therapy in the posterior eye we investigated the relative expression levels of the C5a receptor, complement anaphylatoxin receptor 5 (*C5aR1*), in mouse and human retina, RPE, and choroid/sclera and human choroid tissues. The relative expression of *C5aR1* was measured by RT-PCR in different regions of the mouse eye using posterior eye tissue-enriched RNA isolated from the neural retina, RPE, and choroid. We examined the expression of rhodopsin (*Rho*) (Fig. 11A), retinaldehyde-binding protein 1 (*Rlbp1*) (Fig. 11B), RPE-specific protein 65 kDa (*Rpe65*) (Fig. 11B), and tyrosine kinase with immunoglobulin and epidermal growth factor homology domain-2 (*Tie2*) (Fig. 11C) to confirm the enrichment of the retinal, RPE, and choroidal/scleral RNA samples, respectively. The majority of *C5ar1* (Fig. 11D) was in choroid/sclera-enriched samples compared to RPE-enriched and neural

retina samples.



**Figure 11: *C5ar1* expression in mouse retina, RPE, and choroid/sclera.** RNA was isolated from mouse retinal, RPE, and choroid/scleral tissue. Enrichment of cell- or tissue-specific transcripts was tested by RT-PCR amplification of the genes coding for (A) rhodopsin (*Rho*, rod photoreceptor specific, retinal marker), (B) *Rlbp1* (left) and *Rpe65* (right, RPE markers), (C) *Tie2* (endothelial cell, choroid marker) and (D) *C5ar1*. Although *C5ar1* was detected in all the samples, the majority of *C5ar1* expression is confined to the choroid/sclera, suggesting that expression detected in the RPE is due to contamination from the choroid. The data represent two independent experiments.

Based on the low levels of *C5ar1* transcript detected in the mouse RPE-enriched sample compared to the amount detected in the choroid/sclera, it is possible that the RPE signal is due to contamination of the mouse RPE-enriched RNA with choroidal RNA, and that murine RPE cells do not express the *C5ar1*. To support this, we examined the relative expression of the human *C5AR1* in human RPE- and choroid-enriched RNA samples as well as ARPE-19 cells, an immortalized human RPE cell line that has been shown to express *C5AR* (209). The purity of the RPE- and choroid-enriched tissues we isolated was tested by RT-PCR, as described above, for human *RPE65* (Fig. 12A), *RLBP1* (Fig. 12A), and *TIE2* (Fig. 12B). Expression of *RLBP1*, but not *RPE65*, was detected in

ARPE-19 cells (Fig. 12A) and confirms previously published findings (216). Examination of *C5AR1* expression using these samples revealed no *C5AR1* expression in the human RPE-enriched sample while *C5AR1* was abundantly expressed in the human choroid-enriched sample (Fig. 12C). Interestingly, there was no detection of *C5AR1* in ARPE-19 cells (Fig. 12C). In summary, we conclude that the majority of *C5AR1* occurs in the choroid while there is little or no expression of *C5AR1* in the RPE.

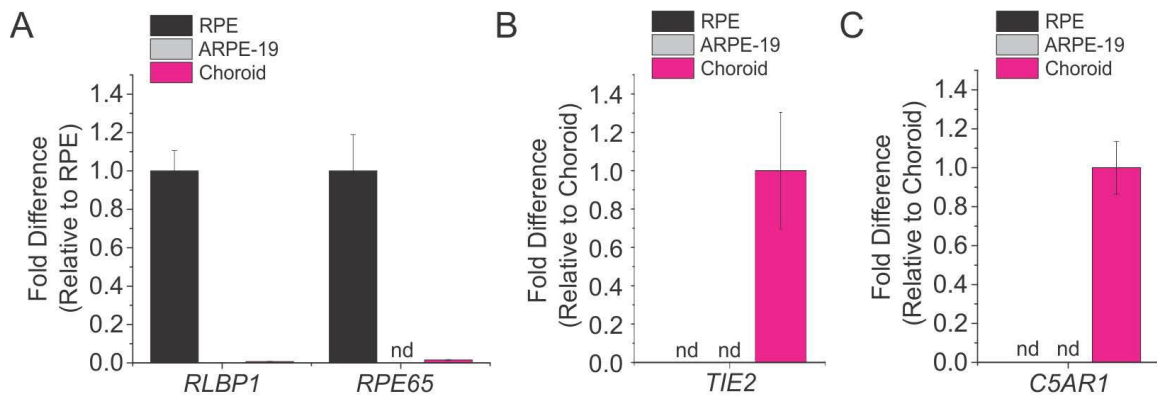


**Figure 12: *C5AR1* expression in human RPE and Choroid and immortalized human RPE.** RNA was isolated from RPE and choroid of a human donor eye as well as cultured ARPE19 RPE cells. (A) Expression of two RPE markers (*RLBP1* and *RPE65*) and (B) one choroid marker (*TIE2*) was examined in these RNA samples. (C) *C5AR1* expression was examined using these samples. *C5AR1* was abundantly detected in choroid-enriched RNA. No *C5AR1* expression was detected in isolated RPE or cultured ARPE19 cells. This supports the *C5ar1* expression pattern seen in primary mouse posterior tissues. nd: none detected

### 2.2.7 Anti-C5a Therapy Ameliorates Classical Monocytosis Seen in *Cfh*<sup>+/-</sup>~HFC Mice

In our previous study of aged *Cfh*<sup>+/-</sup> and *Cfh*<sup>-/-</sup> mice fed a HFC diet we found a correlation between complement dysregulation in the *Cfh*<sup>+/-</sup> mice with peripheral

monocytosis and increased MNPs in the choroid (80). These findings made the *Cfh<sup>+/-</sup>*-HFC a relevant model to test the effects of anti-C5a therapy on monocyte levels and MNP recruitment to the choroid. In the peripheral blood an established gating strategy (81, 217) was used to determine the percentage of classical and nonclassical monocytes (Fig. 13A) (80). As expected, polymorphonuclear leukocytes (PMNs) ( $P < 0.05$ ), classical monocytes ( $P < 0.05$ ), and nonclassical monocyte populations were increased in old *Cfh<sup>+/-</sup>* mice following 8 weeks of HFC diet compared to age-matched controls maintained on a ND. Interestingly, the classical monocyte population in the *Cfh<sup>+/-</sup>*-HFC mice was decreased following anti-C5a treatment, while PMNs were elevated and nonclassical monocytes were unchanged (Fig. 13B). Thus, systemic anti-C5a therapy ameliorates the classical monocytosis ( $P < 0.05$ ) detected in the peripheral blood of *Cfh<sup>+/-</sup>* mice following HFC diet.

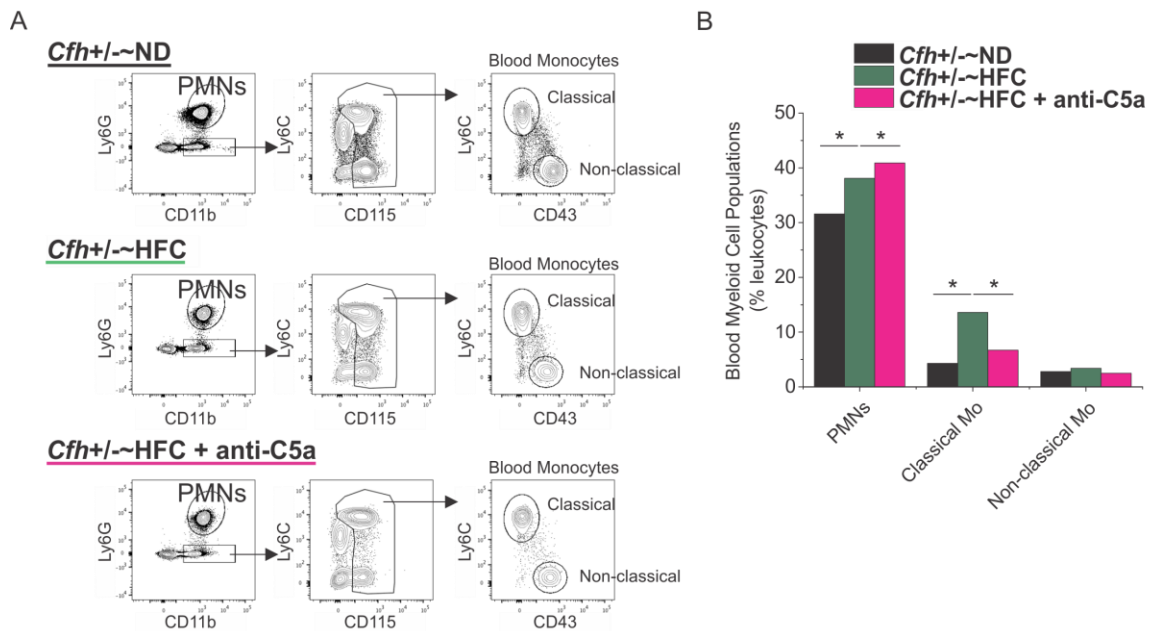


**Figure 13: (A) Flow cytometry was performed on peripheral blood mononuclear phagocytes in *Cfh+/-~ND*, *Cfh+/-~HFC* and *Cfh+/-~HFC + anti-C5a* therapy. (B) An increase in the percentage of classical and non-classical monocytes (Mo) was seen in *Cfh+/-* mice following HFC diet and anti-C5a therapy ameliorated the classical monocytosis. \* represents statistical significance using chi-squared statistical analysis for  $p < 0.05$ . The data presented represents two independent experiments each with a single pooled sample with 3 mice per group. PMN: polymorphonuclear leukocytes.**

## 2.2.8 Anti-C5a Therapy Blocks Recruitment of Monocytes Into the Choroid

Intra- and extravascular flow cytometry was used to test the hypothesis that anti-C5a therapy blocks MNP recruitment in the RPE/choroid. We used a previously established gating strategy to distinguish the intra- and extravascular space using an intravascularly injected anti-CD45 antibody (Fig. 14A) (80). Within the extravascular space there were statistically significant increases in total leukocytes ( $P < 0.05$ ), in PMNs,

and within all MNP populations [Ly6C<sup>hi</sup> (classical monocytes), Ly6C<sup>lo</sup>, and CD64<sup>+</sup>,  $P < 0.05$ ] in *Cfh*<sup>+/-</sup> mice following HFC diet (Fig. 14B). Anti-C5a therapy blocked the increases in total leukocytes ( $P < 0.05$ ), PMNs, classical monocytes, and Ly6C<sup>lo</sup> MNPs ( $P < 0.05$ ) but not CD64<sup>+</sup> MNPs within the RPE/choroid extravascular space (Fig. 14B). Together these results demonstrate that systemic anti-C5a therapy blocks monocyte recruitment to the choroid of *Cfh*<sup>+/-</sup>~HFC mice.

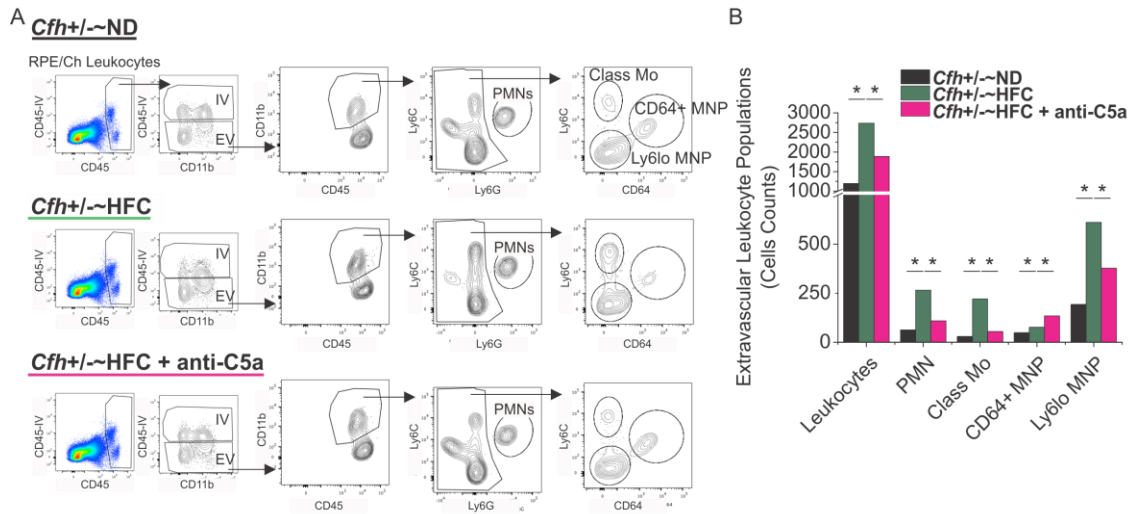


**Figure 14: Extravascular choroidal mononuclear phagocytes are increased in *Cfh*<sup>+/-</sup>~HFC mice and are ameliorated by anti-C5a therapy. (A) RPE/choroid leukocytes were gated for an intravascularly injected anti-CD45 antibody to distinguish the intra- and extravascular space. Gating for polymorphonuclear leukocytes (PMNs) and three previously established populations of mononuclear phagocyte (MNP) (Ly6C<sup>hi</sup> [Class Mo], Ly6C<sup>lo</sup>, and CD64<sup>+</sup>) was performed. (B) Within the extravascular space significant increases were seen in total leukocytes, PMNs, and all the MNP subpopulations (Class Mo, CD64<sup>+</sup> MNP, and Ly6C<sup>lo</sup> MNP). Interestingly, anti-C5a therapy significantly blocked the extravasation of total leukocytes and PMNs, as well as Class Mo and Ly6C<sup>lo</sup> MNP subpopulations. \* $\chi^2$  test for  $P < 0.05$ . Data presented represent a single experiment using a pooled sample from three mice per**

group. A separate independent experiment was performed to confirm trends shown above. Class Mo, classical monocyte.

## **2.3 Discussion**

AMD is a multifactorial disease characterized by early features including reduced rod-mediated light sensitivity, slower dark adaptation, RPE pigmentary changes, and drusen accumulation(17, 218-220). Genetic, biochemical, and clinical studies have converged to implicate the H402 CFH variant in the pathogenesis of AMD development and progression. However, understanding the role of H402 variant in the pathogenesis of AMD is critical for the development of novel therapies. We recently developed an early/intermediate dry AMD mouse model based on advanced age, CFH hemizyosity, and consumption of a HFC diet (80). This aged *Cfh*<sup>+/-</sup>-HFC mouse model of early/intermediate dry AMD can be used to model the pathogenic role of the H402 CFH variant in AMD.

We have previously demonstrated that systemic immunotherapy targeting amyloid beta, a known component of drusen (221-223) that induces complement activation (221, 222, 224, 225), can protect from development of an AMD phenotype in the *APOE4* mouse model of AMD (107). Using a similar approach, in this study we tested the pharmacologic effects of a monoclonal anti-C5a therapy in aged male *Cfh*<sup>+/-</sup>-HFC mice. Aged *Cfh*<sup>+/-</sup> fed a HFC diet have decreased scotopic ERG b-wave responses, increased RPE damage, increased sub-RPE basal laminar deposits, and

increased expression of inflammatory and ECM genes. We show that anti-C5a therapy fails to ameliorate these HFC-induced pathologies in aged *Cfh*<sup>+/-</sup> mice. As a proof of drug efficacy, we used the NaIO<sub>3</sub> model of retinal degeneration and the laser-induced CNV model of wet AMD to confirm the therapeutic potential of systemically delivered anti-C5a antibody in the posterior eye. Although no complement therapies have been tested in the NaIO<sub>3</sub> model to date, our results from the laser-induced CNV model are supported by others (205, 210, 211). Our data suggest that C5a blockade is not sufficient to stop the development of AMD-like pathologies in *Cfh*<sup>+/-</sup>~HFC mice and therefore may not be a viable treatment in early/intermediate dry AMD, although it shows promise as a potential mono- or combinatorial therapy with anti-VEGF in wet AMD.

C5a is a potent anaphylatoxin critical in the recruitment and activation of immune cells to sites of tissue damage. In wet AMD a prominent pathologic hallmark is CNV where choroidal blood vessels proliferate and migrate through BrM into the sub-RPE and subretinal space causing leakage, fibrosis, and eventual tissue damage (16). A role of immune cells such as dendritic cells (226),  $\gamma\delta$  T-cells (210, 227), neutrophils (228), and macrophages (229, 230) in CNV has been implicated using the laser-induced CNV mouse model of wet AMD. All of these immune cells have been shown to express the C5a receptor, C5aR1 (231). Therefore, targeting C5a with either antibodies or aptamers should diminish the exudative lesion size by targeting immune cell populations in the

laser-induced CNV mouse model of wet AMD as confirmed by our results and others (205, 210, 211).

Recruitment of immune cells in early/intermediate dry AMD mouse models has been reported, but the role of immune cells on the development of pathologies in these mouse models is not well understood (38). In addition the H402 variant has been proposed to modulate the clearance of infiltrating immune cells in the posterior eye (85). This study is the first to examine a role for immune cells specifically recruited by C5a during the development of early/intermediate dry AMD-like pathologies in vivo. Our results suggest that recruitment of total leukocytes, PMNs, classical monocytes, and Ly6C<sup>lo</sup> MNPs is sensitive to C5a blockade, but these changes are not sufficient to block the early/intermediate dry AMD-like pathologies seen in *Cfh*<sup>+/-</sup>HFC mice.

In the current study, there was no significant protective effect from RPE damage or vision loss in *Cfh*<sup>+/-</sup>HFC mice treated with systemic immunotherapy blocking C5a. There was increased expression of a subset of inflammation- and ECM-related genes in the RPE/choroid/sclera isolated from *Cfh*<sup>+/-</sup>HFC compared to *Cfh*<sup>+/-</sup>ND, but this increase was not affected by anti-C5a treatment. Because anti-C5a therapy successfully blocked immune cell recruitment to the choroid we suspect that the increased inflammatory and ECM gene expression detected originates from the choroid and/or RPE, and therefore, we measured the relative expression of the *C5AR1* in posterior eye

tissues. Previous studies have examined the expression of the *C5AR1* in human donor eye tissue and found *C5AR1* expression in the choroid and retina (206) as well as in the immortalized human RPE cell line, ARPE-19 (209). We therefore measured the relative *C5ar1* levels in RPE, choroid, and retina isolated from mouse eyes. We found much higher *C5ar1* expression in isolated choroid RNA compared to the RPE and retina RNA obtained from C57BL/6J mice. Although low levels of *C5ar1* expression were detected in the isolated RPE RNA, it is likely that this *C5ar1* expression is due to contamination from the choroid based on the signal detected for the endothelial cell marker, *Tie2*, in the RPE-enriched sample. We obtained similar results using RPE and choroid RNA isolated from a human donor eye and failed to detect *C5AR1* expression in ARPE-19 cells. The *C5AR1* expression in ARPE-19 measured by RT-PCR by Cortright et al. (209) may well be due to genomic DNA contamination since the primers used were nested within a single exon (exon 2). Thus, under normal conditions the majority of *C5ar1* expression is confined to the choroid while RPE cells do not appear to express *C5ar1* in vivo. As a consequence, blocking C5a would not affect the HFC-mediated damage occurring to the RPE and may help explain why anti-C5a therapy did not ameliorate the AMD-like pathologies seen in *Cfh<sup>+/-</sup>~HFC* mice.

Our results suggest that other components of the complement cascade such as the anaphylatoxin C3a and/or the terminal membrane attack complex (MAC) may be

more important for the development of early AMD-like pathologies in *Cfh*<sup>+/-</sup>-HFC mice. A model of Malattia Leventinese/Doyne honeycomb retinal dystrophy, an inherited macular degeneration, using *EFEMP1*<sup>R345W</sup> knock-in mice(59) and RPE cell culture(60), suggests that sub-RPE deposit formation is dependent on complement component 3a (C3a), but not on C5a. These results are consistent with our findings that anti-C5a therapy did not affect sub-RPE deposit formation. In addition, we have previously shown that CFH levels regulate lipoprotein binding and remove endogenous human lipoproteins in BrM (80). In the absence of CFH or decreased CFH, lipoproteins can accumulate and provide a scaffold in which complement activation can occur in the sub-RPE region of the posterior eye and lead to the development of early/intermediate dry AMD. Furthermore, there could be a role of the MAC in our animal model that would not be blocked by anti-C5a therapy.

In summary, targeting the complement activation product C5a is not sufficient to ameliorate the pathologies seen in the aged *Cfh*<sup>+/-</sup>-HFC mouse model of early/intermediate dry AMD; however, it is able to block the recruitment of MNPs to the RPE-choroid and decrease lesion size in the laser-induced CNV mouse model of wet AMD. Other complement components such as C3a or MAC may explain the risk association between the H402 CFH variant and AMD risk. Therefore, new complement-

based therapies and additional mouse models may be needed to elucidate the role of the H402 CFH variant in AMD development and progression.

### 3. Human CFH Y402H Causes an Age-related Macular Degeneration Phenotype in Mice

#### 3.1 Introduction

Although studies on aged *Cfh*<sup>+/-</sup>~HFC mice may provide insight into the role of CFH and AMD, more subtle models of complement dysregulation may be needed to elucidate the molecular mechanisms underlying the risk association between the H402 variant and AMD. It is for this reason we created transgenic mice with bacterial artificial chromosomes spanning the entire human *CFH* gene expressing either the Y402 or H402 human CFH variant that were crossed to *Cfh*<sup>-/-</sup> mice to generate mice that only express the Y402 (*CFH-Y:Cfh*<sup>-/-</sup>) or H402 (*CFH-H:Cfh*<sup>-/-</sup>) variants and no murine *Cfh* (79). This allows for the direct interrogation of the *in vivo* effect of the H402 CFH variant in AMD pathobiology.

Based on the fact that the Y402H *CFH* polymorphism contributes to genetic risk for AMD, but is not a mutation causing AMD, we tested the effect of the *in vivo* expression of the H402 CFH risk variant in combination with two other AMD risk factors, advanced age and HFC diet that we have previously used to generate faithful AMD models (73, 80, 81, 119). Specifically, in the current study we test the hypothesis that the H402 polymorphism contributes to the development of AMD-like pathologies in aged, human CFH-expressing mice after the consumption of an eight week HFC diet. We previously characterized the ocular and kidney phenotypes of aged, hemizygous,

humanized *CFH* mice that express only the Y402 or H402 variant of CFH and no mouse *Cfh* (*CFH-Y:Cfh*<sup>-/-</sup> and *CFH-H:Cfh*<sup>-/-</sup>, respectively) (79). Interpretation of the effect of CFH variants was complicated by the fact that the levels of CFH are twice as high in *CFH-Y:Cfh*<sup>-/-</sup> mice compared to *CFH-H:Cfh*<sup>-/-</sup> mice, prompting us to cross the *CFH-H:Cfh*<sup>-/-</sup> mice to generate homozygous *CFH-HH:Cfh*<sup>-/-</sup> mice (79). *CFH-Y:Cfh*<sup>-/-</sup> and *CFH-HH:Cfh*<sup>-/-</sup> mice have similar levels of CFH resulting in similar C3, C5 and factor B levels and plasma C3 hemolytic activity and can therefore be used to interrogate the impact of expression of the different CFH variants *in vivo* (79) (Fig. 15). Mice were aged to ninety weeks and either maintained on a normal diet (ND) or switched to a HFC diet for eight weeks. Only the aged *CFH-HH:Cfh*<sup>-/-</sup> mice developed decreased rod-mediated visual activity, increased RPE damage and increased basal laminar deposits after the consumption of an eight week HFC diet compared to the age-matched *CFH-Y:Cfh*<sup>-/-</sup> after HFC diet and both mouse lines on ND. Furthermore, none of these pathologies were observed in young *CFH-Y:Cfh*<sup>-/-</sup> and *CFH-HH:Cfh*<sup>-/-</sup> (*CFH:Cfh*<sup>-/-</sup>) mice after HFC diet treatment. Analysis of the plasmas and eyecups from aged *CFH:Cfh*<sup>-/-</sup> mice on and off HFC diet revealed levels of complement activation proteins were similar for both genotypes and suggested the phenotypic differences between these mice is not solely due to complement activation. These findings suggest the CFH Y402H polymorphism effects HFC diet-induced AMD-like pathologies in a complement-independent manner.

## 3.2 Results

### 3.2.1 Fluid Phase Complement Proteins in Human CFH Transgenic Mice

We have previously described the transgenic mouse lines expressing full-length human CFH that were generated to study the Y402H polymorphism *in vivo* (79). Human CFH expressed by these hemizygous *CFH:Cfh*<sup>-/-</sup> mice regulates activation of the mouse alternative complement pathway, effectively replacing the mouse *Cfh*, which is absent in these mice and human CFH rescues the kidney from damage seen in *Cfh*<sup>-/-</sup> mice (79, 180). We also showed that there is two-fold more CFH protein in *CFH-Y:Cfh*<sup>-/-</sup> plasma (~20 µg/mL) than in *CFH-H:Cfh*<sup>-/-</sup> plasma (~10 µg/mL). Hemizygous *CFH-H:Cfh*<sup>-/-</sup> were bred together to generate homozygous *CFH-HH:Cfh*<sup>-/-</sup> mice to correct this problem (79). Concentrations of plasma CFH (Fig. 15A), C3 (Fig. 15B) and FB (Fig. 15C) are the same in homozygous *CFH-HH:Cfh*<sup>-/-</sup> mice compared to hemizygous *CFH-Y:Cfh*<sup>-/-</sup> mice and as much as twice the concentrations of the levels detected in hemizygous *CFH-H:Cfh*<sup>-/-</sup> mice (79). In the current study the effects of expression of *equal* amounts of human normal and AMD-risk associated variants (CFH Y402 and CFH H402, respectively) were compared in hemizygous *CFH-Y:Cfh*<sup>-/-</sup> and homozygous *CFH-HH:Cfh*<sup>-/-</sup> mice.

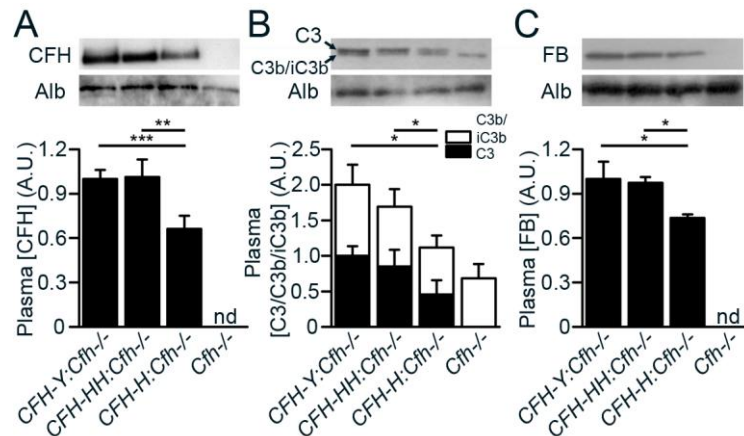


**Figure 15: *CFH-Y:Cfh<sup>-/-</sup>* and *CFH-HH:Cfh<sup>-/-</sup>* mice have equivalent fluid phase complement protein levels. (A-C) Densitometric analysis of CFH (A), C3/C3b/iC3b (B) and FB (C) immunoblots from plasma of young (20-26 week old) *CFH:Cfh<sup>-/-</sup>* mice fed a normal diet. (A) Circulating CFH levels are the same in *CFH-Y:Cfh<sup>-/-</sup>* and *CFH-HH:Cfh<sup>-/-</sup>* mice, half this level in hemizygous *CFH-H:Cfh<sup>-/-</sup>* mice and absent in *Cfh<sup>-/-</sup>* mice. (B) These fluid phase levels of CFH impact levels of plasma C3 such that C3 levels (black bars in graph) are comparable between *CFH-Y:Cfh<sup>-/-</sup>* and *CFH-HH:Cfh<sup>-/-</sup>* mice, reduced in *CFH-H:Cfh<sup>-/-</sup>* mice and absent in *Cfh<sup>-/-</sup>* mice. C3b/iC3b (black bars) is detectable in *CFH:Cfh<sup>-/-</sup>* mice because they express low levels of CFH (79). (C) Circulating levels of FB are the same in *CFH-Y:Cfh<sup>-/-</sup>* and *CFH-HH:Cfh<sup>-/-</sup>* mice, reduced in *CFH-H:Cfh<sup>-/-</sup>* mice and not detected in *Cfh<sup>-/-</sup>* mice reflecting the CFH levels. The asterisks (\*, \*\*, \*\*\*) indicate post hoc Tukey for a  $P < 0.05$ ,  $< 0.01$  and  $< 0.001$ , respectively, following a statistically significant genotype by diet interaction by ANOVA for the densitometric arbitrary units. The data represents two independent experiments. Data is presented as mean  $\pm$  SD. nd, not detected. N=3**

### 3.2.2 Visual Function Decline Associates with Human H402 CFH with Aging and HFC diet

We have previously established that consumption of a HFC diet in aged *Cfh<sup>+/-</sup>* and *Cfh<sup>-/-</sup>* mice for at least 8 weeks causes ‘early/intermediate’ AMD-like pathologies including vision loss, RPE damage and sub-RPE basal laminar deposit accumulation (80). We tested this paradigm in the *CFH:Cfh<sup>-/-</sup>* mice to test the hypothesis that the

Y402H polymorphism would cause an AMD-like phenotype when combined with these risk factors. *CFH-Y:Cfh<sup>-/-</sup>* and *CFH-HH:Cfh<sup>-/-</sup>* mice were aged to at least ninety to ninety-eight weeks and maintained on ND or switched to a HFC diet for eight weeks. Scotopic electroretinography (ERG) was used to measure visual function in the aged *CFH:Cfh<sup>-/-</sup>* mice following the HFC diet as rod photoreceptor dysfunction is an early sign of AMD (232). A diminished scotopic ERG B-wave response has been shown in other AMD mouse models following HFC diet (80, 81, 119). There were no differences in the ERG B-wave responses between the aged *CFH-Y:Cfh<sup>-/-</sup>* mice continued on ND diet (*CFH-Y:Cfh<sup>-/-</sup>~ND*) compared to age-matched *CFH-Y:Cfh<sup>-/-</sup>* mice fed a HFC diet (*CFH-Y:Cfh<sup>-/-</sup>~HFC*) or in *CFH-HH:Cfh<sup>-/-</sup>* mice continued on ND diet (*CFH-HH:Cfh<sup>-/-</sup>~ND*) (Fig. 16). In contrast to all the other aged groups, only aged *CFH-HH:Cfh<sup>-/-</sup>* mice fed a HFC diet (*CFH-HH:Cfh<sup>-/-</sup>~HFC*) developed statistically significant ( $P < 0.01$ ) decrease in their ERG B-wave responses compared to age-matched *CFH-HH:Cfh<sup>-/-</sup>~ND* mice (Fig. 16). Visual function in younger adult (36-40 week old) *CFH-Y:Cfh<sup>-/-</sup>* or *CFH-HH:Cfh<sup>-/-</sup>~HFC* mice fed a ND or switched to HFC was not changed (Figure 30 in Appendix B). Together these findings establish an age-dependent effect of the CFH H402 risk variant on ERG B-wave responses after consumption of a HFC diet in mice.

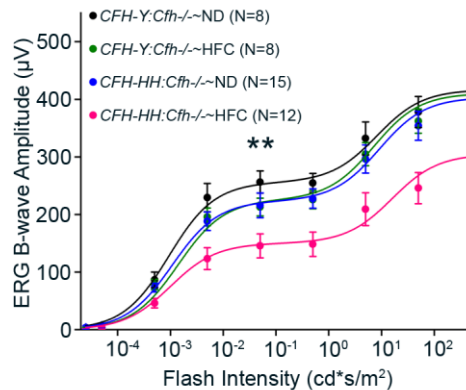


**Figure 16: Decreased visual function loss occurs in only aged *CFH-HH:Cfh-/-~HFC* mice. Scotopic electroretinogram (ERG) flash responses in aged (90+ weeks) *CFH:Cfh-/-* mice fed a ND or HFC diet. Visual function was assessed by scotopic ERG and presented as fitted lines of the B-wave amplitude averages using the equation  $B = (B_{max1} * I / I + I_1) / (B_{max2} * I / I + I_2)$ . No differences in the scotopic ERG B-wave responses were observed between aged *CFH-Y:Cfh-/-~ND* (black), *CFH-Y:Cfh-/-~HFC* (green) mice and *CFH-HH:Cfh-/-~HFC* (blue). Only aged *CFH-HH:Cfh-/-~HFC* mice (pink) develop statistically significant attenuated ERG B-wave responses compared to aged *CFH-HH:Cfh-/-~ND* mice. The asterisks (\*\*) indicate post hoc Tukey for a  $P < 0.01$  following a statistically significant genotype by diet interaction by ANOVA for the mean areas under the B-wave flash response curves.**

Scotopic ERG A-wave responses were analyzed to assess photoreceptor activity (233). There were no statistically significant differences in the ERG A-wave responses between the aged *CFH-Y:Cfh-/-* and *CFH-Y:Cfh-/-* mice fed either diet (Fig. 17A). There was a trend of lower A-wave responses in aged *CFH-HH:Cfh-/-~HFC* compared to all three other groups, but this did not reach statistical significance ( $P=0.11$ ) (Fig. 17A).  $B_{max1}$  and  $B_{max2}$  values representing rod-dominant and cone-dominant responses, respectively, were calculated (233). There was no change in  $B_{max1}$  (Fig. 17B) and  $B_{max2}$  (Fig. 17C) values in aged *CFH-Y:Cfh-/-~ND* and *~HFC* mice. Statistically significant

decreases ( $P < 0.05$ ) were measured in the rod-dominant Bmax1 responses (Fig. 17B), but not in the cone-dominant Bmax2 responses (Fig. 17C), of aged *CFH-HH:Cfh-/-*~HFC mice compared to aged *CFH-HH:Cfh-/-*~ND mice. These results indicate CFH variants modulate rod-dominant visual activity following the HFC diet treatment.

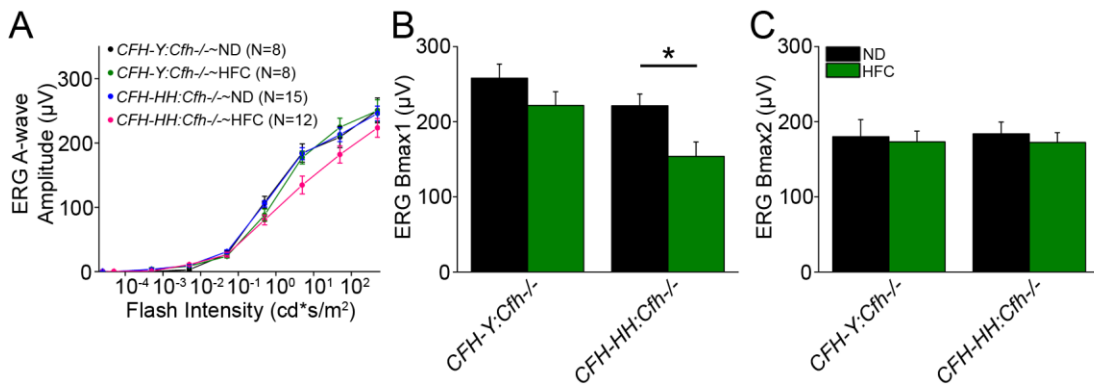


**Figure 17: Rod dominant ERG responses are impaired in aged *CFH-HH:Cfh-/-* mice following HFC diet. (A) Scotopic ERG flash responses in aged *CFH:Cfh-/-* mice fed a ND or HFC diet. Visual function was assessed by scotopic ERG as in Fig. 1A. A-wave responses were unchanged in aged *CFH-Y:Cfh-/-*~ND (black), *CFH-Y:Cfh-/-*~HFC mice (green) and *CFH-HH:Cfh-/-*~ND (blue). Aged *CFH-HH:Cfh-/-*~HFC mice (pink) had lower A-wave responses but this decline did not reach significance ( $P=0.11$ ) compared to aged *CFH-HH:Cfh-/-*~ND mice. (B-C) ERG responses were further analyzed to quantify Bmax1 and Bmax2, measures of rod-dominant and cone-dominant visual activity, respectively (233). (B) Bmax1 values for aged *CFH-Y:Cfh-/-*~ND and *CFH-Y:Cfh-/-*~HFC mice were similar. Aged *CFH-HH:Cfh-/-*~HFC mice had significantly lower Bmax1 values compared to aged *CFH-HH:Cfh-/-*~ND mice. (C) No change was noted in Bmax2 values between these groups of mice. The asterisks (\*) indicate post hoc Tukey for a  $P < 0.05$  following a statistically significant genotype by diet interaction by ANOVA for the Bmax1 values. Data is presented as mean  $\pm$  SEM.**

### 3.2.3 RPE Dysmorphogenesis Increases in Mice Expressing Human H402 CFH with Age and HFC diet

RPE dysmorphogenesis as quantitated by the number of multinucleate RPE cells is associated with AMD (119) and AMD mouse models (80, 81, 119). RPE flat mounts were labeled with an antibody against the tight junction-associated protein zonula occludens 1 (ZO-1) and stained with Hoescht 33258 to quantitate the number of RPE cells with more than 3 nuclei (Fig. 18A). No change in the number of multinucleated RPE cells was detected in aged *CFH-Y:Cfh-/-*~ND and *CFH-Y:Cfh-/-*~HFC mice (Fig. 18B). We found a statistically significant ( $P<0.05$ ) increase in the number of multinucleated RPE cells in aged *CFH-HH:Cfh-/-*~HFC mice compared to aged *CFH-HH:Cfh-/-*~ND mice (Fig. 18B). In younger adult *CFH:Cfh-/-*~ND and ~HFC mice there were fewer numbers of multinucleate RPE cells overall and no statistically significant difference between either genotype fed either diet (Figure 31 in Appendix B). This data demonstrates an age-dependent CFH variant difference contributing to RPE dysmorphogenesis in the old *CFH-HH:Cfh-/-* after eight weeks on a HFC diet.

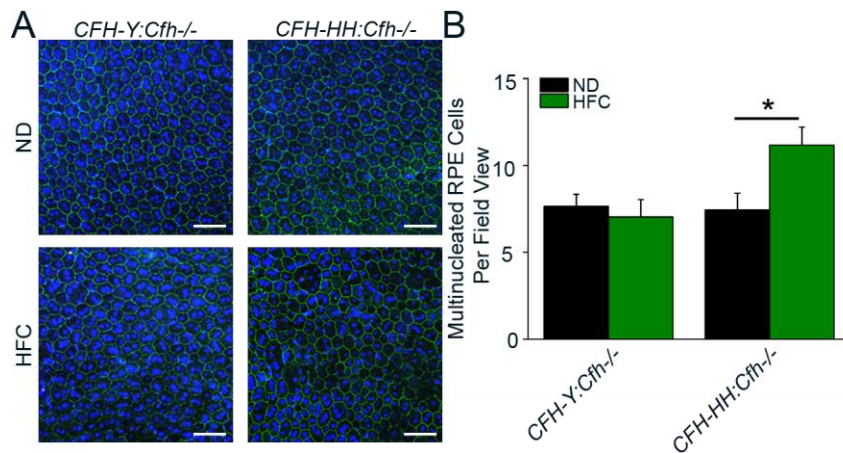


**Figure 18: Increased RPE dysmorphogenesis is only in aged *CFH-HH:Cfh-/-*~HFC mice. ((B) RPE dysmorphogenesis in aged *CFH:Cfh-/-* mice following HFC diet. Representative confocal fluorescence images (40X magnification) of RPE flatmounts near the optic nerve stained with Hoechst 33342 (blue, nuclei) and anti-ZO-1 (green) from aged *CFH:Cfh-/-* mice on ND and HFC diet. RPE dysmorphogenesis in aged *CFH:Cfh-/-* mice was measured by the number of multinucleate ( $n \geq 3$  nuclei) RPE cells within each image. There are more multinucleate RPE cells in aged *CFH-HH:Cfh-/-*~HFC mice. Scale bar = 50  $\mu$ m. (C) Quantitation of multinucleated ( $n \geq 3$  nuclei) RPE cells per field view in aged *CFH:Cfh-/-* mice on ND and HFC diet shows no change in the number of multinucleate RPE cells in aged *CFH-Y:Cfh-/-*~ND (N=8) and *CFH-Y:Cfh-/-*~HFC (N=8) mice. Aged *CFH-HH:Cfh-/-*~HFC mice (N=11) have a statistically larger number of multinucleated cells per field view than *CFH-HH:Cfh-/-*~ND mice (N=7). The asterisk (\*) indicates post hoc Tukey for a  $P < 0.05$  following a statistically significant genotype by diet interaction by ANOVA for the mean number of multinucleate RPE cells. Data is presented as mean  $\pm$  SEM.**

### 3.2.4 HFC Diet-induced Sub-RPE Deposits Increase In Mice Expressing Human H402 CFH

Sub-RPE basal laminal deposits have been shown to accumulate in mouse models of AMD (79-81). However, sub-RPE deposit accumulation can also occur in the absence of other AMD-like changes like visual impairment or RPE damage as we have shown in aged *Cfh-/-* mice after HFC diet which do not develop decreased ERG B-wave

responses or increased numbers of multinucleate RPE cells compared to age-matched *Cfh*<sup>+/-</sup> mice after HFC diet (80). Sub-RPE deposit accumulation was quantitatively measured in aged *CFH:Cfh*<sup>-/-</sup> mice on and off HFC diet by transmission electron microscopy (TEM) as previously described with a slight modification detailed in the methods (79).

All aged *CFH:Cfh*<sup>-/-</sup> mice irrespective of diet treatment had sub-RPE deposits (Fig. 19A). The sub-RPE deposit heights were graphed by their cumulative frequencies revealing that aged *CFH-HH:Cfh*<sup>-/-</sup>~ND mice accumulate less deposits than age-matched *CFH-Y:Cfh*<sup>-/-</sup>~ND mice but the *CFH-HH:Cfh*<sup>-/-</sup>~HFC mice accumulate statistically significantly ( $P < 0.05$ ) more larger deposits than aged *CFH-HH:Cfh*<sup>-/-</sup>~ND mice (Fig. 19). Sub-RPE deposit accumulation was also analyzed in younger adult (36-40 week old) *CFH:Cfh*<sup>-/-</sup>~ND and ~HFC diet to confirm that advanced aging is required for HFC-induced deposit formation. As expected, there was no sub-RPE deposit accumulation in young *CFH:Cfh*<sup>-/-</sup> mice fed either diet (Figure 32 in Appendix B). These results establish a CFH variant difference in age-related and HFC diet-induced sub-RPE deposits.

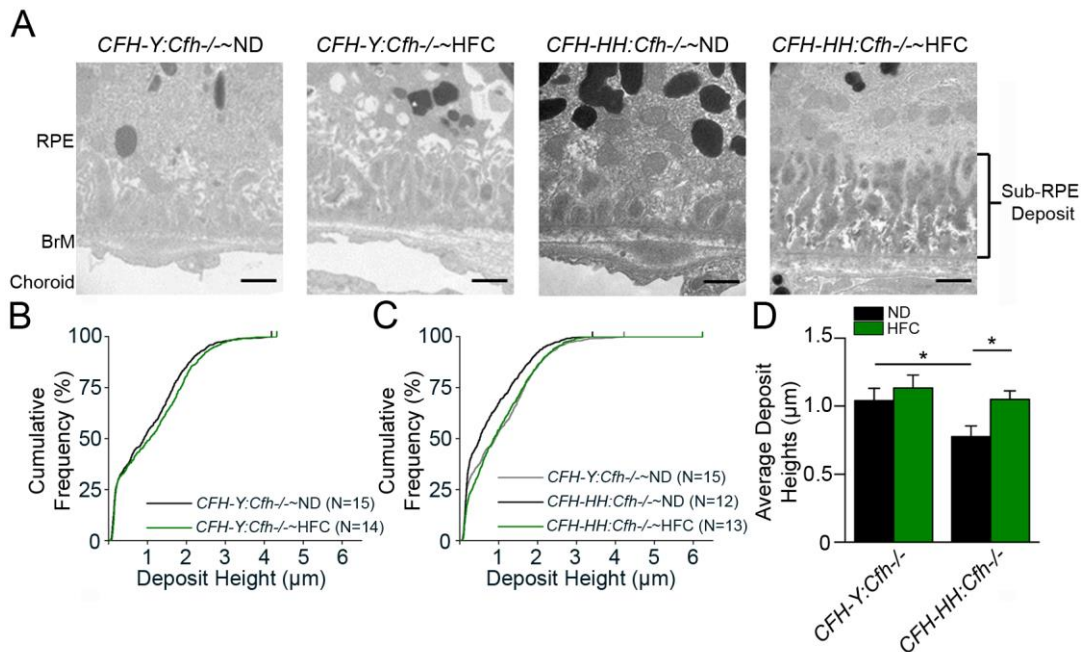


**Figure 19: Aged *CFH-HH:Cfh-/-~HFC* mice have increased sub-RPE deposits.** (A) Transmission electron micrograph (TEM) images (15000X magnification) of the sub-RPE region were used to quantitate the size of sub-RPE deposits in aged *CFH-Y:Cfh-/-* and *CFH-HH:Cfh-/-* mice on ND and HFC diet. Representative TEM images show all aged *CFH-Y:Cfh-/-* and *CFH-HH:Cfh-/-* mice have sub-RPE deposits irrespective of diet treatment. However, deposits in aged *CFH-HH:Cfh-/-~ND* mice appear the smallest compared to the other groups in this study. Scale bar = 1 µm. (B) Sub-RPE deposit heights in aged *CFH-Y:Cfh-/-~ND* and ~HFC mice. Deposits were measured from the elastic layer of Bruch's membrane (BrM) to the top of the largest sub-RPE deposit within each TEM image. Cumulative frequencies of the sub-RPE basal laminal deposit heights were plotted against deposit height to illustrate the distribution of sub-RPE deposit heights for the genotype and diet. There is a slight shift to the right in the distribution of larger sub-RPE deposits and demonstrates an increase in sub-RPE deposit sizes in aged *CFH-Y:Cfh-/-~HFC* mice (green) compared to aged *CFH-Y:Cfh-/-~ND* mice (black). (C) Sub-RPE deposit heights in aged *CFH-HH:Cfh-/-~ND* and *CFH-HH:Cfh-/-~HFC* mice. Aged *CFH-Y:Cfh-/-~ND* mice (gray) have larger sub-RPE deposits compared to aged *CFH-HH:Cfh-/-~ND* mice (black). Aged *CFH-HH:Cfh-/-~HFC* mice (green) have larger sub-RPE deposits than aged *CFH-HH:Cfh-/-~ND* mice but similar sub-RPE deposits as those found in aged *CFH-Y:Cfh-/-~ND* mice. (D) Averages of deposit heights in *CFH:Cfh-/-* mice after HFC diet. The

deposit height averages replicate the trends observed in the cumulative frequency plots. The asterisk (\*) indicates post hoc Tukey for a  $P < 0.05$  following a statistically significant genotype by diet interaction by ANOVA for the mean sub-RPE deposit heights. Data is presented as mean  $\pm$  SEM.

### 3.2.5 HFC Diet-Induced Complement Activation is Independent of CFH 402 Variant Expressed

We have previously shown that complement dysregulation is associated with development of visual loss and increased RPE dysmorphogenesis in aged *Cfh* hemizygous mice following consumption of a HFC diet (80). Here, levels of complement components were compared in aged *CFH-Y:Cfh*<sup>-/-</sup>~HFC and *CFH-HH:Cfh*<sup>-/-</sup>~HFC mice to assess complement activation in response to the HFC diet. There were statistically significant ( $P < 0.05$ ) increases in plasma levels of CFH (Fig. 20A), FB (Fig. 20B) and C3/C3b/iC3b (Fig. 20C) in both the aged *CFH-Y:Cfh*<sup>-/-</sup> and *CFH-HH:Cfh*<sup>-/-</sup> mice after the HFC diet compared to ND fed age-matched controls. Further support for increased complement activation in the plasma was gleaned from analysis of levels of iC3b, a C3 fragment indicative of complement activation, in reduced plasma samples from aged *CFH:Cfh*<sup>-/-</sup>~ND and ~HFC diet mice (Fig. 20D). There was a statistically significant increase of plasma iC3b in both *CFH-Y:Cfh*<sup>-/-</sup>~HFC ( $P < 0.01$ ) and *CFH-HH:Cfh*<sup>-/-</sup>~HFC diet mice ( $P < 0.05$ ) compared to normal diet fed controls (Fig. 20D). No statistically significant differences in the levels of plasma iC3b were measured between aged *CFH-Y:Cfh*<sup>-/-</sup>~HFC and *CFH-HH:Cfh*<sup>-/-</sup>~HFC mice (Fig. 20D). Complement activation in the

eyecup (RPE/BrM/choroid/sclera) lysates of aged *CFH-Y:Cfh-/-*~HFC and *CFH-HH:Cfh-/-*~HFC mice was analyzed by measuring total FB and C3/C3b/iC3b. There was a statistically significant increase in FB levels in the eyecups of both aged *CFH-Y:Cfh-/-* ( $P<0.01$ ) and *CFH-HH:Cfh-/-* ( $P<0.05$ ) mice on HFC compared to normal diet fed controls but the this increase in FB with HFC diet was not different between the genotypes (Fig. 20E). Interestingly, there was no statistically significant increase in the eyecup levels of C3/C3b/iC3b between the genotypes following consumption of the HFC diet (Fig. 20F). This data suggests the phenotypic differences between aged *CFH-Y:Cfh-/-*~HFC and *CFH-HH:Cfh-/-*~HFC mice is not due to HFC-induced complement activation.

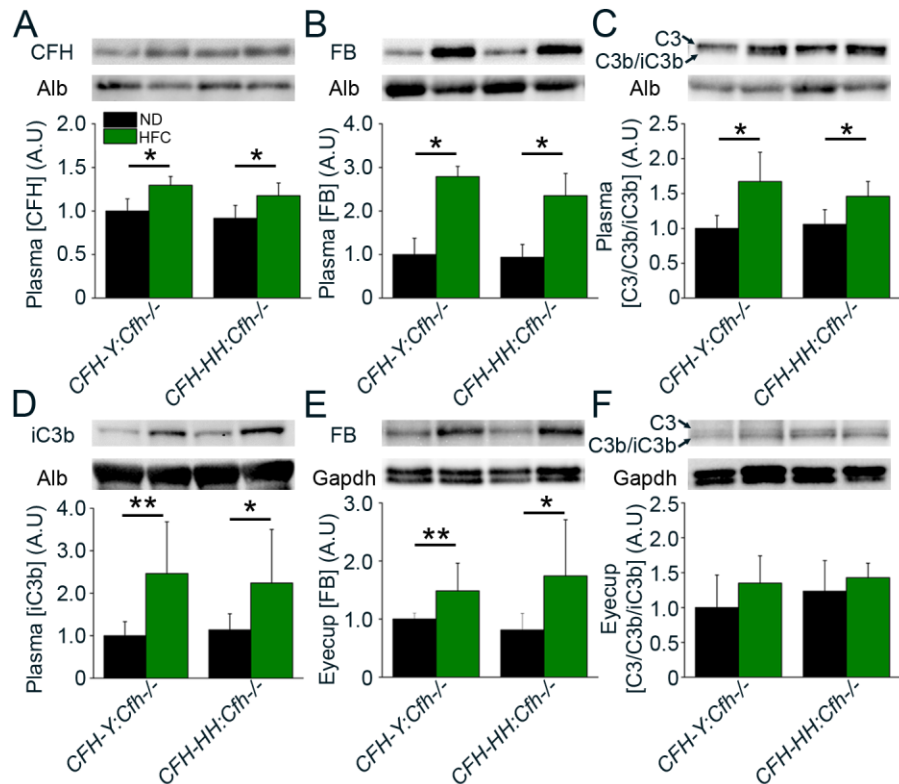


**Figure 20: HFC diet-induced complement activation is *CFH:Cfh*<sup>-/-</sup> genotype independent. (A-D) Densitometric analysis of CFH (A), FB (B), C3/C3b/iC3b (C) and iC3b (D) immunoblots of plasmas from aged *CFH:Cfh*<sup>-/-</sup>~ND and ~HFC mice after fasting. Plasma CFH, FB and C3/C3b/iC3b significantly increased in fasted *CFH-Y:Cfh*<sup>-/-</sup>~HFC and *CFH-HH:Cfh*<sup>-/-</sup>~HFC mice compared to ND fed controls but were no differences in the levels between the genotypes after HFC diet treatment (N=4). (D) Plasma samples were reduced before loading to quantitate iC3b levels (N=8). Both *CFH-Y:Cfh*<sup>-/-</sup>~HFC and *CFH-HH:Cfh*<sup>-/-</sup>~HFC mice had significantly increased levels of plasma iC3b compared to ND fed controls and show similar levels of plasma complement activation between these genotypes after HFC diet. (E-F) Densitometric analysis of FB (E) and C3/C3b/iC3b (F) immunoblots of eyecups (RPE/BrM/choroid/sclera) from fasted, aged *CFH:Cfh*<sup>-/-</sup>~ND and ~HFC mice (N=7). FB levels were significantly higher in fasted *CFH-Y:Cfh*<sup>-/-</sup>~HFC and *CFH-HH:Cfh*<sup>-/-</sup>~HFC mice compared to ND fed controls but not different between the genotypes on HFC diet. Interestingly, no statistically significant differences in the C3/C3b/iC3b levels were detected between the genotypes on ND versus HFC diet (N=7). The asterisks (\*,\*\*) indicate post hoc Tukey for a P<0.05 and <0.01 following a statistically**

significant genotype by diet interaction by ANOVA for the densitometric arbitrary units. Data is presented as mean  $\pm$  SD.

### **3.3 Discussion**

AMD is a complex retinal degeneration presenting in elderly populations with limited therapeutic options for patients. One of the strongest genetic risk factors for AMD is the *CFH* Y402H polymorphism, but the role of the risk-associated H402 CFH in AMD is unclear (146-149). We studied the effects of advanced aging and a HFC diet in mice expressing full-length forms of the normal Y402 (*CFH-Y:Cfh<sup>-/-</sup>*) and risk-associated (*CFH-HH:Cfh<sup>-/-</sup>*) forms of CFH to elucidate the *in vivo* impact of this AMD genetic risk factor. *CFH:Cfh<sup>-/-</sup>* mice were aged to ninety weeks and maintained on a ND diet or switched to a HFC diet for eight weeks to elicit the formation of AMD-like pathologies as observed in other mouse models (73, 80, 81, 119). The HFC diet caused significant phenotypic changes (decreased ERGs, increased RPE multinucleated cells and increased sub-RPE deposits) in the aged *CFH-HH:Cfh<sup>-/-</sup>* mice compared to age-matched control *CFH-HH:Cfh<sup>-/-</sup>* mice maintained on a ND, but these HFC diet induced changes were not documented in the *CFH-Y:Cfh<sup>-/-</sup>* mice or in young adult *CFH:Cfh<sup>-/-</sup>*-HFC mice. While we are not the first laboratory to use mice to investigate the role of the H402 variant in AMD (82, 85, 234), our study is the first to find CFH variant differences in a chronic multifactorial model incorporating advanced aging, genetics and environmental stress.

The risk association between the CFH Y402H polymorphism and AMD is widely believed to result from reduced activity of the CFH H402 variant to regulate C3 activation resulting in complement-mediated inflammation in posterior eye tissues (155). Previous studies have shown that there are increased activated complement components in the plasmas of AMD patients (199-201, 204) and localization of activated complement products within drusen of AMD donor eyes (117, 123, 144), but the role of complement activation in AMD pathogenesis remains unknown. We have previously shown that excess complement activation contributes to the development of HFC-induced visual loss and RPE damage in the *Cfh*<sup>+/-</sup> AMD mouse model (80). In this study the two mouse variants had equal amounts of complement activation yet visual loss and RPE damage was detected only in the *CFH-HH:Cfh*<sup>-/-</sup>~HFC mice, supporting that the H402 CFH variant was in some way damaging or that the Y402 CFH was protective. These CFH variant differences are likely due to a differential binding to a biological molecule or epitope as has been described in previous studies (85, 182, 184-189). The Y402 to H402 change in CFH in the SCR 7 region of the molecule has been shown to have significant consequences in the binding affinity of CFH and other molecules. For example, there is differential binding to heparan sulfate (187), which may result in less CFH H402 binding to the ECM or cell surfaces resulting in increased complement activation. In addition, differential binding of Y402 and H402 variants to CD47 results in

H402 variant inhibiting binding of thrombospondin-1 to CD47 on mononuclear phagocytes, thus preventing their subsequent elimination (85). Finally, differential binding to malondialdehyde (MDA) has been shown in which the Y402 variant has a higher affinity for MDA thereby neutralizing its potentially damaging effects (188). The model of AMD that is described in this paper supports the roles of these or other binding disparities, being responsible for the pathogenic mechanism responsible for the phenotype seen in the old *CFH-HH:Cfh-/-*~HFC mice.

In conclusion, we present differences between how the Y402 and H402 CFH variants modulate the response of aged posterior eye tissues to the consumption of a HFC diet in mice. Our results suggest the molecular differences explaining the phenotypes of aged *CFH-Y:Cfh-/-*~HFC and *CFH-HH:Cfh-/-*~HFC mice are not at the level of complement activation. Understanding the role of the HFC diet in exacerbating AMD-like pathologies in aged *CFH-HH:Cfh-/-* mice will undoubtedly lead to the molecular underpinnings behind the risk association between the H402 variant and AMD risk. These results also provide insight as to why complement inhibitors have not been successful as a treatment for AMD.

## 4. Dietary Cholesterol Causes Visual Loss in a Complement-Dysregulated AMD Mouse Model

### 4.1 Introduction

The consumption of a HFC diet is a critical insult needed to elicit pathological differences between aged *CFH:Cfh<sup>-/-</sup>* mice. Diet and its impact on health (obesity and hypertension) have been mildly associated with AMD risk but these studies are retrospective and notoriously difficult to control due to confounding variables such as genetics, metabolic status and microbiome of the study participants (235, 236). However, some general consensuses are agreed upon in the field. Notably, consuming a Mediterranean-style diet or other diets that are high in vegetables, fruits, nuts and fish appear to lower an individual's risk for AMD (237-239). In contrast, consumption of a Western-style diet that contains saturated fats, cholesterol and processed foods increases the risk for AMD (240).

Only a few mouse models include the consumption of a diet to elicit AMD-like pathologies. The diets tested in these models include a high fat, cholesterol-enriched (HFC) (73, 80, 107), only high fat (87), high glycemic (75) and low glycemic diets (241). Although these diets have different compositions (73, 75, 80, 87, 107, 241), it is unclear the dietary-induced effect required for the development of ocular pathologies in these mice. Understanding the role of diet in eliciting the AMD-like pathologies in mice will

undoubtedly lead to the molecular underpinnings behind the association of the H402 CFH variant and AMD risk.

In this study, we interrogated the role of the HFC diet to determine the molecular differences between aged *CFH-Y:Cfh-/-*~HFC and *CFH-HH:Cfh-/-*~HFC mice. Aged *CFH-Y:Cfh-/-* and *CFH-HH:Cfh-/-* were evaluated for HFC diet-induced systemic pathologies. Both lines of mice develop similar non-alcoholic steatohepatitis (NASH)-like liver pathologies after HFC diet, a common pathological symptom seen in wild type C57 mice after the consumption of dietary cholesterol (242). We hypothesized aged *CFH-HH:Cfh-/-*~HFC mice have impaired ocular cholesterol regulation compared to *CFH-Y:Cfh-/-*~HFC mice and this contributes to the development of AMD-like pathologies in the *CFH-HH:Cfh-/-*~HFC mice. This hypothesis was tested by feeding aged *CFH-HH:Cfh-/-* mice a high fat but with no added cholesterol (HF) or high cholesterol with no added fat (HC) diet to examine the role of dietary cholesterol in AMD-like pathology development. Aged *CFH-HH:Cfh-/-* mice fed a HFC or HC diet developed a statistically significant decrease in visual function that correlated with plasma chylomicrons (CMs), very low-density lipoproteins (VLDLs) and low-density lipoproteins (LDLs) but not with complement activation. To determine if these lipoproteins were changed in mice with different visual responses after HFC diet, lipoprotein levels were assessed in aged *CFH-Y:Cfh-/-*~HFC and *CFH-HH:Cfh-/-*~HFC revealing less circulating LDLs in aged *CFH-*

*HH:Cfh*<sup>-/-</sup> mice compared to aged *CFH-Y:Cfh*<sup>-/-</sup> mice. Strikingly, in the eyecup lysates, we observed increases in ApoA1 in only aged *CFH-HH:Cfh*<sup>-/-</sup> mice after diet. ApoA1 is an HDL-associated apolipoprotein critical for reverse cholesterol transport and is required for lipid efflux from peripheral tissues (243). These findings suggest the CFH Y402H polymorphism effects systemic and local lipoprotein levels *in vivo*.

## **4.2 Results**

### **4.2.1 HFC diet consumption causes NASH-like liver pathologies in *CFH:Cfh*<sup>-/-</sup>~HFC mice**

As shown in Chapter 3, aged *CFH-HH:Cfh*<sup>-/-</sup>, but not *CFH-Y:Cfh*<sup>-/-</sup>, mice develop an AMD-like phenotype after the consumption of an eight week HFC diet. To understand the role of the HFC diet in AMD-like pathology development in aged *CFH-HH:Cfh*<sup>-/-</sup> mice, aged *CFH:Cfh*<sup>-/-</sup>~ND and ~HFC mice were evaluated for systemic pathologies related to the HFC diet consumption. Both aged *CFH-Y:Cfh*<sup>-/-</sup>~HFC and *CFH-HH:Cfh*<sup>-/-</sup>~HFC diet mice develop enlarged, yellowish livers (Fig. 21A) that were twice the size of those seen in ND fed controls (Fig. 21A). Livers were processed and stained with hematoxylin and eosin (H&E) to assess for pathohistological markers of liver disease. Both genotypes displayed vacuole changes representing fat vacuoles and increased inflammation as marked by increased immune cell infiltration (Fig. 21B). These pathohistological signs are characteristic of non-alcoholic steatohepatitis (NASH)-

like pathologies (244). No differences in the severity of NASH-like liver pathologies were seen between aged *CFH-Y:Cfh-/-*~HFC and *CFH-HH:Cfh-/-*~HFC mice.

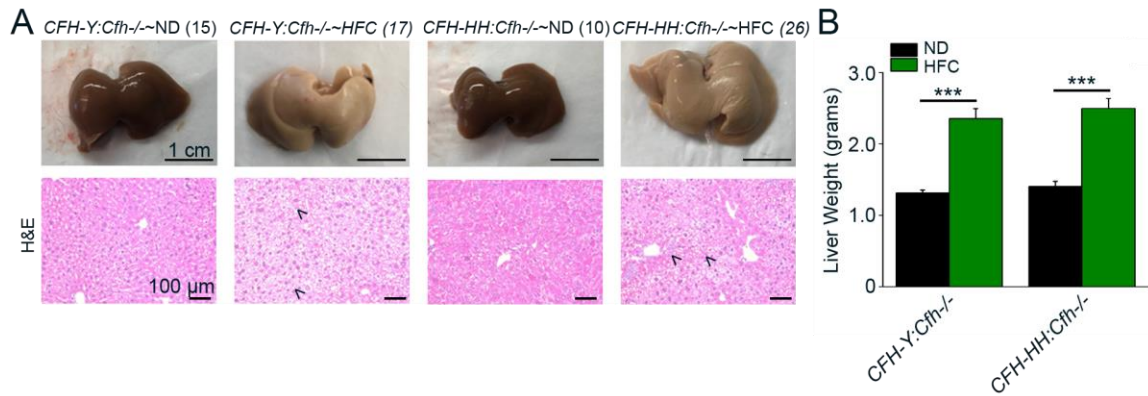


**Figure 21: Aged *CFH:Cfh-/-* mice develop non-alcoholic steatohepatitis-like (NASH) liver pathologies after HFC diet consumption. (A) Aged *CFH-Y:Cfh-/-*~HFC and *CFH-HH:Cfh-/-*~HFC mice develop characteristic pathohistological signs of NASH such as enlarged yellowish livers, macrovacuolar changes and inflammation compared to aged *CFH-Y:Cfh-/-*~ND and *CFH-HH:Cfh-/-*~ND mice (245). Arrowheads depict macrovacuoles and immune cell recruitment. (B) Liver weights show aged *CFH:Cfh-/-*~HFC mice have livers that are significantly larger than those in aged *CFH:Cfh-/-*~ND mice. No difference in liver weights were seen between aged *CFH-Y:Cfh-/-*~HFC and *CFH-HH:Cfh-/-*~HFC mice. The asterisks (\*\*\*) indicate post hoc Tukey for a  $P < 0.001$  following a statistically significant genotype by diet interaction by ANOVA for the liver weights.**

#### 4.2.2 Dietary cholesterol consumption causes NASH in aged *CFH-HH:Cfh-/-* mice

NASH-like liver pathologies result from the consumption of dietary cholesterol in mice (242). Diets based on the HFC diet recipe were generated in which added cholesterol or added cocoa butter fat was omitted to create a high fat (HF) or high cholesterol (HC) diet, respectively. NASH-like liver pathologies were evaluated in aged

*CFH-HH:Cfh<sup>-/-</sup>* mice fed an eight week ND, HFC, HF, or HC diet. Only aged *CFH-HH:Cfh<sup>-/-</sup>* mice consuming diets containing dietary cholesterol developed yellowish livers that had pathohistological signs of NASH such as macrovacuolar changes and immune cell infiltration compared to normal diet and HF fed controls (Fig. 22A). The livers of aged *CFH-HH:Cfh<sup>-/-</sup>~HFC* and *~HC* mice were twice the size of the livers from aged *CFH-HH:Cfh<sup>-/-</sup>~ND* and *~HF* mice (Fig. 22B). These diets are sufficient to modulate systemic cholesterol levels and dietary cholesterol-induced NASH. Next we used these diets to interrogate the role of dietary cholesterol in the age-dependent AMD-like pathologies that develop in the aged *CFH-HH:Cfh<sup>-/-</sup>* mice.

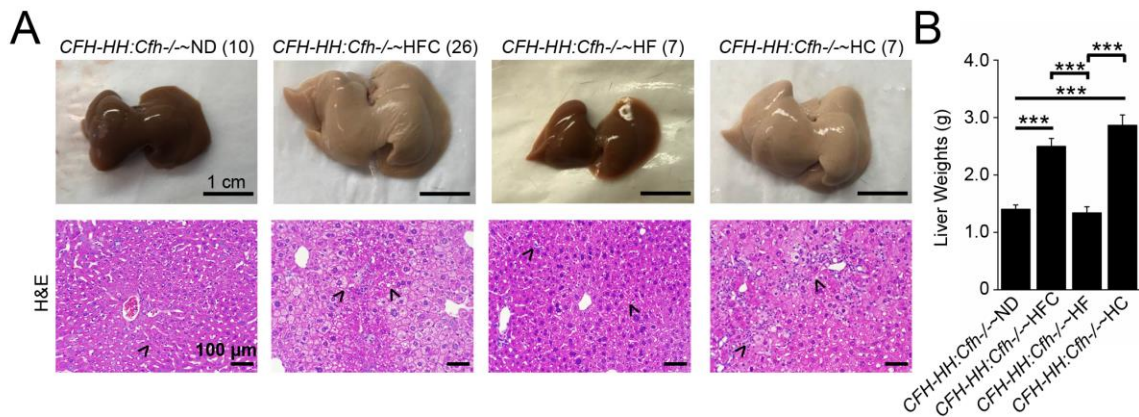


**Figure 22: Aged *CFH-HH:Cfh<sup>-/-</sup>* mice develop NASH liver pathologies that is dietary cholesterol consumption dependent. (A) Aged *CFH-HH:Cfh<sup>-/-</sup>~HFC* and *~HC* mice, but not aged *CFH-HH:Cfh<sup>-/-</sup>~ND* and *~HF*, develop characteristic NASH-like liver pathologies. Arrowheads depict macrovacuoles and immune cell recruitment. (B) Liver weights show aged *CFH:Cfh<sup>-/-</sup>~HFC* and *~HC* mice have livers that are significantly larger than those in aged *CFH:Cfh<sup>-/-</sup>~ND* and *~HF* mice. The asterisks (\*\*\*) indicate post hoc Tukey for a P<0.001 following a statistically significant genotype by diet interaction by ANOVA for the liver weights.**

### 4.2.3 Dietary cholesterol contributes to visual loss in aged *CFH-HH:Cfh*<sup>-/-</sup> mice

Aged *CFH-HH:Cfh*<sup>-/-</sup> develop significant visual loss after the consumption of an eight week HFC diet. Visual function of aged *CFH-HH:Cfh*<sup>-/-</sup> mice was assessed after the consumption of an eight-week HF or HC diet by scotopic ERG. Using another cohort of aged *CFH-HH:Cfh*<sup>-/-</sup> mice, these mice develop a similar decrease of scotopic ERG B-wave responses after the consumption of an eight week HFC diet (Fig. 23A) as previously described in Figure 16. No change was observed in aged *CFH-HH:Cfh*<sup>-/-</sup>~HF mice relative to aged *CFH-HH:Cfh*<sup>-/-</sup>~ND mice (Fig. 23B). Remarkably, aged *CFH-HH:Cfh*<sup>-/-</sup>~HC mice developed significantly attenuated ERG B-wave responses compared to aged *CFH-HH:Cfh*<sup>-/-</sup>~ND mice (Fig 23C) . This data shows the visual loss in aged *CFH-HH:Cfh*<sup>-/-</sup> mice is contingent on consuming dietary cholesterol.

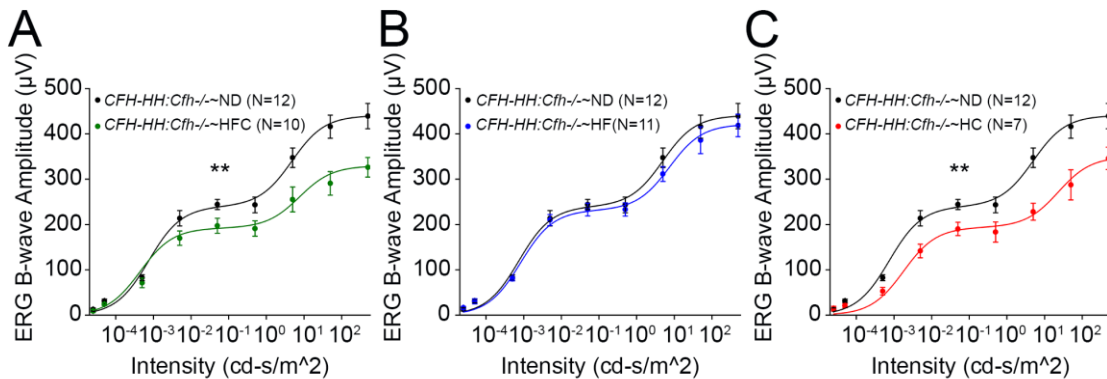


**Figure 23: Visual function loss in aged *CFH-HH:Cfh*<sup>-/-</sup> mice consuming dietary cholesterol. Scotopic ERG flash responses in aged *CFH:Cfh*<sup>-/-</sup> mice fed a ND, HFC, HF or HC diet. Visual function was assessed by scotopic ERG and presented as fitted lines of the B-wave amplitude averages using the equation  $B = (B_{max1} * I / I + I_1) / (B_{max2} * I / I + I_2)$ . (A) Aged *CFH-HH:Cfh*<sup>-/-</sup>~HFC mice have decreased scotopic ERG**

B-wave responses compared to aged *CFH-HH:Cfh-/-*~ND mice. (B) There is no significant difference in aged *CFH-HH:Cfh-/-*~HF mice ERG B-wave responses compared to aged *CFH-HH:Cfh-/-*~ND mice. (C) Aged *CFH-HH:Cfh-/-*~HC mice had decreased ERG B-wave responses relative to aged *CFH-HH:Cfh-/-*~ND mice. The asterisks (\*\*) indicate post hoc Tukey for a  $P < 0.01$  following a statistically significant genotype by diet interaction by ANOVA for the mean areas under the B-wave flash response curves.

#### 4.2.4 Increased complement protein and activation levels in *CFH-HH:Cfh-/-* mice occur in the high fat and high cholesterol diets compared to the normal diet.

Complement protein and activation levels were similarly increased in aged *CFH-Y:Cfh-/-* and *CFH-HH:Cfh-/-* mice after HFC diet but did not correlate with the visual loss observed in aged *CFH-HH:Cfh-/-*~HFC mice. Various complement proteins were quantified in aged *CFH-HH:Cfh-/-* after an eight-week ND, HFC, HF or HC diet using Western Blot analysis. Independent of the diet consumed by aged *CFH-HH:Cfh-/-* mice, there was a similar increase in plasma CFH (Fig. 24A), FB (Fig. 24B) and C3/C3b/iC3b (Fig. 24C) after the HFC, HF or HC diet consumption in aged *CFH-HH:Cfh-/-* mice compared to those fed a normal diet. No change was noted in C5 (Fig. 24D), a downstream effector of the complement cascade. Activation of the complement cascade was measured by the levels of Bb and iC3b, both cleaved protein products indicative of the C3 convertase formation. Bb (Fig. 24E) and iC3b (Fig. 24F) levels were increased in aged *CFH-HH:Cfh-/-* mice fed a HFC, HF, and HC diet compared to *CFH-HH:Cfh-/-*~ND

mice. Based on these results, diet-induced increases of plasma complement components do not correlate with visual loss in aged *CFH-HH:Cfh<sup>-/-</sup>* mice.

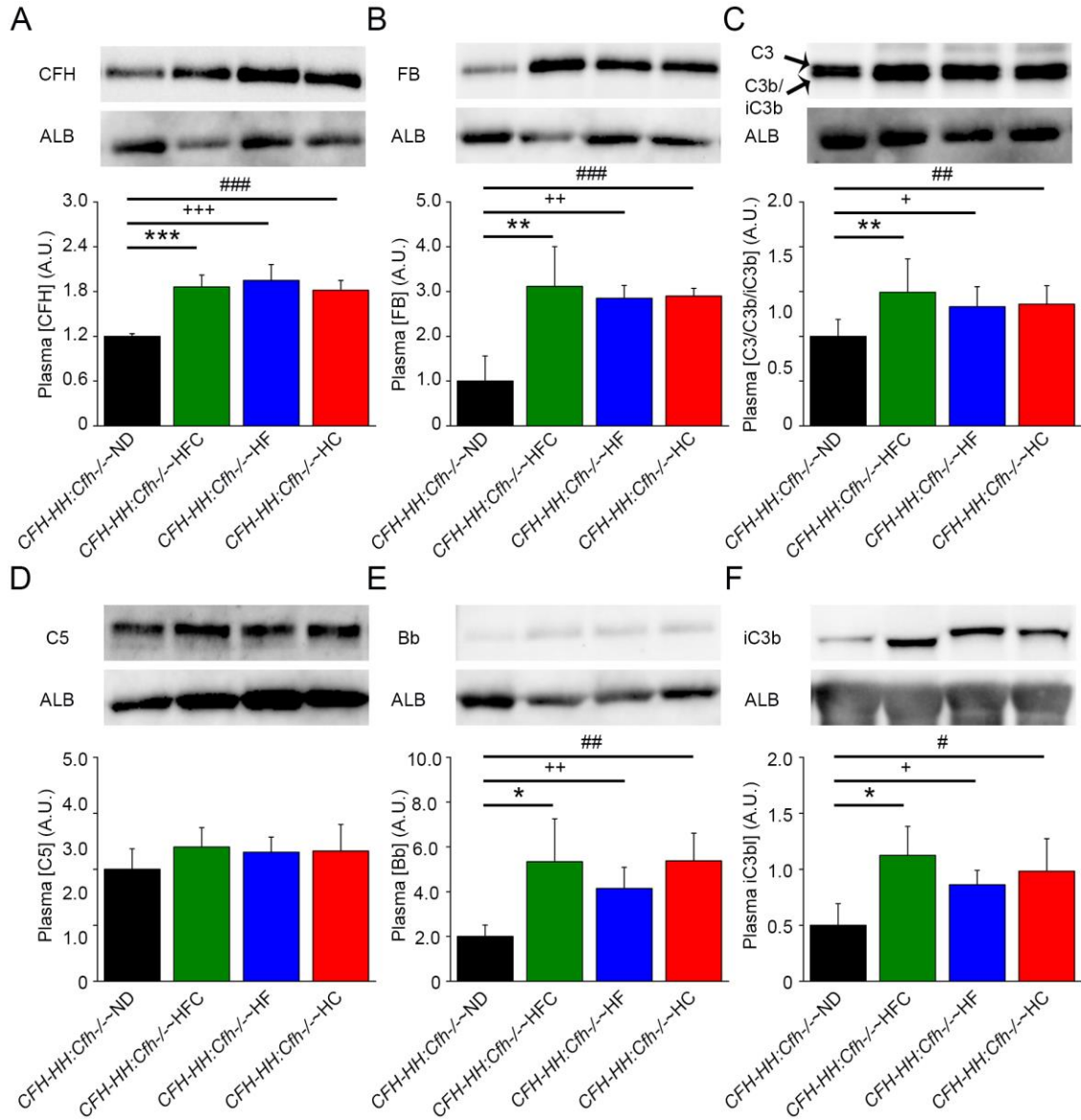


**Figure 24: Diet-induced complement activation is independent of visual function loss in aged *CFH-HH:Cfh<sup>-/-</sup>* mice. (A-D) Densitometric analysis of CFH (A), FB (B), C3/C3b/iC3b (C), C5 (D), Bb (E) and iC3b (F) immunoblots of plasmas from aged *CFH:Cfh<sup>-/-</sup>~ND* and *~HFC* mice after fasting. Plasma CFH, FB and C3/C3b/iC3b**

significantly increased in fasted *CFH-HH:Cfh-/-*~HFC, ~HF and ~HC mice compared to ND fed controls but were no differences in the levels between them after diet treatment (N=4-8). Plasma complement activation levels were quantified by the cleavage products, Bb (E) and iC3b (F). Bb significantly increased in fasted *CFH-HH:Cfh-/-*~HFC, ~HF and ~HC mice compared to *CFH-HH:Cfh-/-*~ND mice (N=8). (F) Plasma samples were reduced before loading to quantitate iC3b levels (N=8). *CFH-HH:Cfh-/-*~HFC, ~HF, and ~HC mice had significantly increased levels of plasma iC3b compared to ND fed controls (N=4). The asterisks (\*, \*\*, \*\*\*) indicate post hoc Tukey for a P<0.05 and <0.01 following a statistically significant genotype by diet interaction by ANOVA for the densitometric arbitrary units. \*, + and # depict HFC, HF and HC diet versus ND diet, respectively. Data is presented as mean ± SD.

#### **4.2.5 Diet modulates the levels of lipoproteins in aged *CFH-HH:Cfh-/-* mice.**

Consumption of an HFC diet increases circulating lipoproteins containing cholesterol in wild type C57 mice (246). Lipoprotein levels in aged *CFH-HH:Cfh-/-* mice after the HFC, HF or HC diet consumption were quantified by fractionating mouse plasma using fast protein liquid chromatography (FPLC). In the normal rodent chow diet fed mice, all the cholesterol is retained within high-density lipoprotein (HDL) particles (Fig. 25A). Aged *CFH-HH:Cfh-/-* mice consuming the HFC and HC have increased chylomicron (CMs), very-low density lipoproteins (VLDLs), and low-density lipoproteins (LDLs) containing cholesterol compared to aged *CFH-HH:Cfh-/-*~HF mice (Fig. 25A). The area under each lipoprotein curve was calculated and confirmed the levels of these lipoproteins were statistically different between these groups (Fig. 25B). The increases in CM/VLDL and LDL containing cholesterol are associated with visual

loss in aged *CFH-HH:Cfh*<sup>-/-</sup> mice.

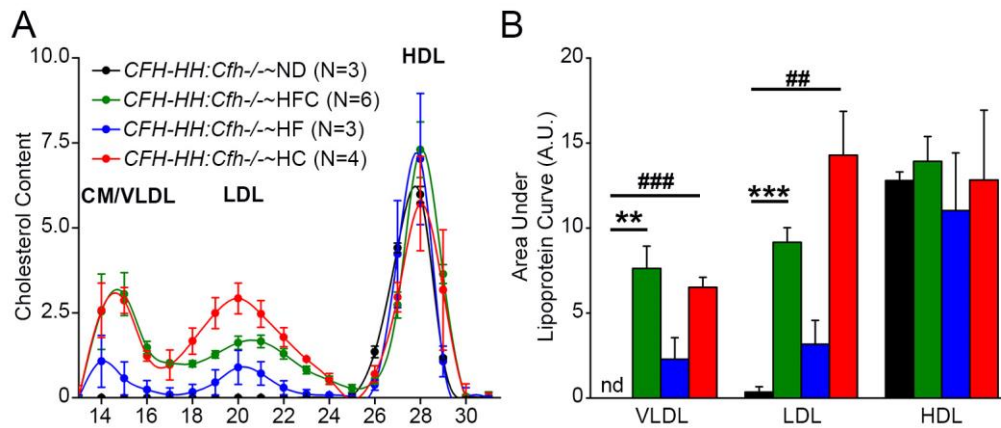


**Figure 25: Dietary cholesterol modulates the circulating lipoprotein levels in aged *CFH:Cfh*<sup>-/-</sup> mice.** Plasmas obtained from fasted *CFH-HH:Cfh*<sup>-/-</sup>~ND (black), ~HFC (green), ~HF (blue) and ~HC (red) mice were fractionated using FPLC. (A) Low to no cholesterol was detected in the fractions associated with chylomicrons CMs, very low-density VLDLs and low-density lipoproteins LDLs in *CFH-HH:Cfh*<sup>-/-</sup>~ND mice. In contrast, increases in CM-, VLDL- and LDL-associated cholesterol were detected in the *CFH-HH:Cfh*<sup>-/-</sup>~HFC, ~HF and ~HC mice. (B) Areas under the lipoprotein curves. Significant increases in VLDL- and LDL-associated cholesterol fractions were measured in *CFH-HH:Cfh*<sup>-/-</sup>~HFC and ~HC, but not ~HF, mice compared to *CFH-HH:Cfh*<sup>-/-</sup>~ND mice. The asterisks (\*\*, \*\*\*) indicate post hoc Tukey for a  $P < 0.01$  and  $< 0.001$  following a statistically significant genotype by diet interaction by ANOVA for the area arbitrary units. \* and # depict HFC and HC diet versus ND diet, respectively. Data is presented as mean  $\pm$  SEM.

These FPLC results were confirmed by measuring apolipoprotein concentrations on Western blot analysis of fasted plasma samples. Plasma from an aged *CFH-HH:Cfh*<sup>-/-</sup>~HFC mouse was fractionated and separated under non-reducing conditions to determine the distribution of apolipoproteins on mouse lipoproteins since there are differences between mouse and human lipoproteins (247). ApoB100 and ApoB48 (Figure 32A in Appendix C) as well as ApoE (Figure 32B in Appendix C) are predominantly

found in the fractions that correlate with CMs, VLDLs and LDLs. In contrast, ApoA1 is only detected in HDL fractions (Figure 32C in Appendix C). ApoB48 (Fig. 26A) increased but ApoB100 (Fig. 26B) was unchanged in aged *CFH-HH:Cfh-/-*~HFC, ~HF, and ~HC diet mice compared to aged *CFH-HH:Cfh-/-*~ND mice. ApoE levels increased in all groups compared to ND fed controls but were significantly increased in mice consuming dietary cholesterol (Fig, 26C). No change in was seen in ApoA1 levels between these groups of mice (Fig, 26D). The increases in plasma ApoE correlated with visual loss in aged *CFH-HH:Cfh-/-* mice.

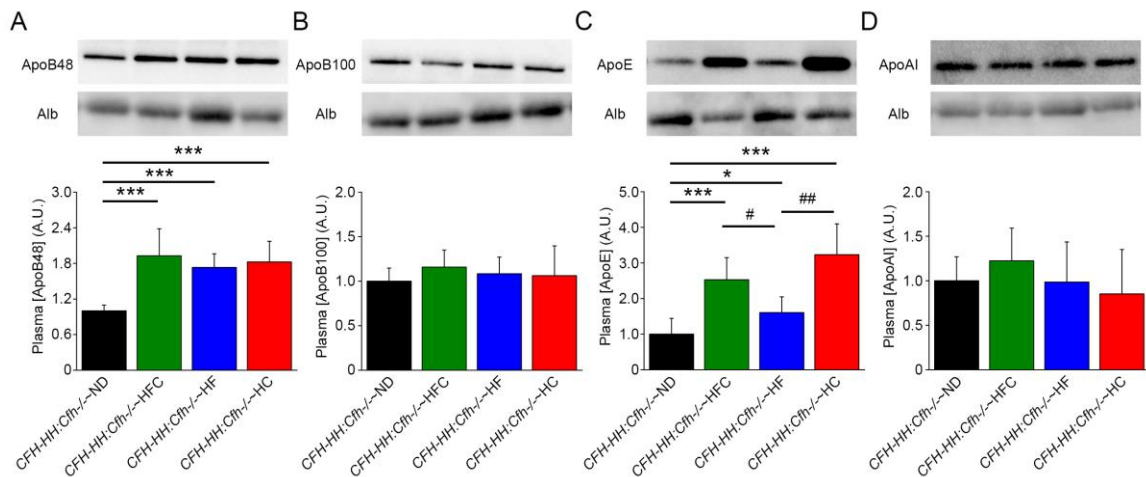


**Figure 26: Plasma ApoE in *CFH-HH:Cfh-/-* is dietary cholesterol dependent. (A-D) Densitometric analysis of ApoB48 (A), ApoB100 (B), ApoE (C) and ApoA1 (D) immunoblots of fasted plasmas from aged *CFH:Cfh-/-*~ND, HFC, ~HF and ~HC mice (N=4-8). ApoB48 levels increased in mice fed a HFC, HF, and HC diet compared to ND fed controls. ApoB100 was unchanged in all groups of mice after diet treatment. ApoE increased significantly in mice fed a HFC, HF, and HC diet compared to ND fed controls. ApoE was significantly higher in *CFH-HH:Cfh-/-*~HFC and ~HC mice compared to *CFH-HH:Cfh-/-*~HF mice. ApoA1 was unchanged after diet treatment. The asterisks (\*, \*\*, \*\*\*) indicate post hoc Tukey for a  $P > 0.05$ ,  $P < 0.01$  and  $P < 0.001$  following a**

statistically significant genotype by diet interaction by ANOVA for the densitometric arbitrary units. \* and # depict HFC and HC diet versus ND diet and HFC and HC diet versus HF diet, respectively. Data is presented as mean  $\pm$  SD.

#### 4.2.6 Plasma Low-Density Lipoprotein (LDL) Levels Are CFH Variant Dependent

Levels of cholesterol-containing CMs, VLDLs and LDLs as well as plasma ApoE correlate with visual loss in aged *CFH-HH:Cfh-/-* mice. To determine if HFC-diet induced increases in cholesterol are different between aged *CFH:Cfh-/-* mice, we measured total plasma cholesterol and found significantly higher levels in both aged *CFH-Y:Cfh-/-~HFC* ( $P<0.001$ ) and *CFH-HH:Cfh-/-~HFC* ( $P<0.001$ ) mice compared to ND fed controls (Fig. 27A). Interestingly, aged *CFH-HH:Cfh-/-~HFC* mice had significantly lower ( $P<0.01$ ) total plasma cholesterol than aged *CFH-Y:Cfh-/-~HFC* mice (Fig. 27A). We fractionated plasmas from aged *CFH:Cfh-/-~ND* and *~HFC* diet mice using FPLC. After the consumption of the HFC diet, we detect cholesterol within CM/VLDL and LDL particles in both aged *CFH-Y:Cfh-/-~HFC* and *CFH-HH:Cfh-/-~HFC* mice (Fig. 27B). We find fractions 17 to 21 and 25, corresponding to LDLs, are significantly lower in aged *CFH-HH:Cfh-/-~HFC* mice compared to *CFH-Y:Cfh-/-~HFC* mice (Fig. 27B). We calculated the area under the lipoprotein curves for each *CFH:Cfh-/-~HFC* diet mouse and found statistically lower ( $P<0.05$ ) LDL curves in aged *CFH-HH:Cfh-/-~HFC* mice compared to *CFH-Y:Cfh-/-~HFC* mice (Fig. 27C). This data reveals decreased cholesterol-containing LDL in aged *CFH-HH:Cfh-/-~HFC* mice compared to aged *CFH-Y:Cfh-/-~HFC* mice.

We confirmed our results by measuring apolipoprotein concentrations by Western blot analysis using fasted plasma samples. There was significantly higher ( $P<0.001$ ) plasma ApoB48 in both aged *CFH-Y:Cfh-/-~HFC* and *CFH-HH:Cfh-/-~HFC* mice compared to ND fed controls but this did not differ between the two genotypes after diet treatment (Fig. 27D). ApoB100 was significantly higher ( $P<0.05$ ) in aged *CFH-Y:Cfh-/-~HFC* mice compared to aged *CFH-Y:Cfh-/-~ND* and *CFH-HH:Cfh-/-~HFC* mice (Fig. 27E). Significantly higher levels of plasma ApoE were observed in *CFH-Y:Cfh-/-~HFC* ( $P<0.001$ ) and *CFH-HH:Cfh-/-~HFC* ( $P<0.01$ ) mice compared to ND controls and these ApoE levels were significantly higher ( $P<0.05$ ) in aged *CFH-Y:Cfh-/-~HFC* mice compared to aged *CFH-HH:Cfh-/-~HFC* mice (Fig. 27F). No difference was detected in plasma ApoA1 levels between the aged *CFH:Cfh-/-* mice after diet treatment (Fig. 27G). Taken together these results support that the CFH Y402H polymorphism impacts plasma LDL levels.

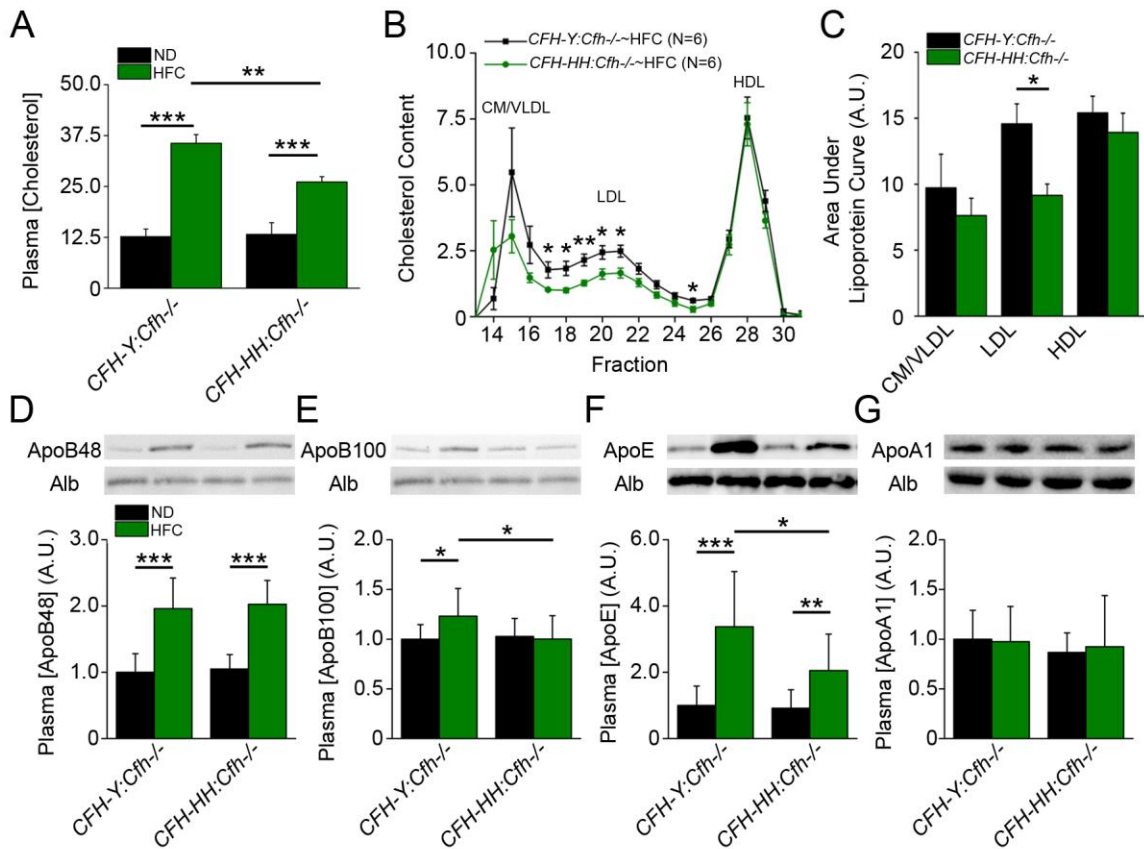


**Figure 27: Plasma lipoprotein levels are *CFH:Cfh-/-* variant dependent.** (A) Total plasma cholesterol in aged *CFH:Cfh-/-*~ND and ~HFC mice was measured by an enzymatic cholesterol assay in plasmas of fasted, aged *CFH:Cfh-/-* mice on ND and HFC diet. Both aged *CFH-Y:Cfh-/-*~HFC (N=11) and *CFH-HH:Cfh-/-*~HFC (N=11) mice have statistically significant higher total plasma cholesterol concentrations than age-matched *CFH-Y:Cfh-/-*~ND (N=8) and *CFH-HH:Cfh-/-*~HFC (N=8) mice, respectively. Aged *CFH-Y:Cfh-/-* mice have statistically higher levels of total plasma cholesterol compared to aged *CFH-HH:Cfh-/-* mice after diet. The asterisks (\*\*, \*\*\*) indicate post hoc Tukey for a  $P < 0.01$  and  $< 0.001$ , respectively, following a statistically significant genotype by diet interaction by ANOVA for the cholesterol concentration. (B-C) FPLC fractionation of plasma from fasted *CFH:Cfh-/-*~HFC mice. 30  $\mu$ l of plasma was FPLC fractionated and analyzed to evaluate chylomicron (CM)/very low-density lipoprotein (VLDL)-, low-density lipoprotein (LDL)- and high-density lipoprotein (HDL)-associated cholesterol peaks. (B) Following the HFC diet, cholesterol was detected in fractions corresponding to CMs, VLDLs and LDLs. There were significant increases in

the fractions 17-21 and 25 that corresponded to LDLs in the plasmas of aged *CFH-Y:Cfh-/-~HFC* mice compared to aged *CFH-HH:Cfh-/-~HFC* mice. The asterisks (\*, \*\*) indicate post hoc Tukey for a  $P < 0.05$  and  $< 0.01$ , respectively, following a statistically significant genotype by diet interaction by ANOVA for the cholesterol concentration in each fraction. (C) The area under the fractionated lipoprotein curve were calculated for each lipoprotein class and confirmed higher plasma LDL levels in aged *CFH-Y:Cfh-/-* mice after diet. The asterisks (\*, \*\*) indicate post hoc Tukey for a  $P < 0.05$  following a statistically significant genotype by diet interaction by ANOVA for the area under the lipoprotein curve corresponding to LDL. (D-G) Densitometric analysis of ApoB48 (D), ApoB100 (E), ApoE (F) and ApoA1 (G) immunoblots of plasmas from fasted, aged *CFH:Cfh-/-~ND* and *CFH:Cfh-/-~HFC* mice (N=8-12). ApoB48 levels were increased in both aged *CFH:Cfh-/-~HFC* murine lines after HFC diet but no difference was observed between genotypes. ApoB100 was significantly higher in aged *CFH-Y:Cfh-/-~HFC* mice compared to aged *CFH-Y:Cfh-/-~ND* but was unchanged in *CFH-HH:Cfh-/-* mice on ND or HFC diet. ApoE increased in both aged *CFH:Cfh-/-* mice lines on HFC diet compared to ND fed controls but aged *CFH-Y:Cfh-/-~HFC* mice had higher levels of ApoE than *CFH-HH:Cfh-/-~HFC* mice. ApoA1 was unchanged in both genotypes after HFC diet. The asterisks (\*, \*\*, \*\*\*) indicate post hoc Tukey for a  $P < 0.05$ ,  $< 0.01$  and  $< 0.001$ , respectively, following a statistically significant genotype by diet interaction by ANOVA for the densitometric arbitrary units. Data is presented as mean  $\pm$  SEM (A-C) and mean  $\pm$  SD (D-G).

#### 4.2.7 Eyecup HDL-associated Apolipoprotein Levels Increase in CFH H402 Mice Fed HFC diet

CFH can compete with ApoB100- and ApoE-containing lipoproteins in BrM (80).

Based on the differences in the amount of sub-RPE deposits and circulating LDLs between aged *CFH-HH:Cfh-/-~ND* and *CFH-HH:Cfh-/-~HFC* mice, we hypothesized that more ApoE and ApoB100 would be retained in the eyecups of aged *CFH-HH:Cfh-/-~HFC*. To test this the apolipoprotein content in eyecups of aged *CFH:Cfh-/-* mice on and off HFC diet by Western blot were analyzed. There were no statistically significant differences in the eyecup levels of ApoB48 (Fig. 28A), ApoB100 (Fig. 28B) and ApoE (Fig.

28C) in aged *CFH:Cfh*<sup>-/-</sup> mice following the HFC diet. Surprisingly, there was a statistically significant ( $P < 0.05$ ) increase in ApoA1 levels in the eyecups of aged *CFH-HH:Cfh*<sup>-/-</sup>~HFC mice compared to all the other groups (Fig. 28D). This result supports a CFH H402 risk variant specific role in increased ApoA1 levels in the eyecup in response to advanced age and the HFC diet.

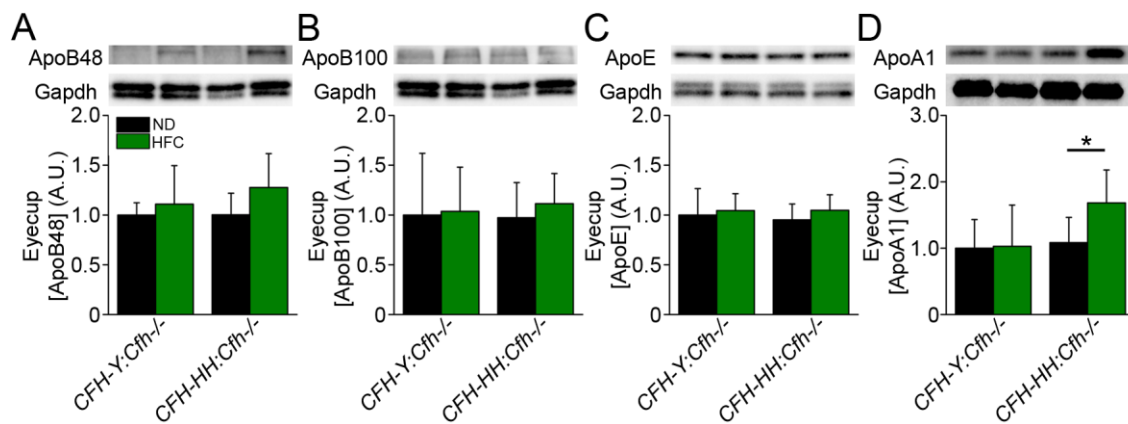


**Figure 28: Posterior eyecup apolipoprotein levels are *CFH:Cfh*<sup>-/-</sup> variant dependent. (A-D) Densitometric analysis of ApoB48 (A), ApoB100 (B), ApoE (C) and ApoA1 (D) immunoblots of eyecup (RPE/BrM/choroid/sclera) lysates isolated from fasted and PBS-perfused, aged *CFH:Cfh*<sup>-/-</sup>~ND and *CFH:Cfh*<sup>-/-</sup>~HFC mice (N=7). ApoB48 levels, on average, were higher in HFC-fed mice but the difference did not reach statistical significance. ApoB100 and ApoE were unchanged after HFC diet in both genotypes. ApoA1, a high density lipoprotein (HDL)-associated apolipoprotein, levels were increased significantly in aged *CFH-HH:Cfh*<sup>-/-</sup>~HFC compared to *CFH-HH:Cfh*<sup>-/-</sup>~ND mice and were unchanged in aged *CFH-Y:Cfh*<sup>-/-</sup>~ND and *CFH-Y:Cfh*<sup>-/-</sup>~HFC mice. The asterisk (\*) indicates post hoc Tukey for a  $P < 0.05$  following a statistically significant genotype by diet interaction by ANOVA for the densitometric arbitrary units. Data is presented as mean  $\pm$  SD.**

### **4.3 Discussion**

The HFC diet is a critical insult needed for AMD-like pathology development in aged *CFH-HH:Cfh<sup>-/-</sup>* mice but the dietary component and its induced effects responsible for these pathologies is unknown. We show dietary cholesterol is the crucial component responsible for visual loss in aged *CFH-HH:Cfh<sup>-/-</sup>* mice. Dietary cholesterol induces NASH-like liver pathologies and increases plasma ApoE-containing LDLs. CFH competes with ApoE-containing lipoproteins for binding to GAGs and prevents their accumulations in porcine and human BrM (80), but the impact of this interaction in mice is unknown. Based on our current study, we observed differences in plasma and eyecup lipoproteins between aged *CFH:Cfh<sup>-/-</sup>~HFC* diet. Plasma LDL levels are increased in aged *CFH-Y:Cfh<sup>-/-</sup>~HFC* mice compared to *CFH-HH:Cfh<sup>-/-</sup>~HFC* mice. LDL originates from VLDL remnants and can migrate through BrM to reach RPE cells in mice (10). We attribute the decrease in plasma LDL in aged *CFH-HH:Cfh<sup>-/-</sup>~HFC* mice to a difference in clearance or retention but not synthesis since we did not observe a change in plasma VLDL levels between aged *CFH:Cfh<sup>-/-</sup>~HFC* mice. However, HDL-associated ApoA1, but not VLDL- or LDL-associated ApoB48, B100 and E, is increased in the eyecups of aged *CFH-HH:Cfh<sup>-/-</sup>~HFC* mice compared to aged *CFH-Y:Cfh<sup>-/-</sup>~HFC* mice. ApoA1 is a critical component of HDL and functions to promote reverse cholesterol transport from peripheral tissues to HDL particles for the removal of excess phospholipid and

cholesterol from the body via the liver (243). Our results suggest the CFH Y402H polymorphism impacts lipoprotein metabolism in aged mice after HFC diet.

The pathological consequences of dysregulated lipoprotein metabolism in aged *CFH-HH:Cfh<sup>-/-</sup>*~HFC mice may be occurring within and/or outside the RPE. RPE cells have LDL receptors and phagocytose circulating LDL (10, 248, 249). Intake of LDL into RPE cells can lead to increased ECM gene expression (250) and contribute to drusen formation by altering BrM composition (11, 251). Furthermore, LDL can become oxidized due to the high oxidative stress environment in eye. Intake of oxidized LDL can lead to increased expression of genes regulating lipid metabolism, oxidative stress, inflammation, and angiogenesis (252-255), as well as increased apoptosis in RPE cells (250, 252, 256). Alternatively, the damage caused by increased LDL in RPE cells may be due to the increased influx of cholesterol. RPE cells are a unique cell type in regards to their daily intake of lipids including cholesterol from photoreceptor outer segments as well as from circulating lipoproteins (257). RPE cells can transport cholesterol derived from photoreceptor outer segments to ApoA1-containing HDL *in vitro* (258). However, advanced aging causes alterations in plasma HDL composition thus preventing these lipoproteins from efficiently participating in reverse cholesterol transport (259, 260). This may force RPE cells, which possess the machinery to assemble and secrete ApoA1-containing lipoproteins, to generate their own supply of ApoA1-containing lipoproteins

to handle their increased intracellular cholesterol (261-263). The increase in ApoA1-containing lipoproteins may explain the increase in sub-RPE deposit formation in aged *CFH-HH:Cfh<sup>-/-</sup>* mice after HFC diet and could create a pro-inflammatory milieu in the sub-RPE that contributes to visual loss and RPE damage. Intriguingly, increased HDL levels are associated with increased risk for AMD (264-267). In addition, AMD risk-associated genetic variants in *APOE*, *LIPC*, *CETP* and *ABCA1* raise HDL concentrations (120, 268, 269). Our studies suggest the risk association between CFH, HDL and AMD may be explained by how aged posterior eye tissues handle intracellular lipids.

In summary, dietary cholesterol is a critical component of the HFC diet required for the development of visual loss in aged *CFH-HH:Cfh<sup>-/-</sup>* mice. A major consequence of dietary cholesterol is the increase of plasma LDL in mice. Since there are differences in the levels of plasma LDL between aged *CFH-Y:Cfh<sup>-/-</sup>*~HFC and *CFH-HH:Cfh<sup>-/-</sup>*~HFC mice, the differences in their ocular phenotypes may be due to how LDL is handled in the posterior eye. Targeting plasma LDL in AMD patients, especially those that are carriers of the CFH H402 variant, may be a viable therapy to treat the disease before it reaches its vision-impairing stages.

## 5. Conclusions

### 5.1 Introduction

Throughout this dissertation, I have presented data elucidating the potential role of the H402 CFH variant in AMD pathobiology using mice. It is widely held that the risk association with the H402 variant and AMD is due to its inability to control complement activation in the posterior eye, but our results do not support this hypothesis (155).

Rather, it appears the CFH Y402H polymorphism impacts systemic and local lipoprotein metabolism in mice. Here, I will discuss a hypothetical model and future experiments to interrogate the importance of complement and lipoproteins in aged *CFH-HH:Cfh-/-~HFC* mice as well as validating our findings using other methods.

### 5.2 *CFH acts a potential regulator of plasma LDL entering the posterior eye*

Based on the data presented, I have devised a possible molecular explanation to explain the ocular phenotypic differences between young and aged *CFH-Y:Cfh-/-~HFC* and *CFH-HH:Cfh-/-~HFC* mice (Fig. 29). The H402 polymorphism impacts the ability of CFH to bind oxidized stress epitopes such as MDA and oxidized phospholipids on oxidized LDL (188, 189). Since oxidized LDL contains heparan sulfate proteoglycan-binding ApoE and ApoB100 (270, 271), the H402 variant allows the interaction of oxidized LDL to bind to heparan sulfate proteoglycans of BrM and facilitate its uptake

into the sub-RPE (Fig. 29D) while the Y402 CFH variant would prevent this interaction (Fig. 29C). Once oxidized LDLs reach the basal side of RPE, oxidized LDL can be ingested by the RPE via CD36, the oxidized LDL receptor (272). The presence of oxidized LDL increases the expression of CD36 in immortalized RPE cells (255) and may lead to large influxes of oxidized LDL into the RPE of aged *CFH-HH:Cfh<sup>-/-</sup>* HFC mice. Our proposed mechanism is supported by previous studies showing CFH can prevent the recognition of oxidized LDLs by RPE cells (188, 189) and circulating oxidized LDL can reach posterior eye tissues and be ingested by RPE cells via CD36 (272). Interestingly, lowering LDLs with atorvastatin in a high-risk subgroup of AMD patients lead to improvement in visual acuity and supports a role of RCT impairment in AMD pathobiology (273).

The role of aging in eliciting the pathologies in *CFH-HH:Cfh<sup>-/-</sup>* HFC may be explained by two possible scenarios. In young *CFH:Cfh<sup>-/-</sup>* mice, there are minimal signs of age-related changes to posterior eye tissues such as visual loss, RPE multinucleated cells and sub-RPE basal laminar deposits as shown in Chapter 3. Of particular importance, the basal laminar deposits are notably absent in young *CFH:Cfh<sup>-/-</sup>* mice (Fig. 29A). These deposits may physically separate the underlying RPE from its supply of plasma HDL causing RPE cells to generate their own supply of lipoproteins to deal with their increased plasma LDL ingestion. Another possible situation is age-related changes

to plasma HDL. Aging alters the composition of plasma HDL and changes its function from participating in reverse cholesterol transport to acting as an antioxidant (259).

Either of these would cause more intracellular LDL-delivered lipids to remain in the RPE of aged *CFH-HH:Cfh<sup>-/-</sup>*-HFC mice.

Diet is a critical component for the eliciting the pathologies in aged *CFH-HH:Cfh<sup>-/-</sup>*- mice. As shown in Chapter 4, cholesterol is a needed component in the diet required for the development of visual loss in aged *CFH-HH:Cfh<sup>-/-</sup>* mice. Interestingly, dietary cholesterol is responsible for the development of NASH-like liver pathologies in mice. From the literature, it has been postulated that oxidized cholesterol, but not cholesterol, causes NASH in mice (242). Thus, it may possible that the HFC diet increases plasma LDLs containing oxidized cholesterol which would be absent in aged *CFH:Cfh<sup>-/-</sup>*-ND mice. Their delivery to the RPE drives the ocular AMD-like phenotype in aged *CFH-HH:Cfh<sup>-/-</sup>*-HFC mice. This proposed model incorporates advanced aging, genetics and environmental stress all of which are important etiological risk factors for AMD. Future studies will examine these proposed ideas through studies on mice, RPE cell culture and population studies.

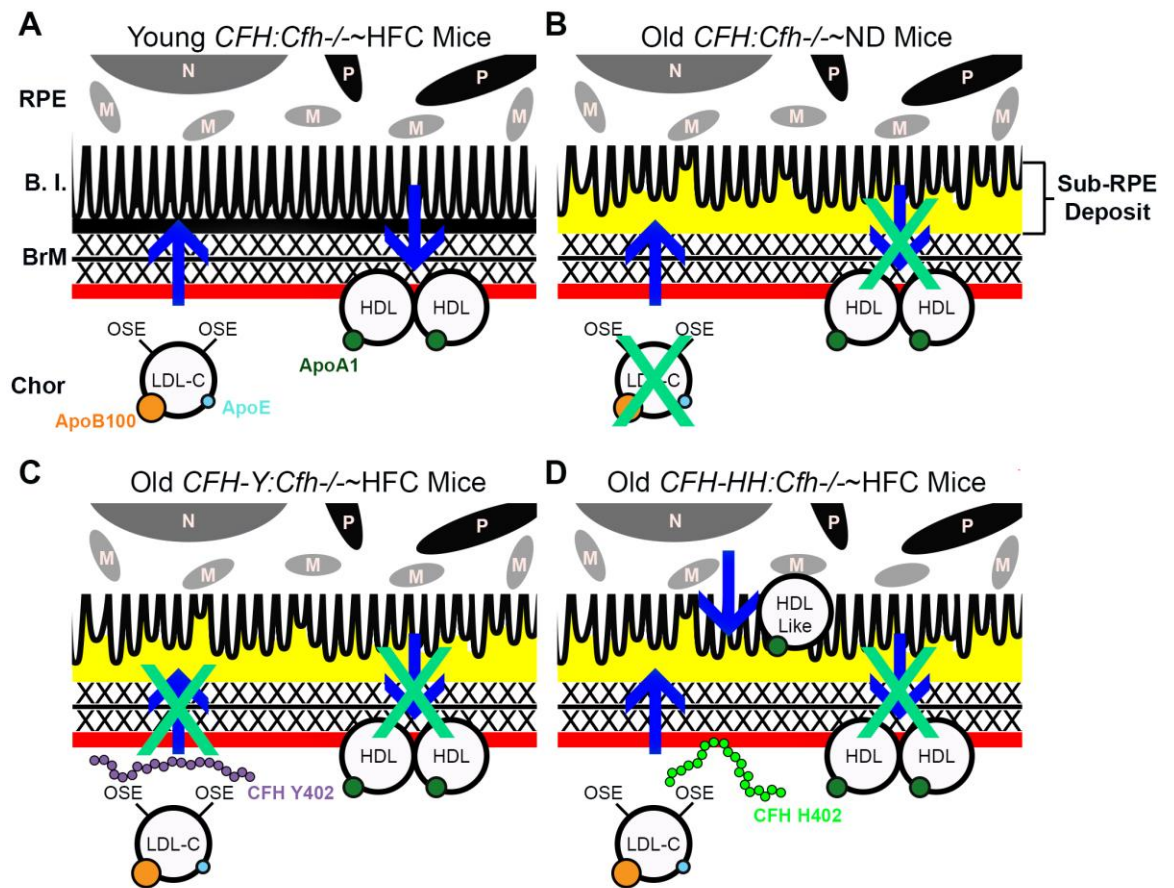


Figure 29: Schematic of CFH-mediated regulation of plasma LDL ingestion by the RPE. (A) Young *CFH:Cfh*<sup>-/-</sup> mice are protected against the development of HFC-induced pathologies that may be explained by the lack of sub-RPE basal laminar deposits. (B) Old *CFH:Cfh*<sup>-/-</sup>~ND mice may not develop a robust AMD-like phenotype due to the absence of oxidized LDL containing cholesterol. (C) Old *CFH-Y:Cfh*<sup>-/-</sup>~HFC mice may be protected against HFC-induced AMD-like pathology development because the Y402 CFH variant binds oxidized LDL-containing cholesterol more efficiently and prevents their intake by RPE and consequent RPE-derived lipoprotein secretion. (D) The CFH H402 variant allows LDL to interact with BrM by ApoE and/or ApoB100 binding to heparan sulfate proteoglycans and facilitate its movement into the sub-retinal pigment epithelium (RPE) region. Once oxidized LDL reaches the RPE, it can be ingested via CD36 and initiate a pathogenic cascade of events that lead to the development of AMD-like pathologies in aged *CFH-HH:Cfh*<sup>-/-</sup>

~HFC mice. N, nucleus; M, mitochondria; P, pigment granule; OSE, oxidative stress epitope.

### **5.3 Determining the Significance of Complement in Aged CFH-HH:Cfh<sup>-/-</sup>~HFC mice**

Complement has been associated with AMD through pathohistological and genetic studies of human specimens but its role in AMD is unknown (144, 146-154, 213). A role of complement driving the formation of AMD-like pathologies was established from studies on aged Cfh<sup>+/-</sup> and Cfh<sup>-/-</sup> mice fed a HFC diet showing only aged Cfh<sup>+/-</sup> mice develop visual loss and RPE damage after diet consumption (80). Cfh<sup>-/-</sup> mice are unable to maintain circulating complement levels of C3 and FB due to the lack of Cfh and lead us to propose that a reservoir of complement proteins is required for the visual loss and RPE damage seen in the Cfh<sup>+/-</sup>~HFC mice (180). Interestingly, aged CFH-HH:Cfh<sup>-/-</sup> mice develop visual loss and RPE damage following consumption of a HFC (or HC) diet but have similar levels of complement components and activation compared to aged CFH-Y:Cfh<sup>-/-</sup> mice, which do not develop visual loss and RPE damage after HFC diet. These results raise the interesting question of the role of complement in eliciting the AMD-like pathologies in mice.

To elucidate the roles of complement in aged CFH-HH:Cfh<sup>-/-</sup>~HFC mice, various complement components will need to be targeted via antibodies or genetic disruptions to determine their significance. The best complement protein to target would be C3. C3

is the main effector protein of the complement cascade and allows for downstream complement activation (274). It is also critical for the formation of sub-RPE deposits in a mouse model of Mallatia Levintene/Doyne's Honeycomb Dystrophy, an inherited retinal degeneration caused by mutations in *EFEMP1* (59). The most straight forward approach would be to cross *CFH-HH:Cfh<sup>-/-</sup>* mice with *C3<sup>-/-</sup>* mice to generate *CFH-HH:Cfh<sup>-/-</sup>C3<sup>-/-</sup>* mice although this would be time- and money-consuming.

Unfortunately, many of the C3 inhibitors such as compstatin developed for human diseases do not work with mouse complement proteins and prevent their utilization in our AMD mouse models (275). It is possible that C3 does not play a role in aged *CFH-HH:Cfh<sup>-/-</sup>~HFC* mice as the levels of C3 and its fragments are similar in *CFH-Y:Cfh<sup>-/-</sup>~HFC* mice but rather downstream complement components may be driving the formation of AMD-like pathologies. Since targeting C5a was not sufficient to ameliorate the AMD-like pathologies in aged *Cfh<sup>+/-</sup>~HFC* mice (81), targeting C5 or other MAC components may prevent AMD-like pathologies in aged *CFH-HH:Cfh<sup>-/-</sup>~HFC* mice.

Another interesting approach to interrogate the role of the complement in AMD-like pathology development in mice would be to phenocopy the ocular damage seen in aged *Cfh<sup>+/-</sup>~HFC* and *CFH-HH:Cfh<sup>-/-</sup>~HFC* mice with other complement-deficient strains of mice. Since CFH is a regulator of the alternative pathway, mice with haploinsufficient amounts of other alternative pathway regulators such as FI would be ideal for these

studies (276). Furthermore, this would aid in identifying the critical complement components needed for HFC-induced AMD-like pathologies and might influence the development of complement-based therapies for human AMD.

The majority of complement proteins are produced by the liver yet many complement proteins are also expressed by the RPE (155). Interestingly, a study examined the presence of AMD in individuals receiving liver transplants that changed their circulating CFH variant status (277). The risk for AMD was unchanged in Y402-expressing individuals that received livers expressing the H402 CFH variant (277). This raises the question about the relative importance of systemic- and local-derived complement components in regulating complement activation and AMD pathology development. Since both aged *Cfh*<sup>+/-</sup>-HFC and *CFH-HH:Cfh*<sup>-/-</sup>-HFC mice are based on CFH perturbations, adding CFH systemically to the circulation or locally to the eyes of these mice will help to determine the importance of the CFH source in maintaining eye health.

#### **5.4 Targeting Dietary Cholesterol and its Effects in Aged *CFH-HH:Cfh*<sup>-/-</sup> mice**

Future studies aimed at identifying the significance of dietary cholesterol-induced plasma LDL in aged *CFH-HH:Cfh*<sup>-/-</sup> mice using pharmacological interventions will be undertaken. Since we know removing cholesterol from the diet is sufficient to protect against visual loss in our mouse models, therapies targeting cholesterol intake

through the small intestine such as ezetimibe (Merck) should prevent visual loss in aged *CFH-HH:Cfh<sup>-/-</sup>~HFC* mice. Ezetimibe interacts with the Neimann Pick C1-like intracellular cholesterol transporter 1 (NPC1) to prevent cholesterol uptake by intestinal enterocytes and lower plasma LDLs containing cholesterol (278). Treating *ApoE<sup>-/-</sup>* mice, a model for both atherosclerosis and AMD, with ezetimibe was sufficient to prevent atherosclerotic lesions, macrophage accumulations and inflammation (279). Another approach to lower plasma LDL containing cholesterol levels is to treat mice with statins. Statins lower the activity of the hydroxymethylglutaryl-CoA reductase (HMGCR) and leads to the formation of less endogenous cholesterol (280). This causes cells to increase their expression of the LDL receptor and ingest more plasma LDL to compensate for their decrease endogenous cholesterol production (280). Statins have been used to treat AMD but the results of these studies are contradictory (273, 281-283). Therefore, aged *CFH-HH:Cfh<sup>-/-</sup>~HFC* mice provides a model to interrogate the effectiveness of statins on modulating AMD-like pathology development.

Alternatively, instead of targeting intracellular components of cholesterol regulation, lipoprotein intake and cholesterol efflux could be modulated by apolipoprotein mimetics. Apolipoprotein mimetics are short synthetic peptides that act similarly as their full-length apolipoprotein (284). Currently, there are ApoB100, ApoE and ApoA1 mimetics being tested in various obese and atherosclerotic mouse models

(285-289). Interestingly, only an ApoA1 mimetic has been tested in an AMD mouse model (290). One-year old *ApoE*<sup>-/-</sup> mice were treated with an intravitreal injection of the ApoA1 mimetic 4F that resulted in less neutral lipid deposition in and thickening of BrM (290). It would be interesting to test these mimetics in aged *CFH-HH:Cfh*<sup>-/-</sup>~HFC mice to determine the impact of the plasma LDL and eye cup HDL on the AMD-like phenotype in these animals. For example, utilizing an ApoE mimetic would prevent the intake of plasma LDL into posterior eye tissues and test whether the intake of lipids is pathogenic in aged *CFH-HH:Cfh*<sup>-/-</sup>~HFC mice (291).

Although pharmacological studies are ideal as it would be translational to the clinic, dietary interventions may serve as a valuable approach to study the roles of dietary cholesterol on the AMD-like pathology development in aged *CFH-HH:Cfh*<sup>-/-</sup>~HFC mice. We have already shown that changing the HFC diet recipe by removing the added cholesterol can prevent the visual loss in aged *CFH-HH:Cfh*<sup>-/-</sup> mice (Chapter 4) . Identifying dietary components capable of modulating the effect of dietary cholesterol in aged *CFH-HH:Cfh*<sup>-/-</sup> mice will aid in our understanding of the pathological mechanisms at play in these mice. One way of approaching these experiments would be adding the AREDS formulation to the HFC diet. AREDS is an antioxidant vitamin and nutrient supplement that can slow the progression of AMD to its later stages (37). The AREDS supplement was given orally to C57 wild type mice before they were subjected to laser-

induced CNV (292). Mice receiving the AREDS-II supplement had smaller CNV lesion sizes than those receiving an oral vehicle (292). The authors suggest the antiangiogenic and antioxidant properties of the AREDS II supplement lessened lesion size in the laser CNV mouse model as evidenced by decreased VEGF gene and protein expression (292). Other possible dietary components to test in aged *CFH-HH:Cfh<sup>-/-</sup>* mice would be niacin which increases HDL particles in humans (293) and a high glycemic diet which can increase cholesterol in mice (75).

### ***5.5 Validating the Role of the H402 CFH Variant on Lipoprotein Metabolism Using In Vitro and Population-based Studies***

As already noted in the introduction of this dissertation, there are advantages and disadvantages of using mice in AMD research. Since we have identified a role of CFH in lipoprotein metabolism, it is important to realize the limitations of mice in metabolic research. Mice are extremely resistant to the development of atherosclerosis requiring sodium cholate for lipid absorption and retention as well as differences in the expression of apolipoproteins, notably ApoB48 (257). ApoB48 is a truncated version of ApoB100 expressed by intestinal enterocytes in humans but it is expressed by both intestinal enterocytes and hepatocytes in mice (294). With these caveats, it is critical to test the role of the H402 CFH variant on lipoprotein metabolism using other methods.

Studies using RPE cell cultures could help to establish the molecular significance of the CFH Y402H polymorphism on lipoprotein metabolism. Similar to studies

described by Weismann *et al.* and Shaw *et al.*, Y402 and H402 CFH variants could be incubated with LDL as well as oxidized LDL with macrophage and RPE cells (188, 295). Instead of measuring the levels of cytokine RNA and secretion, the levels of lipoprotein and cholesterol metabolism genes would be measured and validated by Western Blot analysis. In addition, LDL with fluorescently-labeled cholesterol could be used for these studies and RPE fluorescence measured as an indication for LDL ingestion/uptake. Following the completion of these experiments, macrophages and RPE cells would be collected to assess for oxidative and mitochondrial stress, gene expression changes and sub-RPE deposit formation in RPE cultures maintained for a long period of time as described previously by Johnson *et al.* (296).

There are also studies that could be undertaken using large human populations to validate our findings. It has been shown that early AMD is associated with cardiovascular conditions (297). Risk for cardiovascular disease is strongly linked with increased plasma LDL levels but risk for AMD has been linked with increased plasma HDL levels (264-267, 298). To understand the differences between these diseases, patients involved in epidemiological studies of cardiovascular diseases should be genotyped for their CFH Y402H status and followed longitudinally to determine if they develop AMD. Since the patient's lipoprotein and cholesterol levels would be known

from their involvement in the cardiovascular studies, researchers could evaluate whether there are correlations between CFH, lipoproteins and AMD.

## **5.6 Conclusions**

AMD is a complex retinal degeneration that continues to perplex researchers developing therapies to treat it. In spite of their lack of a macula, the use of mice to probe for the underlying molecular causes of AMD has aided in the development of novel AMD therapies (38). Using the novel AMD mouse models in the Bowes Rickman laboratory, I have uncovered a potential explanation behind the risk association between the H402 CFH variant and AMD. The CFH Y402H polymorphism may impair the ability to regulate lipoprotein metabolism in the posterior eye. This novel finding may explain why clinical trials evaluating complement inhibitors have failed and support targeting lipoprotein metabolism as a viable therapeutic strategy for treating AMD.

## Materials and Methods

### Animals

Aged (>90 week old) *Cfh*<sup>+/-</sup>, *CFH-Y:Cfh*<sup>-/-</sup> and *CFH-HH:Cfh*<sup>-/-</sup> mice were generated and genotyped as described (79, 80). All mice used in this study did not carry the *rd8* mutation (299). All mice were housed conventionally on a middle rack in the same mouse facility under ambient light conditions to control for environmental factors and microbiome fluctuations. Mice were maintained in accordance with the Institutional Animal Care and Use Committee at Duke University. All animal procedures adhered to ARVO's Statement for the Use of Animals in Ophthalmic and Vision Research. The number of mice used for each experiment is provided in the figure or their legends. Mice were randomly assigned to treatment groups with an even distribution by age.

For studies using the laser-induced CNV or the sodium iodate (NaIO<sub>3</sub>) models, male C57BL/6J aged 8 to 10 weeks were obtained from The Jackson Laboratory (Sacramento, CA, USA). A total of 6 to 12 mice were used per dosing group ( $n = 78$  total/model). The care and use of mice for both of these studies adhered to Pfizer's Institutional Animal Care and Use Committee guidelines.

### Diets

Mice were continued on a ND (Isopurina 5001; Prolab) or switched either a HFC (TD 88051; Envigo), HF diet (TD 98232; Envigo) or HC (TD 91342; Envigo) diet for eight weeks. The HFC, HF and HC diets contain 0.5% sodium cholate for lipid absorption.

### **Electroretinography**

Electroretinography was performed on mice following 4 hours of dark adaptation. Pupils were dilated with 0.5% tropicamide and 1.25% phenylephrine then mice were anesthetized with a combined mixture of ketamine (100 mg/kg) and xylazine (10 mg/kg). Scotopic ERGs were recorded using an Espion E2 system (Diagnosys), at increasing flash intensities as described (300). Flash responses were smoothed using a low pass noise filtering script before analysis. The amplitude heights of the A-wave and B-wave for each ERG flash response were calculated and fitted using a previously published equation (300) in OriginPro 9.0 (OriginLab) as previously described (79-81, 119). Bmax1 and Bmax2 values were calculated as described (80).

### **RPE Flat mounts**

Eyes were enucleated following perfusion of the mouse with phosphate buffer solution (PBS). The anterior segment and retina were promptly removed and the remaining RPE/choroid/sclera was fixed overnight in methanol. RPE flat mounts were labeled with the rabbit antibody against ZO-1 (1:100, Invitrogen #40-2200) and nuclear stain Hoechst 33342 (1:500, Invitrogen) as previously described (80, 81, 119). Confocal

images of the north, east, south and west quadrants around the optic nerve were captured on an Eclipse C1 microscope (Nikon). Morphometric analysis was performed by a masked grader that counted the number of multinucleate RPE cells with 3 or more nuclei from each central quadrant.

### **Electron Microscopy**

Eyes were enucleated following PBS and 2% glutaraldehyde/2% paraformaldehyde perfusion of the mouse and then fixed overnight in 2% glutaraldehyde/2% paraformaldehyde. Eyes were processed using routine methods previously described (79). Ultrathin sections of 60-80 nm were sectioned, mounted onto 400 mesh thin-bar copper grids (T400-Cu; Electron Microscopy Sciences) and stained with Sato's lead. Sections were imaged using a Tecnai G2 electron microscope. Deposit sizes were quantified by measuring from the elastic layer of BrM to the top of the largest sub-RPE deposit within the image using Image J software (NIH) as previously described (79) with a slight modification. Images of the RPE/BrM were taken at each intersection with the copper grid and the largest deposit within the EM image was measured, instead of averaging the deposit sizes at the edge of each EM image (79). Approximately 62±8 images per mouse were collected and scored for this study.

### **C5a and VEGF Antibodies**

The anti-C5a antibody, 4C9, was isolated from a phage displayed single chain antibody variable fragment (scFv) library derived from human donors and was provided as a gift from Laird Bloom of Pfizer, Inc. It binds to human and mouse C5a with low nanomolar affinity and blocks binding of C5a to the C5a receptor (C5aR). The affinity of this antibody toward C5a was increased using a yeast surface display system; the resulting higher-affinity clone was subsequently used in the study described here. In brief, the antibody was cloned as a scFv into a yeast display vector (301) and then CDRH2, CDRH3, CDRL1, and CDRL3 of the antibody were individually mutated using look-through mutagenesis (302). *S. cerevisiae* BJ5465 harboring the library was subjected to three rounds of fluorescence-activated cell sorting (FACS) with gating strategies designed to isolate higher-affinity clones (303). DNA encoding the enriched clones was randomly combined and subjected to three additional rounds of FACS followed by individual screening. A higher-affinity clone was identified, expressed as a chimeric monoclonal antibody (human VH and VL domains fused to mouse IgG1 heavy chain and kappa light chain constant regions) from HEK293F cells, purified using standard techniques, binding with human and mouse C5a determined by surface plasmon resonance (SPR) (Biacore, GE Healthcare, Piscataway, NJ, USA), and then used in this study.

Mouse anti-VEGF-A antibody was constructed as murine IgG1 based on the published sequences of the G6-31 antibody (patent CA2533297A1(304)) that was previously shown to bind both mouse and human VEGF with high affinity (304). In brief, the sequences of variable regions of G6-31 were synthesized, cloned into the mouse IgG1 heavy chain and kappa light chain, expressed in the HEK293F cells, and purified using standard techniques, and its interaction with mouse VEGF-A was confirmed by SPR (Biacore, GE Healthcare).

#### **NaIO<sub>3</sub> Treatment and Anti-C5a Dose Response (4C9)**

NaIO<sub>3</sub> treatment was performed as previously described in order to determine the appropriate dose of anti-C5a therapy needed to observe a therapeutic effect in the posterior eye (43). Briefly, 8- to 10-week-old C57BL/6J mice were injected into the intraperitoneal (IP) space with 3, 10, 20, 30, or 60 mg/kg anti-C5a or 60 mg/kg isotype control (day -1). The next day, mice were intravenously injected with 25 mg/kg NaIO<sub>3</sub> or PBS control (day 0). On day 2, mice were dark adapted for 24 hours, and on day 3, ERGs were performed as described below at flash intensities of 1E-4, 1E-3, 1E-1, and 2.5 (cd\*s/m<sup>2</sup>).

#### **Antibody C5a Treatment of *Cfh*<sup>+/-</sup> Mice and Laser CNV Model**

*Cfh*<sup>+/-</sup> mice were treated with 30 mg/kg anti-C5a via a weekly IP injection. Injections began at the onset of HFC diet and were continued during the 8 weeks of diet.

For the laser CNV model, 30 mg/kg anti-C5a was administered with or without anti-VEGF at 3, 5, or 10 mg/kg 1 day prior to CNV induction and at days 5 and 11 post laser CNV.

### **Laser-induced CNV Model**

Experimental CNV was induced bilaterally in C57BL/6J mice at 8 to 10 weeks of age. Animals were anesthetized with IP injection of ketamine (60 mg/kg) and xylazine (9 mg/kg). Animals were pretreated with 1% atropine (atropine sulfate, 1 drop) and tropicamide (1%, 1 drop) eye drops. A coverslip was placed over the cornea with a large drop of Goniosol. Three 532-nm diode laser pulses with a spot size of 50  $\mu$ m, duration of 0.1 second, and power of 110 mW (OcuLight TX; IRIDEX, Mountain View, CA, USA) were applied between retinal vessels at 12, 4, and 8 o'clock, two disc diameters from the optic nerve, with the use of a slit-lamp and ophthalmologic microscope (SL980/5X; IRIDEX). Formation of a bubble at the time of laser application, which indicates rupture of BrM, was an important factor in obtaining laser-induced CNV (44). Only laser burns in which a bubble was produced were included in the study. Any lesions that did not yield the characteristic white "bubble" formation or any hemorrhaging lesions automatically resulted in removal of the animal from the study. A total of 6 to 12 mice were used per dosing group.

### **Analysis of CNV by Scanning Laser Angiography**

Angiography was performed at day 12 post laser treatment with a scanning laser ophthalmoscope (SLO) using the Spectralis Heidelberg Retina Tomograph (HRT)/SLO (Heidelberg Engineering, Dossenheim, Germany), which was used as a digital confocal SLO (cSLO) since it is equipped with four laser wavelengths (488, 514, 788, and 820 nm) and filters for fluorescein and indocyanine green (ICG) fluorescence. To adapt the commercial system to the optics of the mouse eye, we used a 55-diopter lens as a front objective (Linos Optics, Milford, MA, USA) instead of the 40-mm focal lens used for a human eye. Pupils were dilated with topical 1% atropine. Mice were anesthetized by IP injection of ketamine (60 mg/kg) and xylazine (9 mg/kg) and kept on a heated pad during the procedure. Plasma labeling by sodium fluorescein (Akorn, Inc., Lake Forest, IL, USA) was used for choroidal vessel imaging. Five hundred microliters of 2 mg/mL sterile sodium fluorescein solution was injected IP 8 minutes prior to cSLO imaging. Following the recordings, mice were kept in the cage placed on a warming pad until they recovered from anesthesia.

### **Quantitative CNV Lesion Analysis**

In order to analyze the fluorescein fundus angiography, image analysis was performed with open-source software, ImageJ (National Institutes of Health, Bethesda, MD, USA). A masked grader performed quantification of the CNV lesion size. In brief, for the quantification, raw images of angiography were imported into ImageJ and the

CNV lesion was demarcated using the freehand selection tool, avoiding large vessels. The volume and brightness of the lesions were quantitated with background optical density from the neighboring to CNV region subtracted as arbitrary units. Analysis of variance and post hoc *t*-test were used to assess the statistical significance between the treatment groups.

### **Anti-C5a ELISA**

Anti-C5a (4C9) levels were determined by ELISA. Briefly, mC5a (no. 2150-c5; R&D Systems, Minneapolis, MN, USA) was incubated at 4°C overnight in 96-well plates. After washing unbound antibody and blocking with 2% BSA, a 1:1000 dilution of plasma was incubated overnight at 4°C. Following wash steps, the plate was sequentially incubated with biotinylated anti-mouse IgG (H and L) HRP (1:3000; BD Biosciences, San Jose, CA, USA), TMB substrate reagent (BD Biosciences) and the OD 450 nm read; 0.31 to 200 ng/mL anti-C5a (4C9) was used as a standard curve.

### **Leukocyte Adhesion Molecule, Chemokine, and Cytokine RNA Arrays**

Total RNA from four eyecups (RPE/choroid/sclera) from each *Cfh*<sup>+/-</sup> group was extracted using an RNeasy lipid tissue mini kit (Qiagen, Inc., Valencia, CA, USA) according to the manufacturer's instructions. RNA concentrations were determined using the Nanodrop 2000 UV-Vis Spectrophotometer (Thermo Scientific, Waltham, MA, USA). Eyecup RNA (600 ng) was used to synthesize cDNA using the RT<sup>2</sup> First Strand

cDNA kit (Qiagen, Inc.). cDNA was combined with RT<sup>2</sup> SYBR Green qPCR Mastermix (Qiagen, Inc.) and Ultrapure RNase/DNase-free water (Invitrogen). Real-time PCR data analysis of the cDNA was performed on two mouse RT<sup>2</sup> PCR pathway-focused arrays from Qiagen, Inc. (RT<sup>2</sup> Profiler: Inflammatory Response and Autoimmunity [cat. no. PAMM-077ZD] and Extracellular Matrix and Adhesion Molecule [cat. no. PAMM-013ZD]) following the manufacturer's protocol. Prior to RNA expression analysis, quality controls for genomic contamination, reverse transcription, and positive PCR were checked for each plate to confirm that each plate met quality controls. Relative mRNA expression was normalized to five endogenous reference genes, *Actb*, *B2m*, *Gapdh*, *GusB*, and *Hsp90ab1*, for each group using the quantitative  $2^{-\Delta\Delta C_T}$  method (305). All the expression data for the Inflammatory Response and Autoimmunity and the Extracellular Matrix and Adhesion Molecule arrays are presented in Tables 2 and 3 in Appendix A, respectively. For these analyses, a gene was considered to be upregulated or downregulated if the fold change was greater than 1.25 as previously described (306).

Expression of individual genes was examined in triplicate reactions using 25 ng cDNA from a pooled RNA sample consisting of four eyecups from each group (*Cfh*<sup>+/-</sup>~ND, *Cfh*<sup>+/-</sup>~HFC, and *Cfh*<sup>+/-</sup>~HFC + antiC5a), 200 nmol/L each primer, and 12.5  $\mu$ L iQ<sup>TM</sup> SYBR green supermix (Biorad, Hercules, CA, USA) in 25  $\mu$ L total volume. RT-PCR reactions were run in the CFX96 system at 95°C for 3 minutes, followed by 40 cycles

at 95°C for 10 seconds and 60°C for 20 seconds, then 72°C for 15 seconds. Relative mRNA expression was normalized to the endogenous reference murine gene ribosomal protein lateral stalk subunit P0 (*Rplp0*) using the quantitative  $2^{-\Delta\Delta C_T}$  method (305).

### **Tissue and RNA Isolation, and RT-PCR**

Three C57BL/6J mice were euthanized with CO<sub>2</sub> and perfused with 15 mL PBS. After perfusion, eyes were enucleated for dissection where fat, muscle, and anterior segment were removed. Neural retina was carefully separated from the posterior eyecup, placed into a separate Eppendorf tube, and flash frozen. RPE cells were isolated using a modified protocol described previously (307). Briefly, RPE/choroid/sclera was placed into an Eppendorf tube with 1 mL RNAlater Cell Reagent (Qiagen, Inc.) and left overnight at 4°C. The next day, choroid/sclera was removed, rinsed with PBS, and placed in a separate Eppendorf tube for RNA isolation. RPE cells were spun and RNAlater was removed from tube. Both choroid/sclera and RPE tissues were flash frozen. Human RPE cells from a 71-year-old male human donor eye with a 3.5-hour procurement time were isolated by cutting the eye around the ora serrata, removing the vitreous and retina, then adding 500 µL cold PBS to the eyecup and gently rubbing with a rounded glass rod; this step was repeated. The cells were centrifuged at 4° for 10 minutes at 600g; the intact RPE cell pellet was washed one time with cold PBS and spun, the supernatant was removed, and cells were frozen at -80°. More rigorous washing and

mechanical scraping of the eyecup removed any remaining RPE in the eyecup; then a portion, free of RPE cells, was cut out and the BrM and choroid were peeled from the sclera. This “choroid” sample was immediately frozen. Total RNA from each of these tissues, isolated from murine retina, RPE, and choroid/sclera as well as human RPE and choroid, was extracted using an RNeasy lipid tissue mini kit (Qiagen, Inc.) according to the manufacturer's instructions. RNA concentrations were determined using the Nanodrop 2000 UV-Vis Spectrophotometer (Thermo Scientific). RNA from ARPE-19 cells was generously provided by Goldis Malek (Duke University) and was isolated as previously described (308). RNA (150 ng) from each sample was used to synthesize cDNA using ProtoScript II Reverse Transcriptase (NEB, Ipswich, MA, USA). Each RT-PCR reaction contained 7.5 ng cDNA, 200 nmol/L each primer, and 12.5  $\mu$ L iQ SYBR green supermix (Biorad) in 25  $\mu$ L total volume. All primers used in this study span an exon–exon splice junction. RT-PCR reactions were run in triplicate in the CFX96 system at 95°C for 3 minutes, followed by 40 cycles at 95°C for 10 seconds and 60°C for 20 seconds, then 72°C for 15 seconds. Relative mRNA expression was normalized to the endogenous reference gene beta-actin using the quantitative  $2^{-\Delta\Delta C_T}$  method (305).

### **Peripheral Blood and Extravascular RPE/Choroid MNP Analysis by Flow Cytometry**

Intravascular staining of circulating immune cells was performed to differentiate circulating immune cells within the blood vessel from the extravascular immune cells that had migrated into the tissue of the posterior eye as previously described (66, 80). Briefly, 5 minutes prior to euthanasia, mice were injected retro-orbitally with 3  $\mu\text{g}/50 \mu\text{L}$  APC/Cy7 anti-mouse CD45 (BioLegend, San Diego, CA, USA) (CD45-IV) to label the intravascular immune cells. Peripheral blood samples were subjected to red blood cell lysis and staining for cell viability (no. 65-0863; eBiosciences, San Diego, CA, USA) and labeled with antibodies against CD45 (no. 110735, BioLegend), CD11b (no. 562950, BD Biosciences), CD115 (no. 61-1152, eBiosciences), CD43 (no. 562866; BD Pharmingen, San Jose, CA, USA), Ly6C (no. 128022, BioLegend), and Ly6G (no. 127621, BioLegend) to determine the percent of classical and nonclassical monocytes per CD45+ cells based on established methods (80, 217). Both eyes were enucleated, retina was removed, and the RPE/choroid/sclera from each eye was isolated by microdissection. The RPE/choroid was mechanically removed from the subadjacent sclera. Six eyes were pooled to obtain cell numbers sufficient for analysis. RPE/choroid samples then underwent DNase I and collagenase treatment with mechanical stimulation to free immune cells. Subsequently samples were filtered and stained for cell viability, and labeled with antibodies against CD11b, CD45, Ly6C, Ly6G, CCR2 (R&D Systems, no. FAB5538A), CD11c (BD Biosciences, no. 563048), CD64 (BioLegend, no. 139308), F4/80 (BioLegend, no. 123109),

and I-A/E (BioLegend, no. 107629). All samples were run on a BD Biosciences Fortessa flow cytometer using BD FACSDiva software (BD Biosciences). Gating is shown in figures and was performed as previously described in RPE/choroid (80). With  $N = 6$  eyes per group, two independent experiments were performed to confirm the data trend; the average of the peripheral blood analysis experiments is presented, and a representative experiment of the RPE/choroid data is presented.  $\chi^2$  statistical test for  $P < 0.05$  was used to determine the statistical significance of the cell population frequencies normalized to total in the intra- or extravascular space CD45+ cells for a pooled sample.

### **Western Blots of *CFH:Cfh*<sup>-/-</sup> Tissues**

Mice were fasted for five hours from 10 a.m. to 3 p.m. and bled through the submandibular vein into EDTA tubes (BD Microtainer; BD, Franklin Lakes, NJ). Blood was spun for 15 minutes at 1200 rpm and plasma was collected. Mice were then euthanized with CO<sub>2</sub> and promptly perfused with 1X PBS to remove blood contamination from the eyes. Eyes were enucleated and the anterior segment and retina were removed from the posterior eyecup (RPE/choroid/sclera) and stored at -80 °C degrees. Eyecup lysates were made by manually homogenizing tissues with a handheld microgrinder (Argos Technologies) in 80  $\mu$ l of RIPA buffer (ThermoScientific) containing protease inhibitor (Roche) and quantified using the Pierce™ BCA Protein Assay Kit (ThermoScientific). Plasma samples were similarly diluted in 5% XT Sample buffer

(Biorad) and equal dilution volumes were aliquoted while equal eyecup protein concentrations were pipetted to sample buffer before running on 10% Bis-Tris Criterion XT gels (Biorad) in MOPS buffer (Biorad) under nonreducing conditions and transferred to nitrocellulose membranes (Biorad). For the plasma iC3b Westerns, XT reducing agent (Biorad) was added to each sample and each sample was incubated at 105° degrees for seven minutes. Membranes were probed for CFH (goat anti-CFH, A312, Quidel), C3 (rabbit anti-human C3d, A0063, Dako), FB (goat anti-FB, Kent Laboratories), ApoE (goat anti-ApoE, 178479, Calbiochem), ApoB (goat anti-ApoB, AB742) and ApoA1 (goat anti-ApoA, 11A-G2b, Academy Bio-Medical Co.) overnight at 4°C degrees. Blots were washed with TBST buffer and incubated with either peroxidase-conjugated anti-goat or anti-rabbit IgG (Jackson ImmunoResearch Labs, Inc.) depending on the source of the primary antibody. Blots were washed again with TBST and incubated with ECL Plus reagent (Thermo Scientific). Blots were imaged using a ChemiDoc Imaging System (Biorad) and analyzed using ImageJ software (NIH). For loading controls, blots containing plasma samples were reprobed for albumin (rabbit anti-albumin, ab31657-1, abcam) and blots containing eyecup lysates reprobed for GAPDH (rabbit anti-GAPDH, 2118, Cell Signaling) .

### **Cholesterol Measurement**

Plasma cholesterol and lipoprotein-associated cholesterol were measured with the Amplex™ Red Cholesterol Assay Kit (ThermoFisher Scientific) using the manufacturer's guidelines. Fluorescence was measured using a Spectramax M5 plate reader (Molecular Devices).

### **Lipoprotein Fractionation**

30 µl of plasma from each *CFH:Cfh<sup>-/-</sup>*ND and *CFH:Cfh<sup>-/-</sup>*HFC mouse was fractionated on a FPLC system (Pharmacia LKB) with a Superose 6HR 10/30 column (GE Healthcare) into 500 µl fractions. Cholesterol was measured in fractions 13 through 31.

### **Statistical Analysis**

ANOVA statistical analysis with post hoc Tukey test was used to determine the statistical significance for this current study. Detailed descriptions of the comparisons are described in the figure legends. Statistical analyses were performed in JMP Pro-9 software.

## Appendix A

**Table 2: Summary of Inflammatory Process and Autoimmunity Gene Expression Changes in RPE/Choroid Eyecup RNA Isolated from Old *Cfh*<sup>+/-</sup> Fed an HFC Diet Compared to Age-Matched *Cfh*<sup>+/-</sup> Fed a Normal Diet**

Gene	GenBank ID	Fold Change
Cxcl10	NM_021274	4.56
Ccl8	NM_021443	3.23
Ccl12	NM_011331	2.99
Ccl4	NM_013652	2.60
C4b	NM_009780	2.23
Tnfsf14	NM_019418	2.23
Sele	NM_011345	2.13
Ccl7	NM_013654	2.11
Ltb	NM_008518	2.06
Ccl5	NM_013653	2.00
Ccr3	NM_009914	1.89
Cd40	NM_011611	1.87
Tirap	NM_054096	1.80
Il1b	NM_008361	1.79
Il5	NM_010558	1.67
Tlr9	NM_031178	1.66
Tnf	NM_013693	1.66
Ccl2	NM_011333	1.56
Bcl6	NM_009744	1.52
Ccr1	NM_009912	1.48
Il6ra	NM_010559	1.48
Ccl3	NM_011337	1.44
C3ar1	NM_009779	1.41
C3	NM_009778	1.39
Cxcl1	NM_008176	1.39
Cxcl2	NM_009140	1.30
Tlr3	NM_126166	1.27
Tlr6	NM_011604	1.27
Csf1	NM_007778	1.25
Ptgs2	NM_011198	1.24

Tlr1	NM_030682	1.24
Ccr7	NM_007719	1.22
Ccr2	NM_009915	1.17
Cebpb	NM_009883	1.16
Cxcr1	NM_178241	1.16
Fos	NM_010234	1.16
Il1r1	NM_008362	1.16
Tlr4	NM_021297	1.16
Il7	NM_008371	1.16
Itgb2	NM_008404	1.16
Myd88	NM_010851	1.15
Tlr2	NM_011905	1.15
Cxcr2	NM_009909	1.14
Fasl	NM_010177	1.13
Il1rn	NM_031167	1.13
Tollip	NM_023764	1.13
Nfkb1	NM_008689	1.12
Il23r	NM_144548	1.10
Nr3c1	NM_008173	1.09
Cxcl5	NM_009141	1.07
Ccl17	NM_011332	1.04
Il18	NM_008360	1.04
Il1rap	NM_008364	1.03
Ly96	NM_016923	1.02
Cxcr4	NM_009911	-1.02
Tlr5	NM_016928	-1.06
Il1a	NM_010554	-1.07
Il10rb	NM_008349	-1.09
Ccl19	NM_011888	-1.11
Cd14	NM_009841	-1.13
Ccl25	NM_009138	-1.20
Ripk2	NM_138952	-1.20
Tlr7	NM_133211	-1.21
Cxcl11	NM_019494	-1.22
Ccl11	NM_011330	-1.61
Ccl20	NM_016960	nd
Ccl22	NM_009137	nd

Ccl24	NM_0195577	nd
Ccr4	NM_009916	nd
Cd40lg	NM_011616	nd
Crp	NM_007768	nd
Cxcl3	NM_203320	nd
Cxcl9	NM_008599	nd
Ifng	NM_008337	nd
Il10	NM_010548	nd
Il17a	NM_010552	nd
Il22	NM_016971	nd
Il23a	NM_031252	nd
Il6	NM_031168	nd
Il9	NM_008373	nd
Kng1	NM_023125	nd
Lta	NM_010735	nd
Nos2	NM_010927	nd

Yellow, red, green and blue represent a gene that is upregulated, unchanged, downregulated or not detected (nd), in RPE/choroid eyecup RNA isolated from old *Cfh*<sup>+/-</sup> fed an HFC diet compared to age-matched *Cfh*<sup>+/-</sup> fed a normal diet, respectively.

**Table 3: Supplemental Table 2: Summary of Extracellular Matrix and Adhesion Molecule Gene Expression Changes in RPE/Choroid Eyecup RNA Isolated from Old *Cfh*<sup>+/-</sup> Fed an HFC Diet Compared to Age-Matched *Cfh*<sup>+/-</sup> Fed a Normal Diet**

Gene	GenBank ID	HFC/ND
Itgae	NM_008399	3.51
Vcan	NM_001081249	2.78
Mmp13	NM_008607	2.57
Sele	NM_011345	2.54
Cntn1	NM_007727	2.53
Col2a1	NM_031163	2.29
Itgal	NM_008400	2.07
Thbs3	NM_013691	2.05
Selp	NM_011347	1.92
Adamts1	NM_009621	1.78
Spock1	NM_009262	1.78
Mmp1a	NM_032006	1.7
Mmp14	NM_008608	1.62
Adamts5	NM_011782	1.61
Cd44	NM_009851	1.61
Sell	NM_011346	1.6
Vcam1	NM_011693	1.53
Cdh4	NM_009867	1.51
Ecm1	NM_007899	1.49
Fbln1	NM_010180	1.49
Itgb2	NM_008404	1.49
Mmp11	NM_008606	1.49
Mmp12	NM_008605	1.49
Col5a1	NM_015734	1.46
Itgax	NM_021334	1.44
Lama3	NM_010680	1.44
Emilin1	NM_133918	1.42
Icam1	NM_010493	1.42
Itga5	NM_010577	1.41
Itgam	NM_008401	1.41
Tgfbi	NM_009369	1.4
Itgb4	NM_001005608	1.39

Ctnna1	NM_009818	1.38
Itga4	NM_010576	1.35
Itgb1	NM_010578	1.35
Sgce	NM_011360	1.34
Entpd1	NM_009848	1.31
Ctnnb1	NM_007614	1.3
Cdh2	NM_007664	1.29
Lamb2	NM_008483	1.29
Mmp9	NM_013599	1.28
Col4a2	NM_009932	1.27
Ctnna2	NM_009819	1.27
Itgav	NM_008402	1.27
Adamts2	NM_175643	1.26
Adamts8	NM_013906	1.25
Itga3	NM_013565	1.25
Lamc1	NM_010683	1.23
Ncam1	NM_010875	1.23
Thbs1	NM_011580	1.23
Mmp2	NM_008610	1.2
Tnc	NM_011607	1.2
Itga2	NM_008396	1.19
Ctgf	NM_010217	1.17
Mmp15	NM_008609	1.17
Ncam2	NM_010954	1.17
Pecam1	NM_008816	1.16
Timp2	NM_011594	1.15
Col4a1	NM_009931	1.13
Mmp8	NM_008611	1.12
Itgb3	NM_016780	1.1
Lama1	NM_008480	1.1
Col3a1	NM_009930	1.09
Thbs2	NM_011581	1.08
Col4a3	NM_007734	1.06
Sparc	NM_009242	1.06
Spp1	NM_009263	1.06
Cdh1	NM_009864	1.05

Timp1	NM_011593	1.05
Timp3	NM_011595	1.05
Col1a1	NM_007742	1.02
Vtn	NM_011707	-1.03
Lama2	NM_008481	-1.04
Fn1	NM_010233	-1.05
Postn	NM_015784	-1.05
Col6a1	NM_009933	-1.09
Lamb3	NM_008484	-1.28
Hapln1	NM_013500	-1.3
Mmp3	NM_010809	-1.32
Syt1	NM_009306	-1.53
Cdh3	NM_001037809	nd
Hc	NM_010406	nd
Mmp10	NM_019471	nd
Mmp7	NM_010810	nd

Yellow, red, green and blue represent a gene that is upregulated, unchanged, downregulated or not detected (nd), in RPE/choroid eyecup RNA isolated from old *Cfh*<sup>+/-</sup> fed an HFC diet compared to age-matched *Cfh*<sup>+/-</sup> fed a normal diet, respectively.

## Appendix B

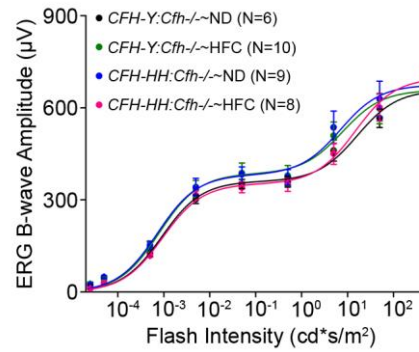
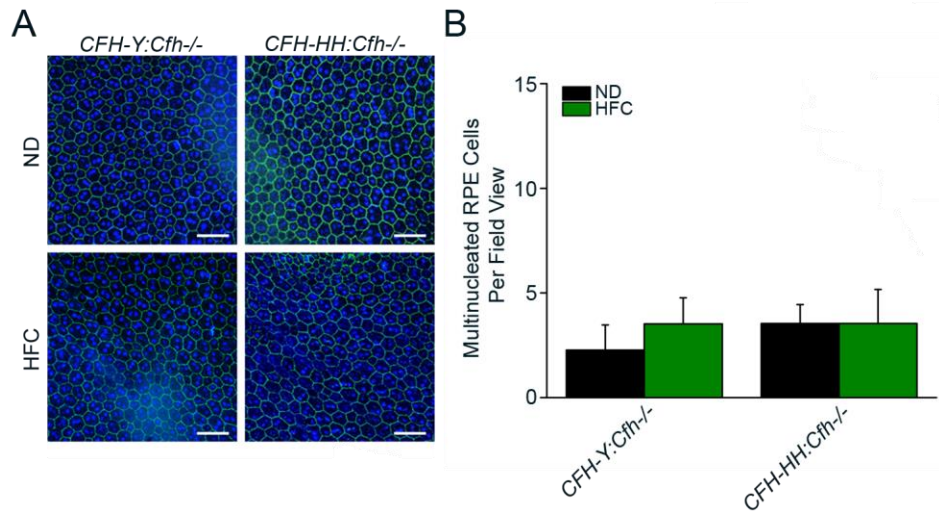
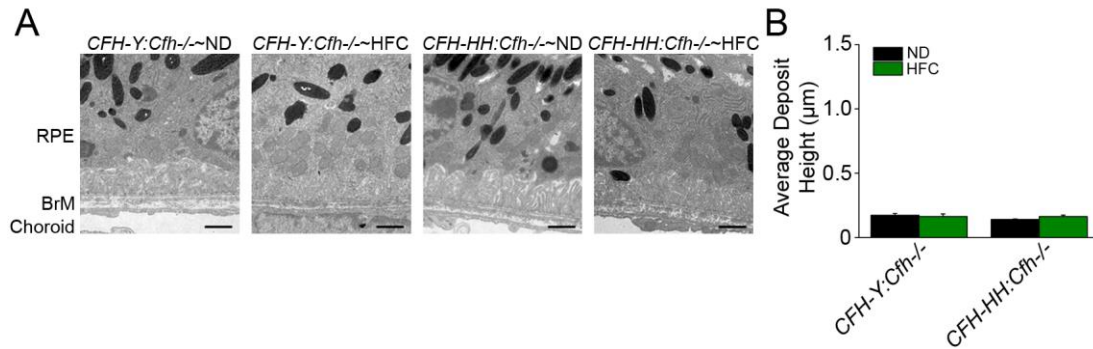


Figure 30: Vision loss in response to the HFC diet in mice expressing human H402 CFH is advanced aging dependent. Scotopic ERG flash responses in young (36-40 week old) *CFH:Cfh*<sup>-/-</sup> mice fed a ND or HFC diet presented as fitted stimulus response curves of B-wave amplitude averages as in Fig. 1A. No differences were observed between the responses for young adult *CFH-Y:Cfh*<sup>-/-</sup>~ND (black), *CFH-Y:Cfh*<sup>-/-</sup>~HFC mice (green), *CFH-HH:Cfh*<sup>-/-</sup>~ND (blue) and *CFH-HH:Cfh*<sup>-/-</sup>~HFC mice (pink). Data is presented as mean ± SEM.



**Figure 31: Increased RPE dysmorphogenesis in response to the HFC diet in mice expressing human H402 CFH is advanced aging dependent. (A) Representative confocal fluorescence images (40X magnification) of RPE flatmounts near the optic nerve stained with Hoechst 33342 (blue, nuclei) and anti-ZO-1 (green) from young (36-40 week old) *CFH:Cfh*<sup>-/-</sup> mice on ND and HFC diet. There are similar numbers of multinucleate RPE cells in young *CFH:Cfh*<sup>-/-</sup>~ND and ~HFC mice. Scale bar = 50  $\mu$ m. (D) Quantitation of multinucleated ( $n \geq 3$  nuclei) RPE cells per field view in young *CFH:Cfh*<sup>-/-</sup> mice on ND and HFC diet shows no statistical significant change in the number of multinucleate RPE cells between these genotypes on ND and HFC diet. Data is presented as mean  $\pm$  SD. N=4**



**Figure 32: Deposit formation in *CFH:Cfh-/-* mice is dependent on advanced age. (A)** Representative TEM (15000X magnification) images of young adult (36-40 week old) *CFH-Y:Cfh-/-* and *CFH-HH:Cfh-/-* mice  $\pm$  HFC diet treatment revealed no detectable sub-RPE deposits. **(B)** TEM images were quantified by measuring from the elastic layer of BrM to the top of the sub-RPE deposits. Since no sub-RPE deposits were observed, measurements are indicative of the distance between the elastic layer of Bruch's membrane (BrM) to the RPE basement membrane. No differences were observed between young *CFH-Y:Cfh-/-* and *CFH-HH:Cfh-/-* mice on and off HFC diet.

## Appendix C

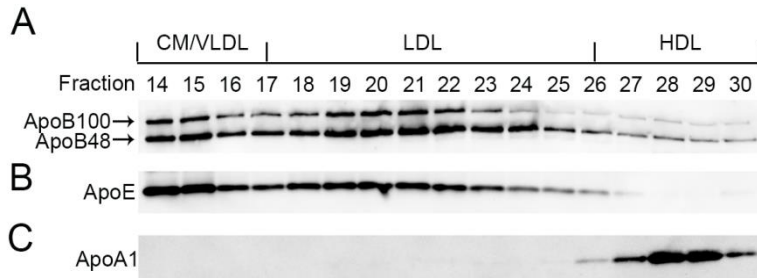


**Figure 33: Apolipoprotein content of FPLC-fractionated *CFH-HH:Cfh*<sup>-/-</sup> plasma after HFC diet. Plasma from an aged *CFH-HH:Cfh*<sup>-/-</sup>HFC mouse was fractionated using FPLC and the isolated fractions were analyzed by Western blot analysis for apolipoproteins B100 (ApoB100) and ApoB48 (A), ApoE (B) and ApoA1 (C). ApoB100, ApoB48 and ApoE are predominantly present in the fractions that correspond to CMs, VLDLs and LDLs. ApoA1 is only found in HDLs.**

## References

1. Toomey CB, Johnson LV, & Bowes Rickman C (2018) Complement factor H in AMD: Bridging genetic associations and pathobiology. *Progress in retinal and eye research* 62:38-57.
2. Hoon M, Okawa H, Della Santina L, & Wong RO (2014) Functional architecture of the retina: development and disease. *Progress in retinal and eye research* 42:44-84.
3. Arshavsky VY & Burns ME (2012) Photoreceptor signaling: supporting vision across a wide range of light intensities. *The Journal of biological chemistry* 287(3):1620-1626.
4. Terakita A (2005) The opsins. *Genome biology* 6(3):213.
5. Palczewski K (2012) Chemistry and biology of vision. *The Journal of biological chemistry* 287(3):1612-1619.
6. Strauss O (2005) The retinal pigment epithelium in visual function. *Physiological reviews* 85(3):845-881.
7. Bhutto I & Luty G (2012) Understanding age-related macular degeneration (AMD): relationships between the photoreceptor/retinal pigment epithelium/Bruch's membrane/choriocapillaris complex. *Molecular aspects of medicine* 33(4):295-317.
8. Marneros AG, *et al.* (2005) Vascular endothelial growth factor expression in the retinal pigment epithelium is essential for choriocapillaris development and visual function. *The American journal of pathology* 167(5):1451-1459.

9. Curcio CA & Johnson M (2013) Structure, Function, and Pathology of Bruch's Membrane., (Elsevier, Inc., London).
10. Tserentsoodol N, *et al.* (2006) Uptake of cholesterol by the retina occurs primarily via a low density lipoprotein receptor-mediated process. *Molecular vision* 12:1306-1318.
11. Curcio CA, Johnson M, Rudolf M, & Huang JD (2011) The oil spill in ageing Bruch membrane. *Br J Ophthalmol* 95(12):1638-1645.
12. Curcio CA, Johnson M, Huang JD, & Rudolf M (2010) Apolipoprotein B-containing lipoproteins in retinal aging and age-related macular degeneration. *Journal of lipid research* 51(3):451-467.
13. Jager RD, Mieler WF, & Miller JW (2008) Age-related macular degeneration. *The New England journal of medicine* 358(24):2606-2617.
14. Klein R, Klein BE, & Linton KL (1992) Prevalence of age-related maculopathy. The Beaver Dam Eye Study. *Ophthalmology* 99(6):933-943.
15. Vingerling JR, *et al.* (1995) The prevalence of age-related maculopathy in the Rotterdam Study. *Ophthalmology* 102(2):205-210.
16. Miller JW (2013) Age-Related Macular Degeneration Revisited - Piecing the Puzzle: The LXIX Edward Jackson Memorial Lecture. *American journal of ophthalmology* 155(1):48.
17. Chew EY, *et al.* (2014) Ten-year follow-up of age-related macular degeneration in the age-related eye disease study: AREDS report no. 36. *JAMA ophthalmology* 132(3):272-277.

18. Jonasson F, *et al.* (2014) Five-year incidence, progression, and risk factors for age-related macular degeneration: the age, gene/environment susceptibility study. *Ophthalmology* 121(9):1766-1772.
19. van Leeuwen R, Klaver CC, Vingerling JR, Hofman A, & de Jong PT (2003) The risk and natural course of age-related maculopathy: follow-up at 6 1/2 years in the Rotterdam study. *Arch Ophthalmol* 121(4):519-526.
20. Fritsche LG, *et al.* (2014) Age-related macular degeneration: genetics and biology coming together. *Annual review of genomics and human genetics* 15:151-171.
21. Fritsche LG, *et al.* (2016) A large genome-wide association study of age-related macular degeneration highlights contributions of rare and common variants. *Nature genetics* 48(2):134-143.
22. Ersoy L, *et al.* (2014) Nutritional risk factors for age-related macular degeneration. *BioMed research international* 2014:413150.
23. Howard KP, Klein BE, Lee KE, & Klein R (2014) Measures of body shape and adiposity as related to incidence of age-related eye diseases: observations from the Beaver Dam Eye Study. *Investigative ophthalmology & visual science* 55(4):2592-2598.
24. Ersoy L, *et al.* (2014) Genetic and environmental risk factors for age-related macular degeneration in persons 90 years and older. *Investigative ophthalmology & visual science* 55(3):1842-1847.
25. Smith W, Mitchell P, & Leeder SR (1996) Smoking and age-related maculopathy. The Blue Mountains Eye Study. *Arch Ophthalmol* 114(12):1518-1523.

26. Vingerling JR, Hofman A, Grobbee DE, & de Jong PT (1996) Age-related macular degeneration and smoking. The Rotterdam Study. *Arch Ophthalmol* 114(10):1193-1196.
27. Armstrong RA & Mousavi M (2015) Overview of Risk Factors for Age-Related Macular Degeneration (AMD). *J Stem Cells* 10(3):171-191.
28. Miller JW (2013) Age-related macular degeneration revisited--piecing the puzzle: the LXIX Edward Jackson memorial lecture. *American journal of ophthalmology* 155(1):1-35 e13.
29. Rudolf M, *et al.* (2008) Prevalence and morphology of druse types in the macula and periphery of eyes with age-related maculopathy. *Investigative ophthalmology & visual science* 49(3):1200-1209.
30. Sarks SH, Arnold JJ, Killingsworth MC, & Sarks JP (1999) Early drusen formation in the normal and aging eye and their relation to age related maculopathy: a clinicopathological study. *Br J Ophthalmol* 83(3):358-368.
31. Bowes Rickman C, Farsiu S, Toth CA, & Klingeborn M (2013) Dry age-related macular degeneration: mechanisms, therapeutic targets, and imaging. *Investigative ophthalmology & visual science* 54(14):ORSF68-80.
32. Wong WL, *et al.* (2014) Global prevalence of age-related macular degeneration and disease burden projection for 2020 and 2040: a systematic review and meta-analysis. *The Lancet. Global health* 2(2):e106-116.
33. Yazdi MH, Faramarzi MA, Nikfar S, Falavarjani KG, & Abdollahi M (2015) Ranibizumab and aflibercept for the treatment of wet age-related macular degeneration. *Expert Opin Biol Ther* 15(9):1349-1358.

34. Ba J, *et al.* (2015) Intravitreal anti-VEGF injections for treating wet age-related macular degeneration: a systematic review and meta-analysis. *Drug design, development and therapy* 9:5397-5405.
35. Yang S, Zhao J, & Sun X (2016) Resistance to anti-VEGF therapy in neovascular age-related macular degeneration: a comprehensive review. *Drug design, development and therapy* 10:1857-1867.
36. Aronow ME & Chew EY (2014) Age-related Eye Disease Study 2: perspectives, recommendations, and unanswered questions. *Curr Opin Ophthalmol* 25(3):186-190.
37. Age-Related Eye Disease Study Research G (2001) A randomized, placebo-controlled, clinical trial of high-dose supplementation with vitamins C and E, beta carotene, and zinc for age-related macular degeneration and vision loss: AREDS report no. 8. *Arch Ophthalmol* 119(10):1417-1436.
38. Pennesi ME, Neuringer M, & Courtney RJ (2012) Animal models of age related macular degeneration. *Molecular aspects of medicine* 33(4):487-509.
39. Gestri G, Link BA, & Neuhauss SC (2012) The visual system of zebrafish and its use to model human ocular diseases. *Developmental neurobiology* 72(3):302-327.
40. Chhetri J, Jacobson G, & Gueven N (2014) Zebrafish--on the move towards ophthalmological research. *Eye (Lond)* 28(4):367-380.
41. Volland S, Esteve-Rudd J, Hoo J, Yee C, & Williams DS (2015) A comparison of some organizational characteristics of the mouse central retina and the human macula. *PloS one* 10(4):e0125631.

42. Franco LM, *et al.* (2009) Decreased visual function after patchy loss of retinal pigment epithelium induced by low-dose sodium iodate. *Investigative ophthalmology & visual science* 50(8):4004-4010.
43. Enzmann V, *et al.* (2006) Behavioral and anatomical abnormalities in a sodium iodate-induced model of retinal pigment epithelium degeneration. *Experimental eye research* 82(3):441-448.
44. Lambert V, *et al.* (2013) Laser-induced choroidal neovascularization model to study age-related macular degeneration in mice. *Nature protocols* 8(11):2197-2211.
45. Jones A, *et al.* (2011) Increased expression of multifunctional serine protease, HTRA1, in retinal pigment epithelium induces polypoidal choroidal vasculopathy in mice. *Proceedings of the National Academy of Sciences of the United States of America* 108(35):14578-14583.
46. Nakayama M, *et al.* (2014) Overexpression of HtrA1 and exposure to mainstream cigarette smoke leads to choroidal neovascularization and subretinal deposits in aged mice. *Investigative ophthalmology & visual science* 55(10):6514-6523.
47. Vierkotten S, Muether PS, & Fauser S (2011) Overexpression of HTRA1 leads to ultrastructural changes in the elastic layer of Bruch's membrane via cleavage of extracellular matrix components. *PLoS ONE* 6(8):e22959.
48. Chavali VR, *et al.* (2011) A CTRP5 gene S163R mutation knock-in mouse model for late-onset retinal degeneration. *Human molecular genetics* 20(10):2000-2014.

49. Dinculescu A, *et al.* (2015) Pathological Effects of Mutant C1QTNF5 (S163R) Expression in Murine Retinal Pigment Epithelium. *Investigative ophthalmology & visual science* 56(11):6971-6980.
50. Fu L, *et al.* (2007) The R345W mutation in EFEMP1 is pathogenic and causes AMD-like deposits in mice. *Human molecular genetics* 16(20):2411-2422.
51. Marmorstein LY, McLaughlin PJ, Peachey NS, Sasaki T, & Marmorstein AD (2007) Formation and progression of sub-retinal pigment epithelium deposits in Efemp1 mutation knock-in mice: a model for the early pathogenic course of macular degeneration. *Human molecular genetics* 16(20):2423-2432.
52. Weber BH, *et al.* (2002) A mouse model for Sorsby fundus dystrophy. *Investigative ophthalmology & visual science* 43(8):2732-2740.
53. Karan G, *et al.* (2005) Lipofuscin accumulation, abnormal electrophysiology, and photoreceptor degeneration in mutant ELOVL4 transgenic mice: a model for macular degeneration. *Proceedings of the National Academy of Sciences of the United States of America* 102(11):4164-4169.
54. Vasireddy V, *et al.* (2006) Elovl4 5-bp-deletion knock-in mice develop progressive photoreceptor degeneration. *Investigative ophthalmology & visual science* 47(10):4558-4568.
55. Weng J, *et al.* (1999) Insights into the function of Rim protein in photoreceptors and etiology of Stargardt's disease from the phenotype in abcr knockout mice. *Cell* 98(1):13-23.

56. Charbel Issa P, *et al.* (2013) Fundus autofluorescence in the Abca4(-/-) mouse model of Stargardt disease--correlation with accumulation of A2E, retinal function, and histology. *Investigative ophthalmology & visual science* 54(8):5602-5612.
57. Radu RA, *et al.* (2011) Complement system dysregulation and inflammation in the retinal pigment epithelium of a mouse model for Stargardt macular degeneration. *The Journal of biological chemistry* 286(21):18593-18601.
58. Chen Y, *et al.* (2013) Systems pharmacology identifies drug targets for Stargardt disease-associated retinal degeneration. *The Journal of clinical investigation* 123(12):5119-5134.
59. Garland DL, *et al.* (2014) Mouse genetics and proteomic analyses demonstrate a critical role for complement in a model of DHRD/ML, an inherited macular degeneration. *Human molecular genetics* 23(1):52-68.
60. Fernandez-Godino R, Garland DL, & Pierce EA (2015) A local complement response by RPE causes early-stage macular degeneration. *Human molecular genetics* 24(19):5555-5569.
61. Mandal NA, *et al.* (2014) In vivo effect of mutant ELOVL4 on the expression and function of wild-type ELOVL4. *Investigative ophthalmology & visual science* 55(4):2705-2713.
62. Qi JH, *et al.* (2009) S156C mutation in tissue inhibitor of metalloproteinases-3 induces increased angiogenesis. *The Journal of biological chemistry* 284(30):19927-19936.

63. Lundh von Leithner P, *et al.* (2009) Complement factor h is critical in the maintenance of retinal perfusion. *The American journal of pathology* 175(1):412-421.
64. Choudhary M, *et al.* (2015) Aryl hydrocarbon receptor knock-out exacerbates choroidal neovascularization via multiple pathogenic pathways. *The Journal of pathology* 235(1):101-112.
65. Combadiere C, *et al.* (2007) CX3CR1-dependent subretinal microglia cell accumulation is associated with cardinal features of age-related macular degeneration. *The Journal of clinical investigation* 117(10):2920-2928.
66. O'Koren EG, Mathew R, & Saban DR (2016) Fate mapping reveals that microglia and recruited monocyte-derived macrophages are definitively distinguishable by phenotype in the retina. *Scientific reports* 6:20636.
67. Cingolani C, *et al.* (2006) Retinal degeneration from oxidative damage. *Free radical biology & medicine* 40(4):660-669.
68. Espinosa-Heidmann DG, *et al.* (2006) Cigarette smoke-related oxidants and the development of sub-RPE deposits in an experimental animal model of dry AMD. *Investigative ophthalmology & visual science* 47(2):729-737.
69. Wang J, Iacovelli J, Spencer C, & Saint-Geniez M (2014) Direct effect of sodium iodate on neurosensory retina. *Investigative ophthalmology & visual science* 55(3):1941-1953.
70. Tarallo V, *et al.* (2012) DICER1 loss and Alu RNA induce age-related macular degeneration via the NLRP3 inflammasome and MyD88. *Cell* 149(4):847-859.

71. Longbottom R, *et al.* (2009) Genetic ablation of retinal pigment epithelial cells reveals the adaptive response of the epithelium and impact on photoreceptors. *Proceedings of the National Academy of Sciences of the United States of America* 106(44):18728-18733.
72. Fujihara M, Bartels E, Nielsen LB, & Handa JT (2009) A human apoB100 transgenic mouse expresses human apoB100 in the RPE and develops features of early AMD. *Experimental eye research* 88(6):1115-1123.
73. Malek G, *et al.* (2005) Apolipoprotein E allele-dependent pathogenesis: a model for age-related retinal degeneration. *Proceedings of the National Academy of Sciences of the United States of America* 102(33):11900-11905.
74. Hu P, *et al.* (2013) Aryl hydrocarbon receptor deficiency causes dysregulated cellular matrix metabolism and age-related macular degeneration-like pathology. *Proceedings of the National Academy of Sciences of the United States of America* 110(43):E4069-4078.
75. Rowan S, *et al.* (2017) Involvement of a gut-retina axis in protection against dietary glycemia-induced age-related macular degeneration. *Proceedings of the National Academy of Sciences of the United States of America* 114(22):E4472-E4481.
76. Doyle SL, *et al.* (2012) NLRP3 has a protective role in age-related macular degeneration through the induction of IL-18 by drusen components. *Nature medicine* 18(5):791-798.
77. Cruz-Guilloty F, *et al.* (2013) Infiltration of proinflammatory m1 macrophages into the outer retina precedes damage in a mouse model of age-related macular degeneration. *International journal of inflammation* 2013:503725.

78. Coffey PJ, *et al.* (2007) Complement factor H deficiency in aged mice causes retinal abnormalities and visual dysfunction. *Proceedings of the National Academy of Sciences of the United States of America* 104(42):16651-16656.
79. Ding JD, *et al.* (2015) Expression of human complement factor h prevents age-related macular degeneration-like retina damage and kidney abnormalities in aged cfh knockout mice. *The American journal of pathology* 185(1):29-42.
80. Toomey CB, Kelly U, Saban DR, & Bowes Rickman C (2015) Regulation of age-related macular degeneration-like pathology by complement factor H. *Proceedings of the National Academy of Sciences of the United States of America* 112(23):E3040-3049.
81. Toomey CB, *et al.* (2018) Effect of Anti-C5a Therapy in a Murine Model of Early/Intermediate Dry Age-Related Macular Degeneration. *Invest Ophthalmol Vis Sci* 59(2):662-673.
82. Ufret-Vincenty RL, *et al.* (2010) Transgenic mice expressing variants of complement factor H develop AMD-like retinal findings. *Investigative ophthalmology & visual science* 51(11):5878-5887.
83. Hadziahmetovic M, *et al.* (2011) The oral iron chelator deferiprone protects against iron overload-induced retinal degeneration. *Investigative ophthalmology & visual science* 52(2):959-968.
84. Levy O, *et al.* (2015) APOE Isoforms Control Pathogenic Subretinal Inflammation in Age-Related Macular Degeneration. *The Journal of neuroscience : the official journal of the Society for Neuroscience* 35(40):13568-13576.

85. Calippe B, *et al.* (2017) Complement Factor H Inhibits CD47-Mediated Resolution of Inflammation. *Immunity* 46(2):261-272.
86. Zhao Z, *et al.* (2011) Age-related retinopathy in NRF2-deficient mice. *PLoS ONE* 6(4):e19456.
87. Zhao Z, *et al.* (2014) gammadelta T Cells as a Major Source of IL-17 Production During Age-Dependent RPE Degeneration. *Investigative ophthalmology & visual science* 55(10):6580-6589.
88. Dong A, *et al.* (2006) Superoxide dismutase 1 protects retinal cells from oxidative damage. *Journal of cellular physiology* 208(3):516-526.
89. Qi X, *et al.* (2017) Systemic Injection of RPE65-Programmed Bone Marrow-Derived Cells Prevents Progression of Chronic Retinal Degeneration. *Mol Ther* 25(4):917-927.
90. Hayward C, *et al.* (2003) Mutation in a short-chain collagen gene, CTRP5, results in extracellular deposit formation in late-onset retinal degeneration: a genetic model for age-related macular degeneration. *Human molecular genetics* 12(20):2657-2667.
91. Stone EM, *et al.* (1999) A single EFEMP1 mutation associated with both Malattia Leventinese and Doyme honeycomb retinal dystrophy. *Nature genetics* 22(2):199-202.
92. Weber B, Vogt G, Pruetz R, Stohr H, & Felbor U (1994) Mutations in the tissue inhibitor of metalloproteinases-3 (TIMP3) in patients with Sorsby's fundus dystrophy. *Nature genetics* 8(4):352-356.

93. Zhang K, *et al.* (2001) A 5-bp deletion in ELOVL4 is associated with two related forms of autosomal dominant macular dystrophy. *Nature genetics* 27(1):89-93.
94. Allikmets R, *et al.* (1997) Mutation of the Stargardt disease gene (ABCR) in age-related macular degeneration. *Science* 277(5333):1805-1807.
95. Maeda A, Golczak M, Maeda T, & Palczewski K (2009) Limited roles of Rdh8, Rdh12, and Abca4 in all-trans-retinal clearance in mouse retina. *Investigative ophthalmology & visual science* 50(11):5435-5443.
96. Maeda A, *et al.* (2009) Involvement of all-trans-retinal in acute light-induced retinopathy of mice. *The Journal of biological chemistry* 284(22):15173-15183.
97. Espinosa-Heidmann DG, *et al.* (2006) Cigarette smoke-related oxidants and the development of sub-RPE deposits in an experimental animal model of dry AMD. *Investigative ophthalmology & visual science* 47(2):729-737.
98. Cachafeiro M, *et al.* (2013) Hyperactivation of retina by light in mice leads to photoreceptor cell death mediated by VEGF and retinal pigment epithelium permeability. *Cell death & disease* 4:e781.
99. Grimm C & Reme CE (2013) Light damage as a model of retinal degeneration. *Methods in molecular biology* 935:87-97.
100. Chen L, *et al.* (2004) Light damage induced changes in mouse retinal gene expression. *Experimental eye research* 79(2):239-247.

101. Krzystolik MG, *et al.* (2002) Prevention of experimental choroidal neovascularization with intravitreal anti-vascular endothelial growth factor antibody fragment. *Archives of ophthalmology* 120(3):338-346.
102. Grossniklaus HE, Kang SJ, & Berglin L (2010) Animal models of choroidal and retinal neovascularization. *Progress in retinal and eye research* 29(6):500-519.
103. Poor SH, *et al.* (2014) Reliability of the mouse model of choroidal neovascularization induced by laser photocoagulation. *Investigative ophthalmology & visual science* 55(10):6525-6534.
104. Justilien V, *et al.* (2007) SOD2 knockdown mouse model of early AMD. *Investigative ophthalmology & visual science* 48(10):4407-4420.
105. Mao H, *et al.* (2014) Mitochondrial oxidative stress in the retinal pigment epithelium leads to localized retinal degeneration. *Investigative ophthalmology & visual science* 55(7):4613-4627.
106. Imamura Y, *et al.* (2006) Drusen, choroidal neovascularization, and retinal pigment epithelium dysfunction in SOD1-deficient mice: a model of age-related macular degeneration. *Proceedings of the National Academy of Sciences of the United States of America* 103(30):11282-11287.
107. Ding JD, *et al.* (2011) Anti-amyloid therapy protects against retinal pigmented epithelium damage and vision loss in a model of age-related macular degeneration. *Proceedings of the National Academy of Sciences of the United States of America* 108(28):E279-287.
108. Hollyfield JG, *et al.* (2008) Oxidative damage-induced inflammation initiates age-related macular degeneration. *Nature medicine* 14:194-198.

109. Hahn P, *et al.* (2004) Disruption of ceruloplasmin and hephaestin in mice causes retinal iron overload and retinal degeneration with features of age-related macular degeneration. *Proceedings of the National Academy of Sciences of the United States of America* 101(38):13850-13855.
110. Weikel KA, *et al.* (2012) Natural history of age-related retinal lesions that precede AMD in mice fed high or low glycemic index diets. *Investigative ophthalmology & visual science* 53(2):622-632.
111. Kaneko H, *et al.* (2011) DICER1 deficit induces Alu RNA toxicity in age-related macular degeneration. *Nature* 471(7338):325-330.
112. Hadziahmetovic M, *et al.* (2008) Ceruloplasmin/hephaestin knockout mice model morphologic and molecular features of AMD. *Investigative ophthalmology & visual science* 49(6):2728-2736.
113. Fujihara M, Nagai N, Sussan TE, Biswal S, & Handa JT (2008) Chronic cigarette smoke causes oxidative damage and apoptosis to retinal pigmented epithelial cells in mice. *PLoS ONE* 3(9):e3119.
114. Rodriguez IR, Clark ME, Lee JW, & Curcio CA (2014) 7-ketocholesterol accumulates in ocular tissues as a consequence of aging and is present in high levels in drusen. *Experimental eye research* 128:151-155.
115. Wang L, *et al.* (2010) Abundant lipid and protein components of drusen. *PloS one* 5(4):e10329.
116. Li CM, Clark ME, Chimento MF, & Curcio CA (2006) Apolipoprotein localization in isolated drusen and retinal apolipoprotein gene expression. *Investigative ophthalmology & visual science* 47(7):3119-3128.

117. Crabb JW, *et al.* (2002) Drusen proteome analysis: an approach to the etiology of age-related macular degeneration. *Proceedings of the National Academy of Sciences of the United States of America* 99(23):14682-14687.
118. Huebbe P & Rimbach G (2017) Evolution of human apolipoprotein E (APOE) isoforms: Gene structure, protein function and interaction with dietary factors. *Ageing research reviews* 37:146-161.
119. Ding JD, *et al.* (2011) Anti-amyloid therapy protects against retinal pigmented epithelium damage and vision loss in a model of age-related macular degeneration. *Proc Natl Acad Sci U S A* 108(28):E279-287.
120. McKay GJ, *et al.* (2011) Evidence of association of APOE with age-related macular degeneration: a pooled analysis of 15 studies. *Human mutation* 32(12):1407-1416.
121. Yamauchi Y, *et al.* (2008) Role of the N- and C-terminal domains in binding of apolipoprotein E isoforms to heparan sulfate and dermatan sulfate: a surface plasmon resonance study. *Biochemistry* 47(25):6702-6710.
122. Rogers J, *et al.* (1992) Complement activation by beta-amyloid in Alzheimer disease. *Proceedings of the National Academy of Sciences of the United States of America* 89(21):10016-10020.
123. Anderson DH, Mullins RF, Hageman GS, & Johnson LV (2002) A role for local inflammation in the formation of drusen in the aging eye. *American journal of ophthalmology* 134(3):411-431.
124. Kanda A, Abecasis G, & Swaroop A (2008) Inflammation in the pathogenesis of age-related macular degeneration. *Br J Ophthalmol* 92(4):448-450.

125. Devasthanam AS & Tomasi TB (2014) Dicer in immune cell development and function. *Immunological investigations* 43(2):182-195.
126. Gelfand BD, *et al.* (2015) Iron Toxicity in the Retina Requires Alu RNA and the NLRP3 Inflammasome. *Cell reports* 11(11):1686-1693.
127. Ardeljan D, Tuo J, & Chan CC (2011) Carboxyethylpyrrole plasma biomarkers in age-related macular degeneration. *Drugs of the future* 36(9):712-718.
128. Hollyfield JG, *et al.* (2008) Oxidative damage-induced inflammation initiates age-related macular degeneration. *Nature medicine* 14(2):194-198.
129. Ambati J, *et al.* (2003) An animal model of age-related macular degeneration in senescent Ccl-2- or Ccr-2-deficient mice. *Nature medicine* 9(11):1390-1397.
130. Doyle SL, *et al.* (2014) IL-18 attenuates experimental choroidal neovascularization as a potential therapy for wet age-related macular degeneration. *Science translational medicine* 6(230):230ra244.
131. Ijima R, *et al.* (2014) Interleukin-18 induces retinal pigment epithelium degeneration in mice. *Investigative ophthalmology & visual science* 55(10):6673-6678.
132. Doyle SL, *et al.* (2015) IL-18 Immunotherapy for Neovascular AMD: Tolerability and Efficacy in Nonhuman Primates. *Investigative ophthalmology & visual science* 56(9):5424-5430.
133. Majewski J, *et al.* (2003) Age-related macular degeneration--a genome scan in extended families. *American journal of human genetics* 73(3):540-550.

134. Kenealy SJ, *et al.* (2004) Linkage analysis for age-related macular degeneration supports a gene on chromosome 10q26. *Molecular vision* 10:57-61.
135. Wang G (2014) Chromosome 10q26 locus and age-related macular degeneration: a progress update. *Experimental eye research* 119:1-7.
136. Dewan A, *et al.* (2006) HTRA1 promoter polymorphism in wet age-related macular degeneration. *Science* 314(5801):989-992.
137. Yang Z, *et al.* (2006) A variant of the HTRA1 gene increases susceptibility to age-related macular degeneration. *Science* 314(5801):992-993.
138. Iejima D, *et al.* (2014) High-Temperature Requirement A Serine Peptidase 1 Gene is Transcriptionally Regulated by Insertion/Deletion Nucleotides Located at the 3 Prime End of Age-Related Maculopathy Susceptibility 2 Gene in Patients with Age-Related Macular Degeneration. *The Journal of biological chemistry*.
139. Yannuzzi LA, Sorenson J, Spaide RF, & Lipson B (1990) Idiopathic polypoidal choroidal vasculopathy (IPCV). *Retina* 10(1):1-8.
140. Spaide RF, Yannuzzi LA, Slakter JS, Sorenson J, & Orlich DA (1995) Indocyanine green videoangiography of idiopathic polypoidal choroidal vasculopathy. *Retina* 15(2):100-110.
141. Smith W, *et al.* (2001) Risk factors for age-related macular degeneration: Pooled findings from three continents. *Ophthalmology* 108(4):697-704.

142. Woodell A, *et al.* (2013) Alternative complement pathway deficiency ameliorates chronic smoke-induced functional and morphological ocular injury. *PLoS ONE* 8(6):e67894.
143. Fu S, Zhu M, Wang C, & Le YZ (2014) Efficient induction of productive Cre-mediated recombination in retinal pigment epithelium. *Molecular vision* 20:480-487.
144. Johnson LV, Leitner WP, Staples MK, & Anderson DH (2001) Complement activation and inflammatory processes in Drusen formation and age related macular degeneration. *Experimental eye research* 73(6):887-896.
145. Johnson LV, Ozaki S, Staples MK, Erickson PA, & Anderson DH (2000) A potential role for immune complex pathogenesis in drusen formation. *Experimental eye research* 70(4):441-449.
146. Hageman GS, *et al.* (2005) A common haplotype in the complement regulatory gene factor H (HF1/CFH) predisposes individuals to age-related macular degeneration. *Proceedings of the National Academy of Sciences of the United States of America* 102(20):7227-7232.
147. Klein RJ, *et al.* (2005) Complement factor H polymorphism in age-related macular degeneration. *Science* 308(5720):385-389.
148. Edwards AO, *et al.* (2005) Complement factor H polymorphism and age-related macular degeneration. *Science* 308(5720):421-424.
149. Haines JL, *et al.* (2005) Complement factor H variant increases the risk of age-related macular degeneration. *Science* 308(5720):419-421.

150. Raychaudhuri S, *et al.* (2011) A rare penetrant mutation in CFH confers high risk of age-related macular degeneration. *Nature genetics* 43(12):1232-1236.
151. Seddon JM, *et al.* (2013) Rare variants in CFI, C3 and C9 are associated with high risk of advanced age-related macular degeneration. *Nature genetics*.
152. Helgason H, *et al.* (2013) A rare nonsynonymous sequence variant in C3 is associated with high risk of age-related macular degeneration. *Nature genetics*.
153. Maller JB, *et al.* (2007) Variation in complement factor 3 is associated with risk of age-related macular degeneration. *Nature genetics* 39(10):1200-1201.
154. Gold B, *et al.* (2006) Variation in factor B (BF) and complement component 2 (C2) genes is associated with age-related macular degeneration. *Nature genetics* 38(4):458-462.
155. Anderson DH, *et al.* (2010) The pivotal role of the complement system in aging and age-related macular degeneration: hypothesis re-visited. *Progress in retinal and eye research* 29(2):95-112.
156. Yehoshua Z, *et al.* (2014) Systemic complement inhibition with eculizumab for geographic atrophy in age-related macular degeneration: the COMPLETE study. *Ophthalmology* 121(3):693-701.
157. Elvington M, Liszewski MK, & Atkinson JP (2016) Evolution of the complement system: from defense of the single cell to guardian of the intravascular space. *Immunol Rev* 274(1):9-15.

158. Hajishengallis G, Reis ES, Mastellos DC, Ricklin D, & Lambris JD (2017) Novel mechanisms and functions of complement. *Nat Immunol* 18(12):1288-1298.
159. Holers VM (2014) Complement and its receptors: new insights into human disease. *Annu Rev Immunol* 32:433-459.
160. Ahearn JM, *et al.* (1996) Disruption of the Cr2 locus results in a reduction in B-1a cells and in an impaired B cell response to T-dependent antigen. *Immunity* 4(3):251-262.
161. Nielsen CH, Fischer EM, & Leslie RG (2000) The role of complement in the acquired immune response. *Immunology* 100(1):4-12.
162. Kremlitzka M, Macsik-Valent B, & Erdei A (2016) Regulation of B cell functions by Toll-like receptors and complement. *Immunol Lett* 178:37-44.
163. Stevens B, *et al.* (2007) The classical complement cascade mediates CNS synapse elimination. *Cell* 131(6):1164-1178.
164. Chu Y, *et al.* (2010) Enhanced synaptic connectivity and epilepsy in C1q knockout mice. *Proceedings of the National Academy of Sciences of the United States of America* 107(17):7975-7980.
165. Pocklington AJ, O'Donovan M, & Owen MJ (2014) The synapse in schizophrenia. *Eur J Neurosci* 39(7):1059-1067.
166. Sekar A, *et al.* (2016) Schizophrenia risk from complex variation of complement component 4. *Nature* 530(7589):177-183.

167. Liszewski MK, *et al.* (2013) Intracellular complement activation sustains T cell homeostasis and mediates effector differentiation. *Immunity* 39(6):1143-1157.
168. Kolev M, *et al.* (2015) Complement Regulates Nutrient Influx and Metabolic Reprogramming during Th1 Cell Responses. *Immunity* 42(6):1033-1047.
169. Paglialunga S, *et al.* (2008) Acylation-stimulating protein deficiency and altered adipose tissue in alternative complement pathway knockout mice. *Am J Physiol Endocrinol Metab* 294(3):E521-529.
170. Liu Q, Siloto RM, Lehner R, Stone SJ, & Weselake RJ (2012) Acyl-CoA:diacylglycerol acyltransferase: molecular biology, biochemistry and biotechnology. *Prog Lipid Res* 51(4):350-377.
171. Moreno-Navarrete JM & Fernandez-Real JM (2017) The complement system is dysfunctional in metabolic disease: Evidences in plasma and adipose tissue from obese and insulin resistant subjects. *Semin Cell Dev Biol.*
172. Rohrer B, *et al.* (2009) A targeted inhibitor of the alternative complement pathway reduces angiogenesis in a mouse model of age-related macular degeneration. *Investigative ophthalmology & visual science* 50(7):3056-3064.
173. Lyzogubov VV, *et al.* (2010) Role of ocular complement factor H in a murine model of choroidal neovascularization. *The American journal of pathology* 177(4):1870-1880.
174. Rohrer B, Coughlin B, Bandyopadhyay M, & Holers VM (2012) Systemic human CR2-targeted complement alternative pathway inhibitor

- ameliorates mouse laser-induced choroidal neovascularization. *J Ocul Pharmacol Ther* 28(4):402-409.
175. Yaspan BL, *et al.* (2017) Targeting factor D of the alternative complement pathway reduces geographic atrophy progression secondary to age-related macular degeneration. *Science translational medicine* 9(395).
  176. Waugh N, *et al.* (2018) Treatments for dry age-related macular degeneration and Stargardt disease: a systematic review. *Health Technol Assess* 22(27):1-168.
  177. Toomey CB, Johnson LV, & Bowes Rickman C (2017) Complement factor H in AMD: Bridging genetic associations and pathobiology. *Progress in retinal and eye research*.
  178. DiScipio RG (1992) Ultrastructures and interactions of complement factors H and I. *J Immunol* 149(8):2592-2599.
  179. Sharma AK & Pangburn MK (1996) Identification of three physically and functionally distinct binding sites for C3b in human complement factor H by deletion mutagenesis. *Proceedings of the National Academy of Sciences of the United States of America* 93(20):10996-11001.
  180. Pickering MC, *et al.* (2002) Uncontrolled C3 activation causes membranoproliferative glomerulonephritis in mice deficient in complement factor H. *Nature genetics* 31(4):424-428.
  181. Kelly U, *et al.* (2010) Heparan sulfate, including that in Bruch's membrane, inhibits the complement alternative pathway: implications for age-related macular degeneration. *J Immunol* 185(9):5486-5494.

182. Skerka C, *et al.* (2007) Defective complement control of factor H (Y402H) and FHL-1 in age-related macular degeneration. *Molecular immunology* 44(13):3398-3406.
183. Clark SJ, Bishop PN, & Day AJ (2010) Complement factor H and age-related macular degeneration: the role of glycosaminoglycan recognition in disease pathology. *Biochemical Society transactions* 38(5):1342-1348.
184. Ormsby RJ, *et al.* (2008) Functional and structural implications of the complement factor H Y402H polymorphism associated with age-related macular degeneration. *Investigative ophthalmology & visual science* 49(5):1763-1770.
185. Yu J, *et al.* (2007) Biochemical analysis of a common human polymorphism associated with age-related macular degeneration. *Biochemistry* 46(28):8451-8461.
186. Molins B, *et al.* (2016) Complement factor H binding of monomeric C-reactive protein downregulates proinflammatory activity and is impaired with at risk polymorphic CFH variants. *Scientific reports* 6:22889.
187. Clark SJ, *et al.* (2010) Impaired binding of the age-related macular degeneration-associated complement factor H 402H allotype to Bruch's membrane in human retina. *The Journal of biological chemistry* 285(39):30192-30202.
188. Weismann D, *et al.* (2011) Complement factor H binds malondialdehyde epitopes and protects from oxidative stress. *Nature* 478(7367):76-81.
189. Shaw PX, *et al.* (2012) Complement factor H genotypes impact risk of age-related macular degeneration by interaction with oxidized phospholipids.

*Proceedings of the National Academy of Sciences of the United States of America* 109(34):13757-13762.

190. Rougier N, *et al.* (1998) Human complement factor H deficiency associated with hemolytic uremic syndrome. *J Am Soc Nephrol* 9(12):2318-2326.
191. Levy M, *et al.* (1986) H deficiency in two brothers with atypical dense intramembranous deposit disease. *Kidney Int* 30(6):949-956.
192. Bomback AS & Appel GB (2012) Pathogenesis of the C3 glomerulopathies and reclassification of MPGN. *Nat Rev Nephrol* 8(11):634-642.
193. Mullins RF, Aptsiauri N, & Hageman GS (2001) Structure and composition of drusen associated with glomerulonephritis: implications for the role of complement activation in drusen biogenesis. *Eye (Lond)* 15(Pt 3):390-395.
194. Hoh Kam J, Lenassi E, Malik TH, Pickering MC, & Jeffery G (2013) Complement component C3 plays a critical role in protecting the aging retina in a murine model of age-related macular degeneration. *The American journal of pathology* 183(2):480-492.
195. Ding JD, *et al.* (2014) Expression of human complement factor H (CFH) prevents AMD-like retina damage and kidney abnormalities in aged Cfh knock-out mice. *The American Journal of Pathology*.
196. Hoh Kam J, Morgan JE, & Jeffery G (2016) Aged complement factor H knockout mice kept in a clean barriered environment have reduced retinal pathology. *Experimental eye research* 149:116-125.

197. Faber C, *et al.* (2012) Complement factor H deficiency results in decreased neuroretinal expression of Cd59a in aged mice. *Investigative ophthalmology & visual science* 53(10):6324-6330.
198. Ansari M, *et al.* (2013) Genetic influences on plasma CFH and CFHR1 concentrations and their role in susceptibility to age-related macular degeneration. *Human molecular genetics* 22(23):4857-4869.
199. Silva AS, *et al.* (2012) Plasma levels of complement proteins from the alternative pathway in patients with age-related macular degeneration are independent of Complement Factor H Tyr(4)(0)(2)His polymorphism. *Molecular vision* 18:2288-2299.
200. Reynolds R, *et al.* (2009) Plasma complement components and activation fragments: associations with age-related macular degeneration genotypes and phenotypes. *Investigative ophthalmology & visual science* 50(12):5818-5827.
201. Scholl HP, *et al.* (2008) Systemic complement activation in age-related macular degeneration. *PLoS ONE* 3(7):e2593.
202. Mandal MN & Ayyagari R (2006) Complement factor H: spatial and temporal expression and localization in the eye. *Investigative ophthalmology & visual science* 47(9):4091-4097.
203. Merle NS, Noe R, Halbwachs-Mecarelli L, Fremeaux-Bacchi V, & Roumenina LT (2015) Complement System Part II: Role in Immunity. *Front Immunol* 6:257.
204. Lechner J, *et al.* (2016) Higher plasma levels of complement C3a, C4a and C5a increase the risk of subretinal fibrosis in neovascular age-related

macular degeneration: Complement activation in AMD. *Immunity & ageing : I & A* 13:4.

205. Nozaki M, *et al.* (2006) Drusen complement components C3a and C5a promote choroidal neovascularization. *Proceedings of the National Academy of Sciences of the United States of America* 103(7):2328-2333.
206. Skeie JM, Fingert JH, Russell SR, Stone EM, & Mullins RF (2010) Complement component C5a activates ICAM-1 expression on human choroidal endothelial cells. *Investigative ophthalmology & visual science* 51(10):5336-5342.
207. Liu B, *et al.* (2011) Complement component C5a promotes expression of IL-22 and IL-17 from human T cells and its implication in age-related macular degeneration. *J Transl Med* 9:1-12.
208. Cao S, *et al.* (2016) CFH Y402H polymorphism and the complement activation product C5a: effects on NF-kappaB activation and inflammasome gene regulation. *Br J Ophthalmol* 100(5):713-718.
209. Cortright DN, Meade R, Waters SM, Chenard BL, & Krause JE (2009) C5a, but not C3a, increases VEGF secretion in ARPE-19 human retinal pigment epithelial cells. *Current eye research* 34(1):57-61.
210. Coughlin B, *et al.* (2016) Connecting the innate and adaptive immune responses in mouse choroidal neovascularization via the anaphylatoxin C5a and gammadeltaT-cells. *Scientific reports* 6:23794.
211. Brockmann C, *et al.* (2015) Intravitreal inhibition of complement C5a reduces choroidal neovascularization in mice. *Graefe's archive for clinical and experimental ophthalmology = Albrecht von Graefes Archiv fur klinische und experimentelle Ophthalmologie* 253(10):1695-1704.

212. Ishibashi T, Miller H, Orr G, Sorgente N, & Ryan SJ (1987) Morphologic observations on experimental subretinal neovascularization in the monkey. *Investigative ophthalmology & visual science* 28(7):1116-1130.
213. Hageman GS, *et al.* (2001) An integrated hypothesis that considers drusen as biomarkers of immune-mediated processes at the RPE-Bruch's membrane interface in aging and age-related macular degeneration. *Progress in retinal and eye research* 20(6):705-732.
214. Tsau C, *et al.* (2011) Barx2 and Fgf10 regulate ocular glands branching morphogenesis by controlling extracellular matrix remodeling. *Development* 138(15):3307-3317.
215. Kuny S, Gaillard F, & Sauve Y (2012) Differential gene expression in eyecup and retina of a mouse model of Stargardt-like macular dystrophy (STGD3). *Investigative ophthalmology & visual science* 53(2):664-675.
216. Carr AJ, *et al.* (2011) The expression of retinal cell markers in human retinal pigment epithelial cells and their augmentation by the synthetic retinoid fenretinide. *Molecular vision* 17:1701-1715.
217. Carlin LM, *et al.* (2013) Nr4a1-dependent Ly6C(low) monocytes monitor endothelial cells and orchestrate their disposal. *Cell* 153(2):362-375.
218. Rudnicka AR, *et al.* (2012) Age and gender variations in age-related macular degeneration prevalence in populations of European ancestry: a meta-analysis. *Ophthalmology* 119(3):571-580.
219. van Leeuwen R, *et al.* (2005) Dietary intake of antioxidants and risk of age-related macular degeneration. *JAMA* 294(24):3101-3107.

220. VandenLangenberg GM, *et al.* (1998) Associations between antioxidant and zinc intake and the 5-year incidence of early age-related maculopathy in the Beaver Dam Eye Study. *Am J Epidemiol* 148(2):204-214.
221. Anderson DH, *et al.* (2004) Characterization of beta amyloid assemblies in drusen: the deposits associated with aging and age-related macular degeneration. *Experimental eye research* 78(2):243-256.
222. Dentchev T, Milam AH, Lee VM, Trojanowski JQ, & Dunaief JL (2003) Amyloid-beta is found in drusen from some age-related macular degeneration retinas, but not in drusen from normal retinas. *Molecular vision* 9:184-190.
223. Johnson LV, *et al.* (2002) The Alzheimer's A beta -peptide is deposited at sites of complement activation in pathologic deposits associated with aging and age-related macular degeneration. *Proceedings of the National Academy of Sciences of the United States of America* 99(18):11830-11835.
224. Kurji KH, *et al.* (2010) Microarray analysis identifies changes in inflammatory gene expression in response to amyloid-beta stimulation of cultured human retinal pigment epithelial cells. *Investigative ophthalmology & visual science* 51(2):1151-1163.
225. Wang J, *et al.* (2009) Amyloid-beta up-regulates complement factor B in retinal pigment epithelial cells through cytokines released from recruited macrophages/microglia: Another mechanism of complement activation in age-related macular degeneration. *Journal of cellular physiology* 220(1):119-128.
226. Nakai K, *et al.* (2008) Dendritic cells augment choroidal neovascularization. *Investigative ophthalmology & visual science* 49(8):3666-3670.

227. Hasegawa E, *et al.* (2013) IL-23-independent induction of IL-17 from gammadeltaT cells and innate lymphoid cells promotes experimental intraocular neovascularization. *J Immunol* 190(4):1778-1787.
228. Zhou J, *et al.* (2005) Neutrophils promote experimental choroidal neovascularization. *Molecular vision* 11:414-424.
229. Caicedo A, Espinosa-Heidmann DG, Pina Y, Hernandez EP, & Cousins SW (2005) Blood-derived macrophages infiltrate the retina and activate Muller glial cells under experimental choroidal neovascularization. *Experimental eye research* 81(1):38-47.
230. Espinosa-Heidmann DG, *et al.* (2003) Macrophage depletion diminishes lesion size and severity in experimental choroidal neovascularization. *Investigative ophthalmology & visual science* 44(8):3586-3592.
231. Monk PN, Scola AM, Madala P, & Fairlie DP (2007) Function, structure and therapeutic potential of complement C5a receptors. *Br J Pharmacol* 152(4):429-448.
232. Owsley C, *et al.* (2016) Delayed Rod-Mediated Dark Adaptation Is a Functional Biomarker for Incident Early Age-Related Macular Degeneration. *Ophthalmology* 123(2):344-351.
233. Travis AM, Heflin SJ, Hirano AA, Brecha NC, & Arshavsky VY (2018) Dopamine-Dependent Sensitization of Rod Bipolar Cells by GABA Is Conveyed through Wide-Field Amacrine Cells. *J Neurosci* 38(3):723-732.
234. Aredo B, *et al.* (2015) A chimeric Cfh transgene leads to increased retinal oxidative stress, inflammation, and accumulation of activated subretinal microglia in mice. *Investigative ophthalmology & visual science* 56(6):3427-3440.

235. Lambert NG, *et al.* (2016) Risk factors and biomarkers of age-related macular degeneration. *Progress in retinal and eye research* 54:64-102.
236. Stanhope KL, *et al.* (2018) Pathways and mechanisms linking dietary components to cardiometabolic disease: thinking beyond calories. *Obes Rev.*
237. Nunes S, *et al.* (2018) Adherence to a Mediterranean diet and its association with age-related macular degeneration. The Coimbra Eye Study-Report 4. *Nutrition* 51-52:6-12.
238. Hogg RE, *et al.* (2017) Mediterranean Diet Score and Its Association with Age-Related Macular Degeneration: The European Eye Study. *Ophthalmology* 124(1):82-89.
239. Merle BM, Silver RE, Rosner B, & Seddon JM (2015) Adherence to a Mediterranean diet, genetic susceptibility, and progression to advanced macular degeneration: a prospective cohort study. *Am J Clin Nutr* 102(5):1196-1206.
240. Chiu CJ, *et al.* (2014) The relationship of major American dietary patterns to age-related macular degeneration. *American journal of ophthalmology* 158(1):118-127 e111.
241. Rowan S, *et al.* (2014) Cfh genotype interacts with dietary glycemic index to modulate age-related macular degeneration-like features in mice. *Investigative ophthalmology & visual science* 55(1):492-501.
242. Wouters K, *et al.* (2008) Dietary cholesterol, rather than liver steatosis, leads to hepatic inflammation in hyperlipidemic mouse models of nonalcoholic steatohepatitis. *Hepatology* 48(2):474-486.

243. Tall AR, Yvan-Charvet L, Terasaka N, Pagler T, & Wang N (2008) HDL, ABC transporters, and cholesterol efflux: implications for the treatment of atherosclerosis. *Cell metabolism* 7(5):365-375.
244. Lau JK, Zhang X, & Yu J (2017) Animal models of non-alcoholic fatty liver disease: current perspectives and recent advances. *The Journal of pathology* 241(1):36-44.
245. Hansen HH, *et al.* (2017) Mouse models of nonalcoholic steatohepatitis in preclinical drug development. *Drug discovery today* 22(11):1707-1718.
246. Vergnes L, Phan J, Strauss M, Tafuri S, & Reue K (2003) Cholesterol and cholate components of an atherogenic diet induce distinct stages of hepatic inflammatory gene expression. *The Journal of biological chemistry* 278(44):42774-42784.
247. Gordon SM, *et al.* (2015) A comparison of the mouse and human lipoproteome: suitability of the mouse model for studies of human lipoproteins. *Journal of proteome research* 14(6):2686-2695.
248. Hayes KC, Lindsey S, Stephan ZF, & Brecker D (1989) Retinal pigment epithelium possesses both LDL and scavenger receptor activity. *Investigative ophthalmology & visual science* 30(2):225-232.
249. Gordiyenko N, *et al.* (2004) RPE cells internalize low-density lipoprotein (LDL) and oxidized LDL (oxLDL) in large quantities in vitro and in vivo. *Investigative ophthalmology & visual science* 45(8):2822-2829.
250. Yu AL, Lorenz RL, Haritoglou C, Kampik A, & Welge-Lussen U (2009) Biological effects of native and oxidized low-density lipoproteins in cultured human retinal pigment epithelial cells. *Experimental eye research* 88(3):495-503.

251. Fernandez-Godino R, Pierce EA, & Garland DL (2016) Extracellular Matrix Alterations and Deposit Formation in AMD. *Adv Exp Med Biol* 854:53-58.
252. Yamada Y, *et al.* (2008) Oxidized low density lipoproteins induce a pathologic response by retinal pigmented epithelial cells. *Journal of neurochemistry* 105(4):1187-1197.
253. Yin L, *et al.* (2011) OX-LDL up-regulates the vascular endothelial growth factor-to-pigment epithelium-derived factor ratio in human retinal pigment epithelial cells. *Current eye research* 36(4):379-385.
254. Ebrahimi KB, Fijalkowski N, Cano M, & Handa JT (2013) Decreased membrane complement regulators in the retinal pigmented epithelium contributes to age-related macular degeneration. *The Journal of pathology* 229(5):729-742.
255. Gnanaguru G, Choi AR, Amarnani D, & D'Amore PA (2016) Oxidized Lipoprotein Uptake Through the CD36 Receptor Activates the NLRP3 Inflammasome in Human Retinal Pigment Epithelial Cells. *Investigative ophthalmology & visual science* 57(11):4704-4712.
256. Yating Q, *et al.* (2015) Oxidized LDL induces apoptosis of human retinal pigment epithelium through activation of ERK-Bax/Bcl-2 signaling pathways. *Current eye research* 40(4):415-422.
257. Pikuleva IA & Curcio CA (2014) Cholesterol in the retina: the best is yet to come. *Progress in retinal and eye research* 41:64-89.
258. Storti F, *et al.* (2017) Regulated efflux of photoreceptor outer segment-derived cholesterol by human RPE cells. *Experimental eye research* 165:65-77.

259. Holzer M, *et al.* (2013) Aging affects high-density lipoprotein composition and function. *Biochimica et biophysica acta* 1831(9):1442-1448.
260. Berrougui H, Isabelle M, Cloutier M, Grenier G, & Khalil A (2007) Age-related impairment of HDL-mediated cholesterol efflux. *Journal of lipid research* 48(2):328-336.
261. Zheng W, *et al.* (2012) Spatial distribution of the pathways of cholesterol homeostasis in human retina. *PLoS ONE* 7(5):e37926.
262. Li CM, *et al.* (2005) Retina expresses microsomal triglyceride transfer protein: implications for age-related maculopathy. *Journal of lipid research* 46(4):628-640.
263. Klingeborn M, *et al.* (2017) Directional Exosome Proteomes Reflect Polarity-Specific Functions in Retinal Pigmented Epithelium Monolayers. *Scientific reports* 7(1):4901.
264. Fan Q, *et al.* (2017) HDL-cholesterol levels and risk of age-related macular degeneration: a multiethnic genetic study using Mendelian randomization. *International journal of epidemiology* 46(6):1891-1902.
265. Cheung CMG, *et al.* (2017) Plasma lipoprotein subfraction concentrations are associated with lipid metabolism and age-related macular degeneration. *Journal of lipid research* 58(9):1785-1796.
266. Burgess S & Davey Smith G (2017) Mendelian Randomization Implicates High-Density Lipoprotein Cholesterol-Associated Mechanisms in Etiology of Age-Related Macular Degeneration. *Ophthalmology* 124(8):1165-1174.

267. Paun CC, *et al.* (2015) Genetic Variants and Systemic Complement Activation Levels Are Associated With Serum Lipoprotein Levels in Age-Related Macular Degeneration. *Investigative ophthalmology & visual science* 56(13):7766-7773.
268. Neale BM, *et al.* (2010) Genome-wide association study of advanced age-related macular degeneration identifies a role of the hepatic lipase gene (LIPC). *Proceedings of the National Academy of Sciences of the United States of America* 107(16):7395-7400.
269. Chen W, *et al.* (2010) Genetic variants near TIMP3 and high-density lipoprotein-associated loci influence susceptibility to age-related macular degeneration. *Proceedings of the National Academy of Sciences of the United States of America* 107(16):7401-7406.
270. Libeu CP, *et al.* (2001) New insights into the heparan sulfate proteoglycan-binding activity of apolipoprotein E. *The Journal of biological chemistry* 276(42):39138-39144.
271. Boren J, *et al.* (1998) Identification of the principal proteoglycan-binding site in LDL. A single-point mutation in apo-B100 severely affects proteoglycan interaction without affecting LDL receptor binding. *The Journal of clinical investigation* 101(12):2658-2664.
272. Picard E, *et al.* (2010) CD36 plays an important role in the clearance of oxLDL and associated age-dependent sub-retinal deposits. *Aging* 2(12):981-989.
273. Vavvas DG, *et al.* (2016) Regression of Some High-risk Features of Age-related Macular Degeneration (AMD) in Patients Receiving Intensive Statin Treatment. *EBioMedicine* 5:198-203.

274. Delanghe JR, Speeckaert R, & Speeckaert MM (2014) Complement C3 and its polymorphism: biological and clinical consequences. *Pathology* 46(1):1-10.
275. Sahu A, Morikis D, & Lambris JD (2003) Compstatin, a peptide inhibitor of complement, exhibits species-specific binding to complement component C3. *Molecular immunology* 39(10):557-566.
276. Nilsson SC, Sim RB, Lea SM, Fremeaux-Bacchi V, & Blom AM (2011) Complement factor I in health and disease. *Molecular immunology* 48(14):1611-1620.
277. Khandhadia S, *et al.* (2013) Age-related macular degeneration and modification of systemic complement factor H production through liver transplantation. *Ophthalmology* 120(8):1612-1618.
278. Savarese G, De Ferrari GM, Rosano GM, & Perrone-Filardi P (2015) Safety and efficacy of ezetimibe: A meta-analysis. *Int J Cardiol* 201:247-252.
279. Tie C, *et al.* (2015) Ezetimibe Attenuates Atherosclerosis Associated with Lipid Reduction and Inflammation Inhibition. *PLoS ONE* 10(11):e0142430.
280. Sirtori CR (2014) The pharmacology of statins. *Pharmacol Res* 88:3-11.
281. Ma L, *et al.* (2015) The association between statin use and risk of age-related macular degeneration. *Scientific reports* 5:18280.
282. Al-Holou SN, *et al.* (2015) The Association of Statin Use with Age-Related Macular Degeneration Progression: The Age-Related Eye Disease Study 2 Report Number 9. *Ophthalmology* 122(12):2490-2496.

283. VanderBeek BL, Zacks DN, Talwar N, Nan B, & Stein JD (2013) Role of statins in the development and progression of age-related macular degeneration. *Retina* 33(2):414-422.
284. Leman LJ (2015) The potential of apolipoprotein mimetic peptides in the treatment of atherosclerosis. *Clin Lipidol* 10(3):215-217.
285. Kong SK, *et al.* (2017) An ApoB100-mimetic vaccine prevents obesity and liver steatosis in ApoE<sup>-/-</sup> mice. *Pharmacol Rep* 69(6):1140-1144.
286. Qin S, *et al.* (2012) Reverse D4F, an apolipoprotein-AI mimetic peptide, inhibits atherosclerosis in ApoE-null mice. *J Cardiovasc Pharmacol Ther* 17(3):334-343.
287. Nayyar G, *et al.* (2012) Apolipoprotein E mimetic is more effective than apolipoprotein A-I mimetic in reducing lesion formation in older female apo E null mice. *Atherosclerosis* 224(2):326-331.
288. Sharifov OF, *et al.* (2011) Apolipoprotein E mimetics and cholesterol-lowering properties. *Am J Cardiovasc Drugs* 11(6):371-381.
289. Pal M & Pillarisetti S (2007) HDL elevators and mimetics--emerging therapies for atherosclerosis. *Cardiovasc Hematol Agents Med Chem* 5(1):55-66.
290. Rudolf M, *et al.* (2018) ApoA-I Mimetic Peptide 4F Reduces Age-Related Lipid Deposition in Murine Bruch's Membrane and Causes Its Structural Remodeling. *Current eye research* 43(1):135-146.

291. Anantharamaiah GM, Garber DW, & White CR (2016) Apolipoprotein Mimetic Peptides as Modulators of Lipoprotein Function. *Protein Pept Lett* 23(11):1024-1031.
292. Ivanescu AA, *et al.* (2015) Modifying Choroidal Neovascularization Development with a Nutritional Supplement in Mice. *Nutrients* 7(7):5423-5442.
293. Ronsein GE, *et al.* (2016) Niacin Therapy Increases High-Density Lipoprotein Particles and Total Cholesterol Efflux Capacity But Not ABCA1-Specific Cholesterol Efflux in Statin-Treated Subjects. *Arteriosclerosis, thrombosis, and vascular biology* 36(2):404-411.
294. Damsteegt EL, Davie A, & Lokman PM (2018) The evolution of apolipoprotein B and its mRNA editing complex. Does the lack of editing contribute to hypertriglyceridemia? *Gene* 641:46-54.
295. Shaw PX, *et al.* (2012) Complement factor H genotypes impact risk of age-related macular degeneration by interaction with oxidized phospholipids. *Proceedings of the National Academy of Sciences of the United States of America* 109(34):13757-13762.
296. Johnson LV, *et al.* (2011) Cell culture model that mimics drusen formation and triggers complement activation associated with age-related macular degeneration. *Proceedings of the National Academy of Sciences of the United States of America* 108(45):18277-18282.
297. Cheng Q, *et al.* (2017) Early Age-related Macular Degeneration with Cardiovascular and Renal Comorbidities: An Analysis of the National Health and Nutrition Examination Survey, 2005-2008. *Ophthalmic epidemiology* 24(6):413-419.

298. Wadhera RK, Steen DL, Khan I, Giugliano RP, & Foody JM (2016) A review of low-density lipoprotein cholesterol, treatment strategies, and its impact on cardiovascular disease morbidity and mortality. *J Clin Lipidol* 10(3):472-489.
299. Mattapallil MJ, *et al.* (2012) The Rd8 mutation of the Crb1 gene is present in vendor lines of C57BL/6N mice and embryonic stem cells, and confounds ocular induced mutant phenotypes. *Investigative ophthalmology & visual science* 53(6):2921-2927.
300. Herrmann R, *et al.* (2010) Phosducin regulates transmission at the photoreceptor-to-ON-bipolar cell synapse. *J Neurosci* 30(9):3239-3253.
301. Van Blarcom T, *et al.* (2015) Precise and efficient antibody epitope determination through library design, yeast display and next-generation sequencing. *Journal of molecular biology* 427(6 Pt B):1513-1534.
302. Rajpal A, *et al.* (2005) A general method for greatly improving the affinity of antibodies by using combinatorial libraries. *Proceedings of the National Academy of Sciences of the United States of America* 102(24):8466-8471.
303. Boder ET & Wittrup KD (1997) Yeast surface display for screening combinatorial polypeptide libraries. *Nature biotechnology* 15(6):553-557.
304. Uehara H, *et al.* (2013) Dual suppression of hemangiogenesis and lymphangiogenesis by splice-shifting morpholinos targeting vascular endothelial growth factor receptor 2 (KDR). *FASEB J* 27(1):76-85.
305. Livak KJ & Schmittgen TD (2001) Analysis of relative gene expression data using real-time quantitative PCR and the 2<sup>-</sup>(Delta Delta C(T)) Method. *Methods* 25(4):402-408.

306. Kurihara T, *et al.* (2016) Hypoxia-induced metabolic stress in retinal pigment epithelial cells is sufficient to induce photoreceptor degeneration. *eLife* 5.
307. Xin-Zhao Wang C, Zhang K, Aredo B, Lu H, & Ufret-Vincenty RL (2012) Novel method for the rapid isolation of RPE cells specifically for RNA extraction and analysis. *Experimental eye research* 102:1-9.
308. Choudhary M, *et al.* (2016) PPARbeta/delta selectively regulates phenotypic features of age-related macular degeneration. *Aging* 8(9):1952-1978.

## Biography

Michael Landowski was born on May 4<sup>th</sup>, 1987 in Hampton, Virginia and was raised in Wisconsin. He attended the University of Wisconsin-Madison from 2005-2009 where he received his B.S. in Genetics. As an undergraduate, he became interested in research when working in Dr. Herbert Chen's laboratory studying the mechanisms contributing to the development of neuroendocrine cancers. After graduating, Michael took a research technician position at the Children's Hospital Boston with Dr.'s Alan Beggs and Hanna Gazda. He studied the genetic causes of Diamond-Blackfan anemia and published his first first author paper titled, "Novel deletion of RPL15 identified by array-comparative genomic hybridization in Diamond-Blackfan anemia." Michael became interested in understanding the genetic basis of human disease and decided to pursue his graduate studies at Duke University under the guidance of Dr. Catherine Bowes Rickman in the University Program in Genetics and Genomics (UPGG) in 2011. During his PhD training, Michael received two conference travel awards from the Association for Research in Vision and Ophthalmology (ARVO) and Association of Ocular Pharmacology and Therapeutics (AOPT) to present his work as well as attended the prestigious National Eye Institute's Fundamentals of Vision Research course at Woods Hole, Massachusetts.